EVALUATION OF CO_2 FLOODING IN MULTI-LAYERED HETEROGENEOUS RESERVOIR

Mr. Satavee Summapo

A Thesis Submitted in Partial Fulfillment of the Requirements

for the Degree of Master of Engineering Program in Petroleum Engineering

Department of Mining and Petroleum Engineering

Faculty of Engineering

Chulalongkorn University

Academic Year 2013

Copyright of Chulalongkorn University

การประเมินประสิทธิภาพของการฉีดอัดก๊าซคาร์บอนไดออกไซด์

ในแหล่งกักเก็บวิวิธพันธุ์หลายชั้น

นายสาธวี สัมมาโพธิ์

Thesis title	EVALUATION OF CO_2 FLOODING IN MULTI-LAYERED HETEROGENEOUS RESERVOIR
By	Mr. Satavee Summapo
Field of Study	Petroleum Engineering
Thesis Advisor	Falan Srisuriyachai, Ph.D.
Thesis Co-advisor	Assistant Professor Suwat Athichanagorn, Ph.D.

Accepted by the Faculty of Engineering, Chulalongkorn University in Partial Fulfillment of the Requirements for the Master's Degree

………………………….… Dean of the Faculty of Engineering

(Professor Bundhit Eua-Arporn, Ph.D.)

THESIS COMMITEE

…………………………………….… Chairman

(Associate Professor Sarithdej Pathanasethpong)

…………………………………….... Thesis Advisor

(Falan Srisuriyachai, Ph.D.)

…………………………………….... Thesis Co-advisor

(Assistant Professor Suwat Athichanagorn, Ph.D.)

…………………………………….… Examiner

(Assistant Professor Jirawat Chewaroungroaj, Ph.D.)

…………………………………….… External Examiner

(Siree Nasakul, Ph.D.)

สาธวี สัมมาโพธิ์ : การประเมินประสิทธิภาพของการฉีดอัดก๊าซคาร์บอนไดออกไซด์ใน
แหล่งกักเก็บวิวิธพันธุ์หลายชั้น. (EVALUATION OF CO_2 FLOOING IN
MULTI-LAYERED   HETEROGENEOUS   RESERVOIR)
อ. ที่ปรึกษาวิทยานิพนธ์หลัก: อ.ดร. ฟ้าลั่น ศรีสุริยชัย, อ. ที่ปรึกษาวิทยานิพนธ์ร่วม:
ผศ.ดร.สุวัฒน์ อธิชนากร, 138 หน้า.

ปัจจุบันกระบวนการฉีดอัดก๊าซคาร์บอนไดออกไซด์แบบเนื้อเดียวได้ถูกนำมาใช้อย่าง
แพร่หลายเนื่องจากก๊าซดังกล่าวสามารถช่วยเพิ่มประสิทธิภาพในการผลิตน้ำมันโดยอาศัยหลักการ
รวมตัวเป็นเนื้อเดียวซึ่งเกิดขึ้นระหว่างก๊าซคาร์บอนไดออกไซด์และน้ำมันดิบในแหล่งกักเก็บ
อย่างไรก็ตาม การที่ก๊าซคาร์บอนไดออกไซด์มีความหนาแน่นน้อยกว่าน้ำมันนั้นเป็นสาเหตุของ
การไหลขึ้นสู่ด้านบนและยังก่อให้เกิดความไม่มีเสถียรภาพของแนวผิวหน้าของการฉีดอัด ซึ่งทำให้
ประสิทธิภาพในการผลิตน้ำมันจากแหล่งกักเก็บลดลง ดังนั้นวัตถุประสงค์ของการศึกษานี้คือการ
ประเมินผลของตัวแปรที่ไม่สามารถควบคุมได้ อันได้แก่ ดรรชนีวิวิธพันธุ์ของแหล่งกักเก็บ ลำดับ
การทับถมของหินกักเก็บและความลาดเอียงของแหล่งกักเก็บ เมื่อรวมตัวแปรดังกล่าวกับผลจากตัว
แปรที่สามารถควบคุมได้ อันได้แก่ อัตราการฉีดอัดของก๊าซคาร์บอนไดออกไซด์และช่วงความยาว
ในหลุมฉีดอัด จะได้สภาวะที่เหมาะสมในการดำเนินการผลิต ดรรชนีวิวิธพันธุ์ของแหล่งกักเก็บ ถูก
กำหนดโดยสัมประสิทธิ์ลอเรนซ์ซึ่งได้มาจากการปรับค่าความสามารถในการซึมผ่านได้ของหินกัก
เก็บในแต่ละชั้น

ผลการศึกษาด้วยแบบจำลองแหล่งกักเก็บระบุว่าการฉีดอัดน้ำลงไปก่อนการฉีดอัดก๊าซ
คาร์บอนไดออกไซด์ช่วยให้การผลิตดีขึ้นและปริมาณน้ำที่เหมาะสมควรเป็น 0.2 เท่าของปริมาตรรู
พรุนทั้งหมด ผลการศึกษายังแสดงให้เห็นว่าแบบจำลองนี้สามารถผลิตน้ำมันถึงร้อยละ 68 จาก
ปริมาณน้ำมันที่มีทั้งหมด ซึ่งสูงกว่าการฉีดอัดน้ำเพียงอย่างเดียวร้อยละ 8 อีกทั้งผลการศึกษายัง
สามารถสรุปได้ว่าการที่น้ำปริมาณมากมาถึงหลุมผลิตในช่วงท้ายของการผลิตนั้นเป็นการช่วยให้
กระบวนการผลิตดำเนินได้ยาวนานขึ้นเนื่องจากก้อนน้ำนี้ไปช่วยผลักดันน้ำมันให้มีอัตราการผลิต
สูงเกินกว่าอัตราขั้นต่ำที่กำหนดไว้ นอกจากนี้ดรรชนีวิวิธพันธุ์ของแหล่งกักเก็บเป็นตัวแปรที่ส่งผล
กระทบต่อเสถียรภาพของแนวหน้าของการอัดฉีดและประสิทธิภาพในการผลิต

ภาควิชา วิศวกรรมเหมืองแร่และปิโตรเลียม   ลายมือชื่อนิสิต
สาขาวิชา วิศวกรรมปิโตรเลียม   ลายมือชื่อ อ.ที่ปรึกษาวิทยานิพนธ์หลัก
ปีการศึกษา 2556   ลายมือชื่อ อ.ที่ปรึกษาวิทยานิพนธ์ร่วม

5471217321: MAJOR PETROLEUM ENGINEERING

KEYWORDS: CO_2 FLOODING/HETEROGENEOUS RESERVOIR

SATAVEE SUMMAPO: EVALUATION OF CO_2 FLOODING IN MULTI-LAYERED HETEROGENEOUS RESERVOIR. ADVISOR: FALAN SRISURIYACHAI, Ph.D., CO-ADVISOR: ASST. PROF. SUWAT ATHICHANAGORN, Ph.D., 138 pp.

Carbon dioxide (CO_2) miscible flooding is widely performed to improve oil recovery. This technique recovers oil through miscibility mechanism between CO_2 and reservoir fluid. Since CO_2 is less dense compared to reservoir oil, this leads to gas overriding and instability of flood front, resulting in poor recovery efficiency. This study aims to investigate effect of uncontrollable parameters consisting reservoir heterogeneity, formation depositional sequence and dip angle. Appropriate conditions combined with controllable parameters including CO_2 injection rate and CO_2 injection perforation interval are also studied. ECLIPSE®300 reservoir simulator is utilized. Each heterogeneous reservoir model is constructed by varying permeability in each layer and it is assigned with Lorenz coefficient (L_c).

Results indicate that pre-flushed water is required and 0.2 PV is found to be optimum. About 68% of oil recovery is achieved from this CO_2 flooding base case, where 8% is higher than just solely waterflood. Although, miscible bank can extract intermediate hydrocarbon, without pressure support from injected water, oil production can be terminated early. The results also show that, with a big slug of water arrival to production well at late period, production can be prolonged due to a bounce of oil rate above well shut-in limit. Reservoir heterogeneity plays a role, affecting stability of flood front and also recovery performance.

Department: <u>Mining and Petroleum Engineering</u>   Student's Signature <u>   </u>

Field of Study: <u>Petroleum Engineering</u>   Advisor's Signature <u>   </u>

Academic Year: <u>2013</u>   Co-advisor's Signature <u>   </u>

Acknowledgements

Contents

List of Tables

List of Figures

List of Abbreviations

BSCF	billion standard cubic feet
C1	methane
C2	ethane
C3	propane
i-C4 or I-C4	isobutane
i-C5 or I-C5	isopentane
n-C4 or N-C4	normal butane
n-C5 or N-C5	normal pentane
C6	hexane
C7+	alkane hydrocarbon from heptanes onward
CO_2	carbon dioxide
EOR	enhanced oil recovery
EOS	equation of state
F or ^{o}F	degree fahrenheit
FCM	first contact miscibility
HCPV	hydrocarbon pore volume
MCM	multi-contact miscibility
mD	millidarcy
MMP	minimum miscibility pressure
MSCFD	thousand standard cubic feet per day
MMSCFD	million standard cubic feet per day
MMSTB	million stock-tank barrel
OOIP	original oil in place
PV	reservoir pore volume
PSIA or psia	pounds per square inch absolute
RB	reservoir barrel
SCAL	special core analysis
STB or stb	stock-tank barrel
STB/D	stock-tank barrels per day

Nomenclatures

ΔP	pressure difference
φ	porosity
μ	viscosity
C_j	fraction of total storage capacity
h	formation thickness
k	absolute permeability
F_j	fraction of flow capacity
L	formation length
L_c	Lorenz's coefficient
k_h	horizontal permeability
k_{rg}	relative permeability to gas
k_{ro}	relative permeability to oil (Oil/Water function)
k_{rog}	relative permeability to oil (Gas/Liquid function)
k_{rw}	relative permeability to water
k_v	vertical permeability
Q_j	flow rate
W	formation width

CHAPTER I

INTRODUCTION

1.1 Background

Oil occupied in reservoir porous media is realized that it could be produced up to one third of Original Oil In Place (OOIP) by natural drive mechanism or primary recovery. As a result of increasing in oil demand on global market together with limited resources, Enhanced Oil Recovery (EOR) can be achieved by injecting materials which are not present in the reservoir to improve flow property of hydrocarbon and/or releasing previously captured hydrocarbon. The EOR techniques can be thermal treatment (steam flooding or fire flooding), chemical injection (surfactant or polymer flooding) or gas injection (nitrogen or carbon dioxide).

Among of the techniques used in EOR, Carbon Dioxide (CO_2) flooding has been commercially proven and has been broadly used as a promising technique. The use of CO_2 is not considered only as an EOR injected fluid to improve oil recovery but the technique also can be adopt to sequestering emitted greenhouse gas. CO_2 flooding can be implemented either in immiscible or miscible mode depending on oil property, CO_2 property, reservoir conditions, and operational conditions. In CO_2 miscible flooding, miscibility can be achieved through a Multi-Contact Miscibility or MCM. Miscibility of CO_2 and reservoir oil is a result from an evaporation of intermediate compounds (C_2-C_6) in reservoir oil. That is, CO_2, which is a potential vaporizer, induces intermediate compounds to vaporize, creating a new intermediate enriched fluid which is completely mixed in all proportions. At certain situation when intermediate compounds are enriched enough with injected CO_2, a miscible bank is formed. However, miscibility of CO_2 and reservoir oil requires reservoir pressure to be greater than Minimum Miscibility Pressure (MMP).

Increment of oil recovery is mainly accomplished by improvement of displacement efficiency. The mechanisms contributing to enhancing recovery of CO_2 flooding are oil viscosity reduction, oil swelling and IFT reduction [1]. CO_2 miscible flooding has been reportedly desirable as it is applicable with a wide range of crude

properties, can achieve MMP at relatively low pressure in comparison to other miscible gases [2] as well as can be applied in both sandstone and carbonate formations [1][3].

The low density of CO_2 compared to oil density, however, can cause instability of flood front as well as gas overriding and consecutively an early breakthrough of the injected CO_2, resulting in a severe displacement condition due to preceded CO_2 production prior to production of oil. Large amount of oil tends to be upswept and low oil recovery is obtained, accordingly. This problem is generally diminished by displacing CO_2 downdip through an inclined reservoir. An early gas breakthrough is mitigated by gravity effect. Not only inclination of reservoir that plays a major role in most gas injection, heterogeneity of reservoir, referring to variation of petrophysical properties mainly permeability, has been identified as one of the most important factors affecting displacement performance by gas. Presence of high permeability streaks generally leads to gas channeling, resulting in gas early breakthrough. This also causes instability of flood front and consecutively affects occurrence of miscible bank.

Reservoir simulation is applied for this study in order to evaluate the effects from various parameters. Reservoir models are constructed by using the commercialized compositional oil simulator "**ECLIPSE®300**" by **GeoQuest Schlumberger**. The study is performed by varying reservoir permeability to illustrate degree of heterogeneity for the multi-layered reservoir. Heterogeneous reservoir models are, then, coupled with other uncontrollable parameters which are depositional sequence and reservoir dip angle as well as controllable parameters consisting of CO_2 injection rate and its injection perforation interval. Field oil recovery factor is used as criteria to compare and to evaluate performance of CO_2 miscible flooding.

1.2 Objectives

1. To study effect of uncontrollable parameters or reservoir parameters including reservoir heterogeneity, formation depositional sequence (lithofacies) and reservoir dip angle on CO_2 miscible flooding performance.

2. To determine the appropriate condition of operation parameters which are CO_2 injection rate and injection perforation interval when combining with uncontrollable parameters for CO_2 miscible flooding.

1.3 Outline of Methodology

1. Develop base case model which is CO_2 flooding in homogeneous reservoir. Flooding scheme of water pre-flushed, CO_2 injection and chasing water will be determined in this base case.

2. Construct heterogeneous reservoir model by varying of reservoir permeability in each layer, to depict fining upward sand. Each constructed model will be represented by a heterogeneity index, Lorenz coefficient (L_c).

3. Simulate heterogeneous model with different reservoir dip angle.

4. Repeat step 2 and 3 with coarsening upward sand model.

5. Run heterogeneous model with earlier mentioned controllable parameters by repeating step 2 to 4, and beginning with CO_2 injection rate, then followed by injection perforation interval.

6. Analyze results mainly in terms of field oil recovery as a function of heterogeneity index, accompanied with other reservoir simulation outcomes such as oil production rate, water production rate, gas production rate, reservoir pressure and bottomhole pressure.

7. Conclude results obtained from each study parameters as appropriate value to be implemented as well as findings in CO_2 miscible flooding in the multi-layered heterogeneous reservoir.

1.4   Thesis Outline

The remaining parts of this thesis contain five chapters outlining as follows:

Chapter II – includes review of published literatures/ previous works which are relevant to the use of CO_2 as injected gas for miscible flooding and also the study parameters on performance of CO_2 miscible flooding.

Chapter III – describes theory related to CO_2 miscible flooding and concepts to be used when constructing model or determining effect from each study parameters.

Chapter IV – gives details of reservoir simulation model construction which is set up in the simulator **ECLIPSE®300**. Details of thesis methodology are also described in this chapter.

Chapter V – shows and discusses simulation results including base case optimization and also study parameters. Discussion is mainly investigated based on field oil recovery as a function of heterogeneity index. Other simulation outcomes will be, however, used to assist in this chapter.

Chapter VI – provides conclusions and recommendations for future or further study.

1.5   Expected Usefulness

This study focuses on CO_2 miscible flooding simulation when reservoir contains degree of heterogeneity and in association with depositional sequence. A range of reservoir dip angles will be run through heterogeneous reservoir models in order to determine appropriate conditions for displacement mechanism by CO_2. Moreover, CO_2 injection rate, and injection perforation interval will be also investigated. Consequently, obtained results should be able to provide suitable value or screening criteria of parameters for CO_2 miscible flooding, particularly in multi-layered heterogeneous formation.

CHAPTER II

LITERATURE REVIEW

This chapter reviews works or studies on previous publications which focus on CO_2 injection as a miscible slug to improve oil recovery from the reservoir.

2.1 Application of CO_2 Miscible Flooding

The use of CO_2 as injectant in EOR process is not a new concept. It was originally presented as a patent since 1952. Its application becomes much more interesting from that day due to a higher availability of CO_2 source. CO_2 flooding has been categorized into two main aspects; miscible and immiscible flooding. Several studies have shown that CO_2 miscible flooding could become a potential method to increase oil recovery; thus, developments of process including experiments, pilot projects and field tests have been conducted to investigate benefits from utilizing this technique.

Qin et al. [4] performed a laboratory study, a reservoir simulation as well as a pilot test for CO_2 miscible flooding in a low permeability with thin-interbedded reservoir of Gao 89-1. In laboratory study, swelling test had been carried out to observe the effect from increasing pressure on oil volume and oil viscosity. Slim tube test was performed in order to determine minimum miscibility pressure and core flooding experiment was also examined to compare displacement efficiency between CO_2 miscible flooding and conventional water flooding. In the simulation part, compositional modeling was used to predict the optimized flooding parameters such as injection scheme. Finally, pilot test had been applied and results showed that an addition of oil recovery about 14.19% was recovered in ten years.

Shedid et al. [5] studied the feasibility of CO_2 flooding in a carbonate heterogeneous reservoir. They performed core flood analysis to evaluate the effects of CO_2 injection pressure, mobile oil saturation, CO_2 slug size, and oil viscosity on efficiency of CO_2 flooding. They also measured minimum miscibility pressure by using empirical correlations and slim tube tests. Results indicated that CO_2 miscible

flooding together with an increasing of injection pressure could recover more oil compared to immiscible flooding due to improvement of displacement efficiency. However, increasing in oil viscosity reduced total oil recovery. The optimum CO_2 slug size was found to be 15% driven by brine. It was also recommended that lighter oil is more suitable for the application of CO_2 miscible flooding than heavy oil.

Ghasemzadeh et al. [6] conducted full field compositional simulation to determine reservoir management and production strategies for Iranian undersaturated reservoir in order to improve oil recovery by comparing three possible recovery schemes including natural depletion, CO_2 injection and water flooding. In addition to the study, they also predicted minimum miscibility pressure (MMP) from various gases such as separator gas, CO_2, N_2, Methane and enriched gas by simulating one-dimensional slim tube displacement using EOS based compositional simulator and results indicated that CO_2 could attain the lowest MMP which was also lower than reservoir pressure. In the full field compositional simulations, optimization of CO_2 injection scenarios was accomplished by identifying CO_2 injection rate and location of additional injection well where there were six existing production wells. Performance of injection showed the highest cumulative oil production when injecting CO_2 from the crest of reservoir because displacement was more stable due to gravity difference. Then, injection rate was examined where injection well was at the crest and oil recovery factor was achieved the optimum value of CO_2 injection rate at 50 MMSCFD. Finally, three production schemes were compared and results showed that CO_2 miscible flooding yielded the highest oil recovery of about 19% additional oil recovery.

Factors leading to a better oil recovery in CO_2 miscible flooding have been summarized by Yongmao et al. [7]. They stated that factors contributing to oil recovery comprised of low interfacial tension, viscosity reduction, oil swelling, formation permeability improvement, solution gas flooding, and density change of oil and water. Results were proven experimentally that the main factors help enhance oil recovery were oil swelling and oil viscosity reduction.

2.2 CO_2 Flooding in Heterogeneous Reservoir

Reservoir heterogeneity can be considered as a major cause of severe problems for many field operations. Reservoir heterogeneity basically expresses reservoir characteristic and it is considered as one of the most important factors because of its implication to flooding displacement efficiency.

Jeschke et al. [8] studied CO_2 flooding in Californian oil reservoirs and possible sources of CO_2. It is mentioned that CO_2 miscible flooding would be a potential method where its performance could recover additional oil from 8 up to 16% of original oil in place (OOIP). This performance was dependent on reservoir depth and characteristics of oil and reservoir. It was reported that maximum oil that could be recovered was estimated to be 10% higher than mature waterflood technique with average CO_2 utilization of 4 to 6 thousand cubic feet per barrel of oil produced. They also stated that ideal CO_2 flooding performed well in homogenous reservoirs; however, most reservoirs were attributed to be heterogeneous. Therefore, reservoir characteristic could be a problem encountered in CO_2 flooding.

To investigate effects of reservoir heterogeneity on CO_2 miscible flooding, Shedid [9] determined this by using three different modes of heterogeneity including inclined single fractured reservoirs, composite reservoirs and layered reservoirs. He performed a slim tube tests and empirical correlation to obtain MMP for oil-CO_2 system as well as carbonate core flood tests to exhibit three different modes of reservoirs. Cores were flooded with super-critical CO_2 at optimized quantity of about 0.15 PV and chased by actual reservoir brine. Results showed that every mode containing reservoir heterogeneity had significant effect on oil recovery performance. With the first mode, performance between fractured and non-fractured reservoir was compared and poor displacement occurred in the case of fractured due to early breakthrough of CO_2 via high permeability fractures. Inclination angles used in this study were 30, 45, 60 and 90 degree and results showed that single fractured reservoir with 30 degree of inclination angle could produce the highest oil recovery. For the composite mode, the highest oil recovery was obtained from LMH (a series of low-medium-high permeability in order) core because of a gradual change of pressure gradient with a gradual increase of permeability. Lastly, layered reservoir mode

results were shown. Core with permeability distribution of MHL (medium-high-low) ordering from top gave the highest oil recovery because flow was at the center of core where high permeability layer exists.

Ahmed et al. [10] examined reservoir models and operating parameters for CO_2 flooding in order to provide guidelines to boost up flooding performance for different degrees of reservoir heterogeneity. Simulation runs were conducted to compare effectiveness of each model. Heterogeneity was estimated to generate different scenarios of reservoir by using Lorenz and Dyskstra Parsons coefficient while other key parameters were also investigated consisting of injection rates, injection patterns, well spacing, injection scheme (WAG, SWAG), WAG cycle length, vertical to horizontal permeability and horizontal injection wells. Oil recovery factor was used in this work as a criterion parameter to evaluate performance of each scenario. Experimental Design techniques were also used to minimize a number of simulation runs and help define effective variables and their combinational effects on the decision variables. It was noticed that different degrees of heterogeneity had a different effect on CO_2 miscible flooding performance at which each heterogeneity index could attain high oil recovery factors when other operating parameters are in the right combination. The results also showed that WAG and horizontal wells significantly increased oil recovery.

2.3   Gas Injection in Inclined Reservoir Formation

Several CO_2 flooding studies are involved with inclination of reservoir formation. As fluids own different densities, this leads to a concept of locating injection and production well for fluid displacement process. Gas, in general, is much lighter than oil; hence, it is preferably injected from top of formation, combining injection force and gravity segregation to maintain stability of flood front.

Mansour et al. [11] studied different scenarios of continuous CO_2 injection in dipping oil and gas condensate reservoirs by using reservoir simulations. Three-layered reservoirs with a dip angle of 10 degree deviated from x-direction were constructed and three different modes of heterogeneity were applied to illustrate permeability distribution. In the first geological scenario, permeability was set equally

in all three layers, while the second scenario was associated with a trend of descending permeability for deeper layers. The last scenario included a trend of ascending permeability for deeper layers. One injector and one producer were located on opposite side of the reservoir. Injection of both updip and downdip were examined as well. As results of this work, the third scenario yielded the highest sweep efficiency due to lower permeability at shallower layers which prevents CO_2 bypassing and flood front fingering. Attempts for CO_2 injection updip and downdip were then compared, and it was shown that injection from updip obtained higher oil recovery which is provided by gravity assists. In summary, it was concluded that in inclined reservoir scenarios, heterogeneity can show both positive and negative results on performance based on type of injection. Therefore, it should be investigated case by case.

The effect of reservoir inclination on CO_2 flooding was also investigated by Abdassah et al. [12]. They studied whether miscible CO_2 injection could be a potential technique to enhance oil recovery by exploiting slim tube experiment simulations to determine the MMP. In this work, injection pressure and reservoir dip angle were varied. Injection pressure was varied at below, equal and above MMP, while dip angle was compared between horizontal and 45 degree inclined reservoir. The results indicated that oil recovery from 45 degree downdip displacement was higher than horizontal displacement for the same injection pressure. This could be described as the effect of gravity segregation occurring from the difference of density between oil and CO_2. For injection pressure, it was shown that injection at pressure above MMP could attain the highest oil recovery; thus, conclusion was that miscible CO_2 injection more potential than immiscible one to improve oil recovery.

CHAPTER III

THEORY AND CONCEPT

This chapter describes the miscibility and its drive mechanism. Technique for measuring miscibility is also presented. Additionally, reservoir heterogeneity and its measures are explained as well.

3.1   Principal of CO_2 Flooding

CO_2 is recognizably known as a powerful hydrocarbon vaporizer. Lighter hydrocarbon portion in heavy oil components can be extracted by injecting CO_2 under suitable conditions including reservoir pressure, reservoir temperature and oil composition. This is a result from Multi-Contact Miscibility (MCM) mechanism between injected CO_2 and intermediate hydrocarbon in crude oil. This technique is currently growing in terms of EOR aspect due to its wide range of applicability.

3.2   Miscibility and Drive Mechanism

In order to get better understanding what is taking place inside porous media for miscible flooding process, ternary diagram are extensively used to explain behaviors of phase equilibrium, particularly for complicated hydrocarbon mixtures.

Ternary diagram is an equilateral triangular plot describing phase behavior of three-hypothetical-component system. It consists of three apexes in which each represents fluid type. At any point of diagram, fraction of each component in the mixture can be identified as shown in Figure 3.1 and it might be either in volume, mole or weight percentage form.
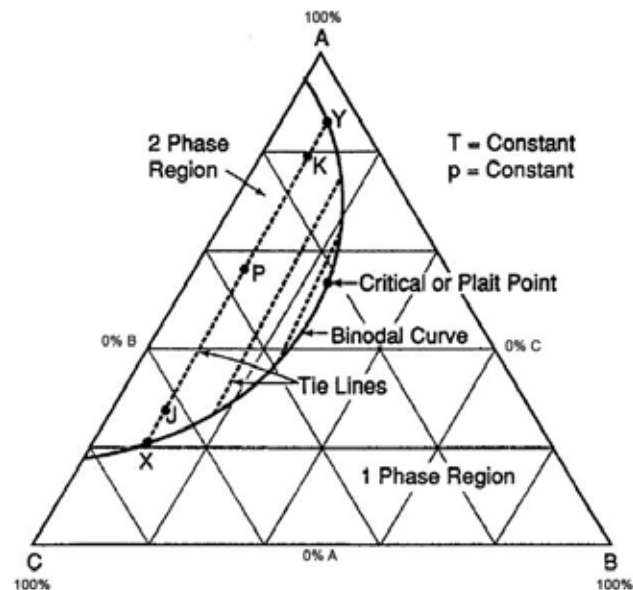
Figure 3.1 Ternary phase diagram of system consisting of three components [13]

A common example of components present in ternary diagram is hydrocarbon including light, intermediate and heavy hydrocarbons. Hydrocarbon in light component apex usually refers to methane (C_1), while intermediate component apex is represented by C_2-C_6 hydrocarbon and heavy component corner belongs to lumped C_7 or C_7 with heavier hydrocarbons; thus, the plot is now called "pseudo-ternary" diagram. Figure 3.2 below shows pseudo-ternary system for hydrocarbon. At particular pressure and temperature, ternary diagram is split into two zones by binodal curve. Zone under the curve is area where two phases appear, whereas above this curve is area where all components are in single phase. Tie lines connect two points on saturated vapor and saturated liquid curves. These two curves are eventually joined at critical point or plait point. Tie lines connecting two points are representation of equilibrium relation between saturated gas and saturated liquid because at any saturated liquid, there is a corresponding saturated vapor where they are in equilibrium. In addition, tie line tangent to two-phase envelope at the critical point and extending to both sides of the pseudo-ternary diagram is the limiting tie line identifying composition at which either oil or CO_2 must lie to the right (zone B or C) in order to produced multi-contact miscibility.
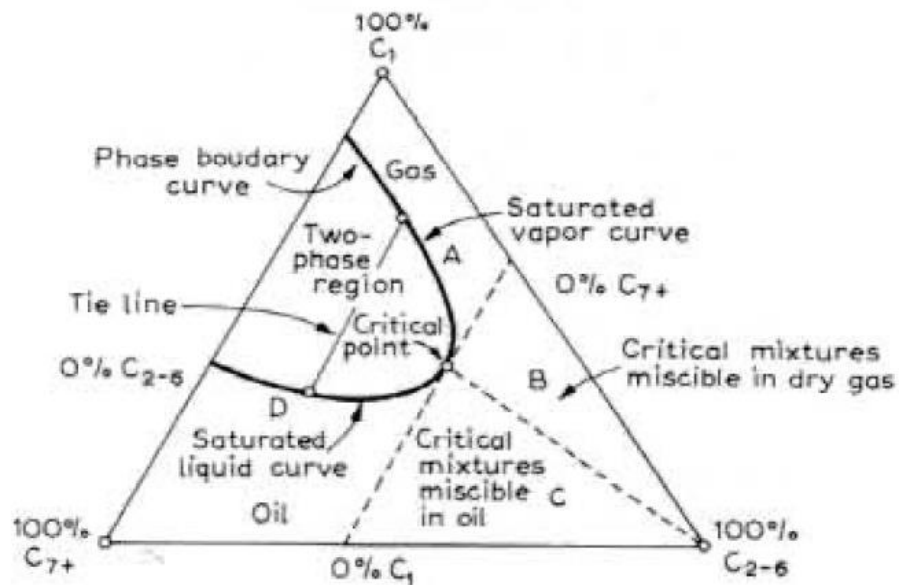
Figure 3.2 Pseudo-Ternary diagram for hydrocarbon system at fixed pressure and
temperature [14]

Appearance of miscibility can be noticed by a formation of new single phase
where all components are mixed in any proportion. Pressure and temperature have
strong influence on miscibility as well as oil composition and gas composition as they
affect behavior of binodal or two-phase zone. Miscibility is categorized into two
types, First Contact Miscibility (FCM) and multi-contact miscibility, where their
behaviors are summarized in Figure 3.3.
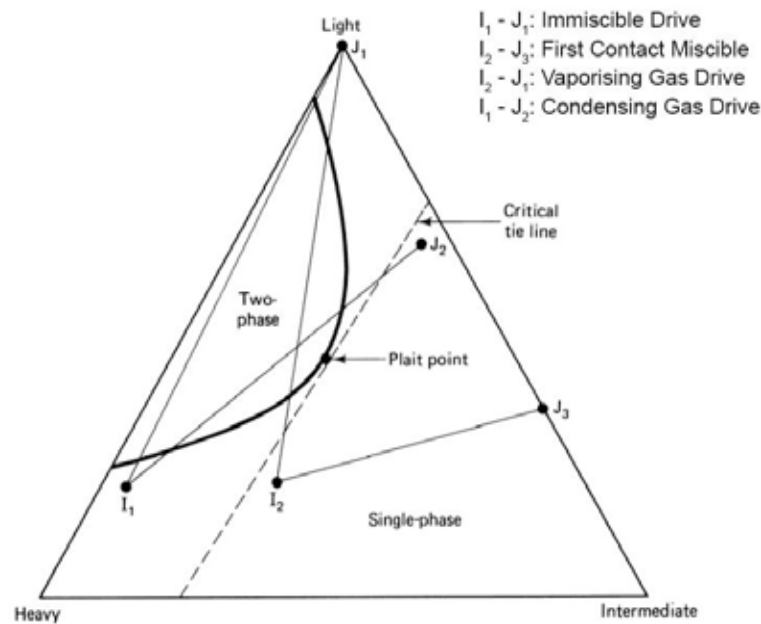
Figure 3.3 Conditions for different types of oil displacement by solvents [15]

Shown in Figure 3.3, path I_1-J_1wholly lying on the two-phase zone is considered as immiscible displacement. Path I_2-J_3 does not pass through two-phase zone or critical tie line, thus, it shows characteristic of first contact miscible displacement, while path I_2-J_1 and path I_1-J_2 passing through the two-phase zone and crossing critical tie line represent multi-contact miscible displacement. The first contact miscibility occurs when injected fluid is directly miscible with reservoir oil at any given pressure and temperature, forming a bank or a new phase where all components are completely mixed in all proportions. The latter case, multi-contact miscibility or dynamic miscibility is achieves by in-situ compositional alteration from mass transfer when crude oil is in contact with injected fluid. Multi-contact miscibility can be classified into two sub-categories which are vaporizing gas drive (high pressure gas injection) and condensing gas drive (enriched gas injection).

Basically, CO_2 injection is not directly miscible with crude oil at normal reservoir pressure and temperature and its miscibility is achieved through vaporizing gas drive. Moreover, phase behavior of CO_2/C_2-C_6/C_{7+} system is also similar to methane gas drive or C_1/C_2-C_6/C_{7+}system. The mechanism of multi-contact of vaporizing gas drive can be explained using Figure 3.4 and Figure 3.5.
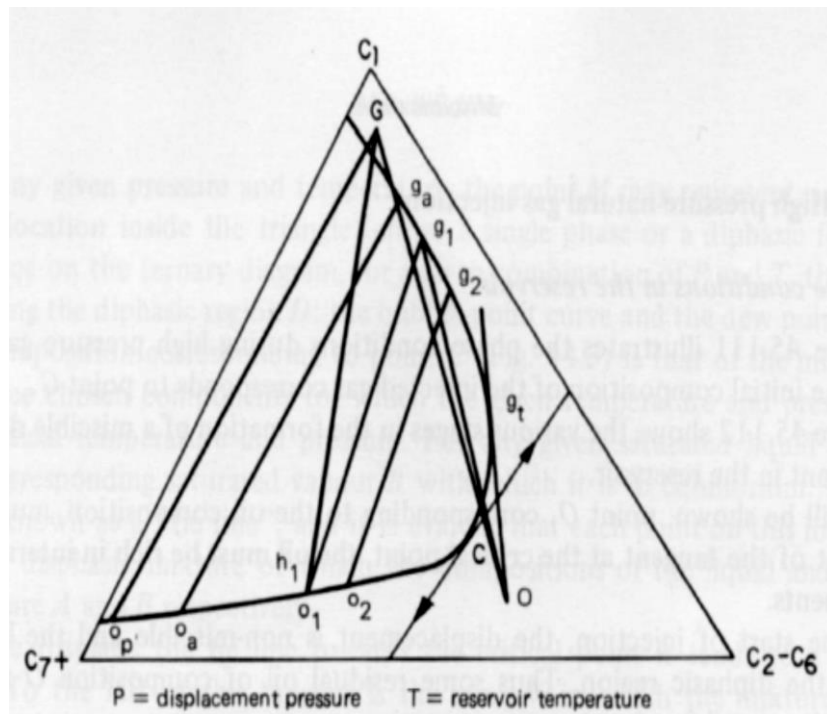
Figure 3.4 Pseudo-ternary diagram of vaporizing gas drive process [16]
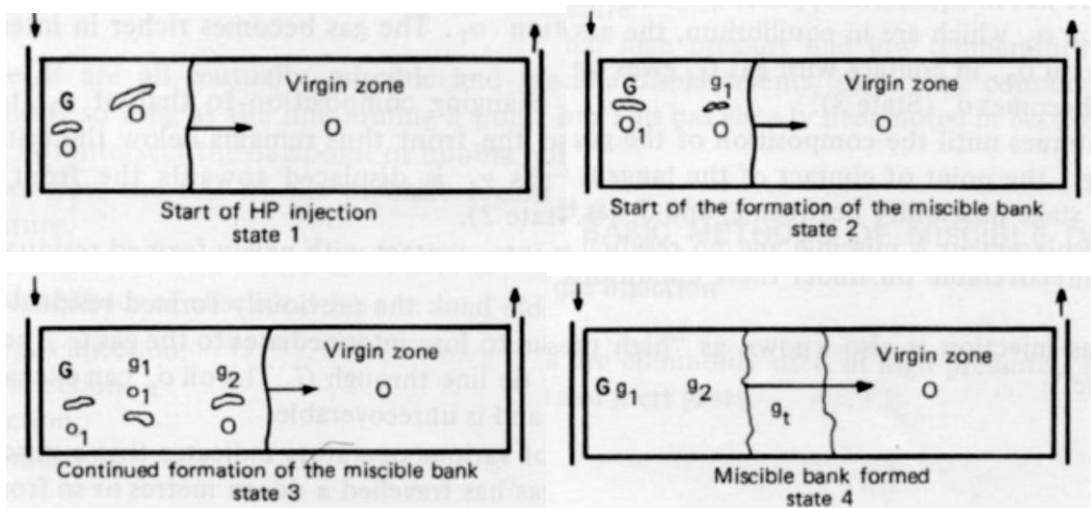
Figure 3.5 Schematic of vaporizing gas drive process [16]

Figure 3.4 shows pseudo-ternary diagram with reservoir having original oil composition O and injected stream having composition of gas G. Figure 3.5 illustrates stages of miscibility mechanism corresponding to changes in Figure 3.4. In the first stage, gas G is injected into oil O and connecting line between oil O and gas G passes through binodal area. This results in appearance of two-phase mixture splitting into gas g_1 and oil o_1 phases, determined by equilibrium tie line. Consequently, in stage 2, gas g_1 with a higher mobility moves toward flood front, leaving o_1 behind to mix with continuing injected gas G. Next stage is that gas g_1 at flood front is in contact with oil O, creating a mixture which is still in the two-phase zone. The mixture created is then splitting into gas g_2 and oil o_2 from equilibrium tie line. Similarly, gas g_2 preferentially moves toward flood front, whereas oil o_2 is trapped behind. Again, oil o_2 is in contact with gas G, releasing intermediate portion to gas phase and its composition turns into o_a. Mechanism continues following these steps until the gas phase will no longer form two phases when mixing with oil O or gas becomes g_t. This is path that is tangential to binodal curve and at this stage multi-contact miscibility has been achieved, forming miscibility. At the same time, previously formed oils such as o_1, o_2 and so on, continue to give their intermediate to gas G behind miscible bank until oil composition reaches the limit or o_p. At composition o_p, oil can no more release intermediate compounds to gas G and is unrecoverable. Therefore, reservoir oil must have sufficient amount of intermediate components (C_2-C_6), unless it is impossible to develop a miscible bank.

Although, CO_2 displacement process is analogous to methane injection or high pressure gas drive process, notable difference is that binodal curve or two-phase envelope for CO_2 process is relatively smaller than that of methane process (Figure 3.6) at the same pressure and temperature. Consequently, this is an advantage of applying CO_2 flooding as miscibility can be achieved at lower pressure.
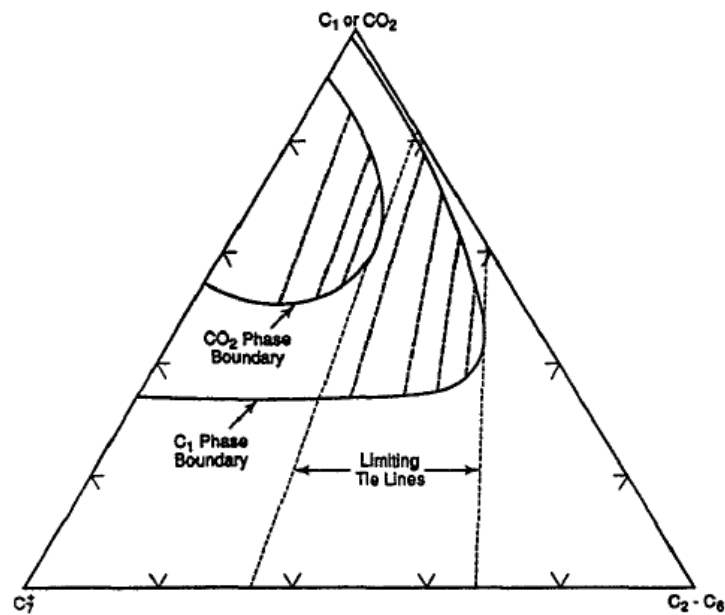
Figure 3.6 Comparison of two-phase envelops of CO_2-hydrocarbon system and
methane-hydrocarbon system [13]

3.3 Miscibility Measurement

CO$_2$ flooding is not directly miscible with most crude oil; therefore, there is a minimum pressure where miscibility will be achieved. This pressure is called "Minimum Miscibility Pressure" or "MMP" which can be dynamically measured by mass transfer between CO_2 and oil using flow experiments in equipment set called slim tube. Equipment includes a very small-diameter tube causing low flow rate inside sand packed coil to avoid an unfavorable mobility ratio condition. Figure 3.7 illustrates a typical schematic of slim tube apparatus operated by Yelig and Metcalfe [17].
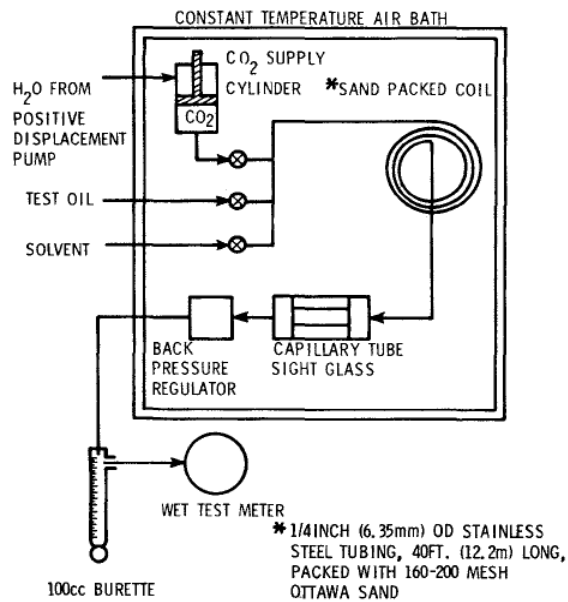
Figure 3.7 Slim tube experiment apparatus for MMP determination [17]

Corresponding oil recovery and injection pressure after a fixed pore volume (PV) of CO_2 has been injected is plotted to determine that miscibility has been attained (Figure 3.8). Sharp break on the curve indicates that immiscible displacement has been changed to miscible displacement as test pressure is increased.
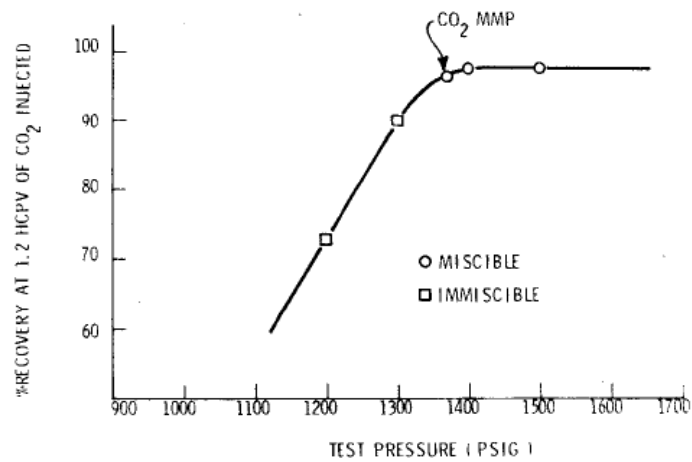
Figure 3.8 Determination of MMP from test result [17]

MMP can be either estimated by empirical correlation which is based on experimental data or by equation of state (EOS) based on known fluid compositions. Many researchers have proposed MMP correlation for miscible CO_2/hydrocarbon system. Yelig and Metcalfe [17] developed a simple correlation with a single MMP curve in Figure 3.9 as a function of temperature alone and it is used when there is limited data of oil properties.
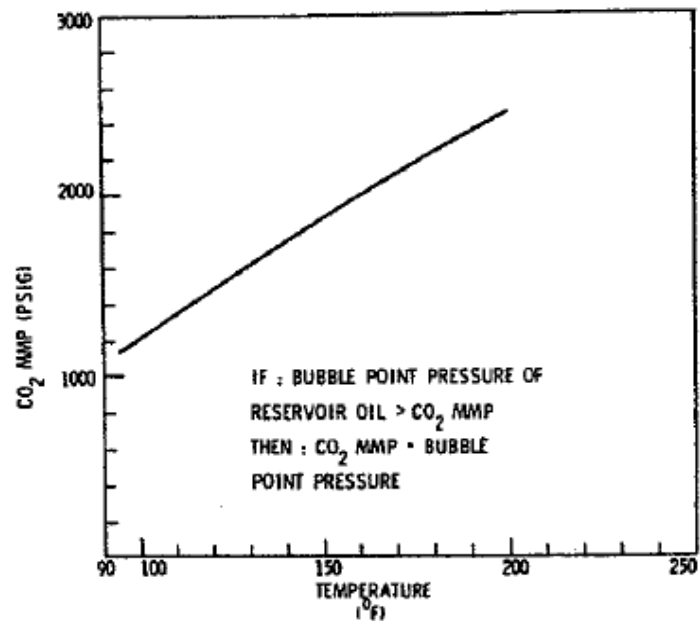
Figure 3.9 Minimum miscibility pressure for CO_2 by Yelig and Metcalfe

Other investigators included component fractions. Holm and Josendal developed a set of curves that give MMP as a function of pressure, temperature, and molecular weight of heavy component of crude oil (C_{5+}). Mungan extended the study to cover wider range for heavier crudes that have molecular weight of C_{5+} higher than 240 as shown in Figure 3.10 [13].
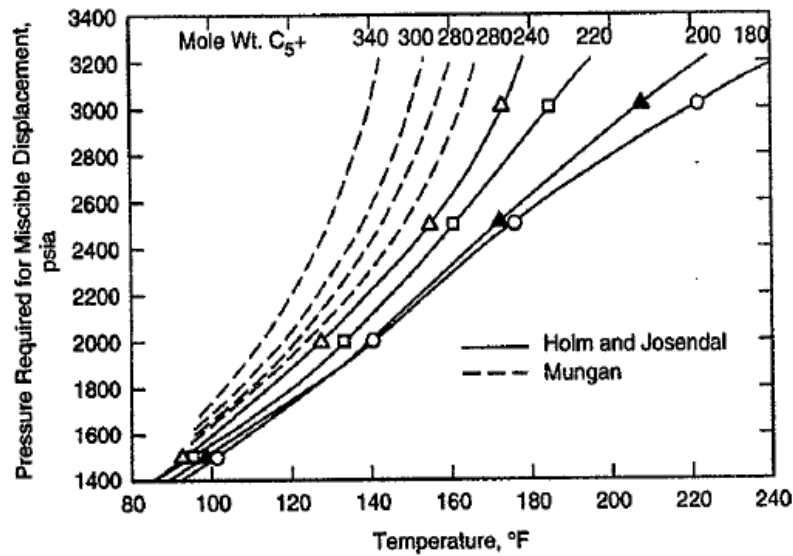
Figure 3.10 MMP of CO_2 considering C_{5+} molecular weight by Holm and Josendal with extended part by Mungan [13]

Even simpler, ones can estimate MMP of CO_2 from mathematical correlation. Many authors have published these equation correlations. Yuan et al. [18] gathered MMP correlation from previous literatures, for example, Yelig and Metcalfe [17] correlation is:

$$MMP_{pure} \text{ (psia)} = 1833.717 + 2.2518055T + 0.01800674T^2 - \frac{103949.9}{T} \quad (3.1)$$

where T is reservoir temperature in ^oF.

It is clear that this estimation of MMP is not accurate because reservoir fluid composition is not taken into account. The Glasø [19] correlation for pure CO_2 flooding, proposed a more accuracy and the correlation is defined as:

For C_2-C_6> 18%:

$$MMP_{pure}(\text{psia}) = 810 - 3.404\,M_{C_{7+}} + (1.700 \times 10^{-9}\,M_{C_{7+}}^{3.730}e^{786.8M_{c7+}^{-1.058}})T \quad (3.2)$$

For C_2-$C_6 < 18\%$:

$$\text{MMP}_{\text{pure}}(\text{psia}) = 2947.3 - 3.404\, M_{C_{7+}} + 1.700 \times 10^{-9} \times M_{C_{7+}}^{3.730} e^{7868 M_{c7+}^{-1.058}}\, T$$
$$- 121.2 F_R \qquad\qquad (3.3)$$

where

$M_{C_{7+}}$ = molecular weight of C_{7+} which equals to $\left(\dfrac{2.622}{\gamma_{o,C_{7+}}}\right)^{6.588}$,

F_R = mole percentage of C_{2-6} and T is temperature in $^{\circ}$F,

$\gamma_{o,C_{7+}}$ = specific gravity of stock-tank oil.

The Conquist correlation [20], using three input parameters, is given by

$$\text{MMP}_{\text{pure}}(\text{psia}) = 15.988\, T^{0.744206+0.0011038 M_{C5+}+0.0015279 C_1} \qquad\qquad (3.4)$$

where

$M_{C_{5+}}$ = molecular weight of pentane (C_5) plus heavier fraction,

C_1 = mole percentage of methane,

T = temperature in $^{\circ}$F.

Their own improved correlation is stately having higher accuracy than the most currently used correlation and is expressed as:

$$\text{MMP}_{\text{pure}}(\text{psia}) = a_1 + a_2\, M_{C_{7+}} + a_3\, P_{C_{2-6}} + (a_4 + a_5\, M_{C_{7+}} + a_6\, \frac{P_{C_{2-6}}}{M_{C_{7+}}^2})T + (a_7 + a_8\, M_{C_{7+}}$$
$$+ a_9\, M_{C_{7+}}^2 + a_{10}\, P_{C_{2-6}})T^2 \qquad\qquad (3.5)$$

where

a_1	=	-1.4634×10^3	a_2	=	0.6612×10^1
a_3	=	-4.4979×10^1	a_4	=	0.2139×10^1
a_5	=	1.1667×10^{-1}	a_6	=	8.1661×10^3
a_7	=	-1.2258×10^{-1}	a_8	=	1.2883×10^{-3}
a_9	=	-4.0152×10^{-6}	a_{10}	=	-9.2577×10^4

$M_{C_{7+}}$ is molecular weight of C7+, $P_{C_{2-6}}$ is the total mole fraction of $C_2 - C_6$, and T is reservoir temperature in ^{o}F.

3.4 Reservoir Heterogeneity

Most naturally-occurring porous and permeable media or reservoir rock are seldom homogeneous from the view of geological properties or rock characteristics e.g. permeability, porosity, thickness and saturation. Ideally, once reservoir is defined as homogeneous, its measured properties can be simply described at any location as its properties are non-location dependent. Reservoir heterogeneity is, then, defined as a variation in properties and most heterogeneity measurement focuses mainly on permeability because permeability changes have a larger influence than other properties. This property variation is considerably controlled by many situations, principally by chemical and physical changes, for example, depositional environment during sedimentation of sandstone, compaction and dolomitization of carbonate reservoir as well as plate tectonic or rock movements.

As a result of variation, reservoir heterogeneity has been broadly recognized as a significant factor affecting fluid displacement performance and influencing oil recovery efficiency as it illustrates distribution property of flood front when displacement is carried out.

Heterogeneous reservoir may be classified into three major types: (1) vertical variations, (2) areal variations, and (3) reservoir-scaled fractures [21]. Vertical permeability variations or vertical heterogeneity represents a stratified or layered formation. Permeability can be viewed differently in each strata and fluid flows in parallel directions. Areal variations are considered when permeability varies in lateral direction and these might be caused by existence of vugs or salt dome. The last category is non-pattern permeability such as fractures that can result in a tremendous thief zone.

3.5   Measures of Reservoir Heterogeneity

Heterogeneity of reservoir can be indicated as a quantitative term. This number characterizes how reservoirs scatter from uniformity or homogeneity. The zero degree of heterogeneity represents homogeneous reservoir, whereas a unity of value is found in fully heterogeneous reservoir. To quantify this value, some authors published techniques such as Schmalz and Rahme, Dykstra and Parson, and Warren and Price [22]. The most widely used, however, appears to be the coefficient introduced by Schmalz-Rahme, denoted as Lorenz coefficient (L_c), for vertical stratified formation due to its simplicity.

Suppose that reservoir consists of N layers and each layer has its own properties consisting of permeability (k_j), porosity (φ_j) and thickness (h_j). The first step to obtain Lorenz coefficient is to rearrange all layers in order, descending value of permeability. That means top layer possess the largest permeability layer assigned as k_1 has thickness of h_1 with porosity φ_1 and bottom layer has the smallest permeability assigned as k_N, thickness of h_N and porosity φ_N, accordingly. Two new parameters, including fraction of flow capacity (F_j) and fraction of total storage capacity (C_j), are introduced and given as:

$$F_j \quad = \quad \frac{\sum_{j=1}^{j=n} k_j h_j}{\sum_{j=1}^{j=N} k_j h_j} \tag{3.6},$$

and

$$C_j \quad = \quad \frac{\sum_{j=1}^{j=n} \phi_j h_j}{\sum_{j=1}^{j=N} \phi_j h_j} \tag{3.7}.$$

These two parameters are plotted on X and Y axis on Figure 3.11. The figure illustrates normalized flow capacity distribution. Diagonal straight line represents uniform system or homogeneous reservoir where permeability values are identical in all layers. As difference between values of permeability increases, the plot is more

concave towards upper left corner, indicating a more heterogeneity condition. Lorenz coefficient is defined as ratio of area between above and below diagonal straight line.

$$L_c \quad = \quad \frac{\text{Area above the straight line}}{\text{Area below the straight line}} \qquad (3.8)$$

The coefficient (L_c) can have value ranging from zero to unity; however, typical value is between 0.3-0.6 [23].
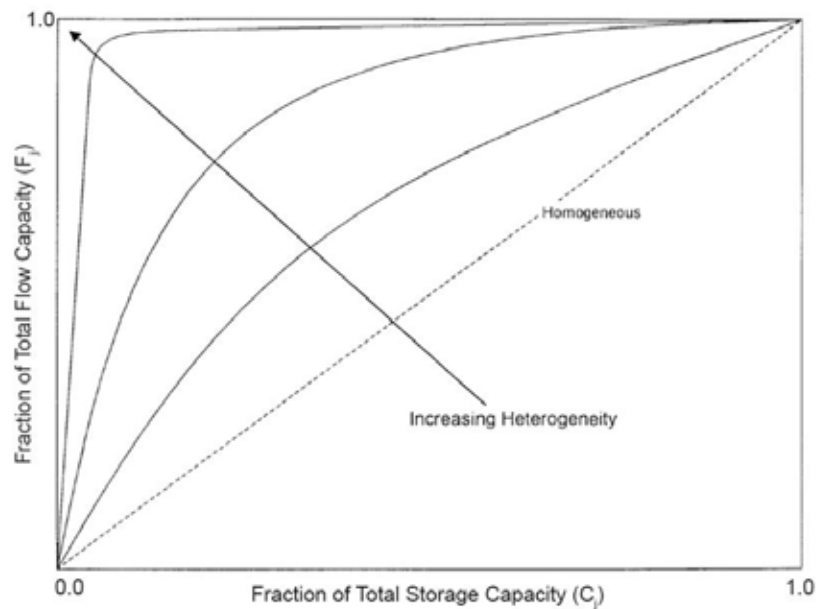
Figure 3.11 Normalized flow capacity distribution [24]

To estimate Lorenz coefficient, area above straight line or area under curve is required as in expression mentioned. This area estimate can be done by using trapezoidal rule or Simson's rule. However, another approach is also published by applying relationship between Lorenz Coefficient and Gini's coefficient of concentration [23].

$$\hat{L}_c \quad = \quad \frac{1}{2n} \frac{\sum_{i=1}^{i=n}\sum_{j=1}^{j=n}\left|k_i - k_j\right|}{\sum_{i=1}^{i=n} k_i} \qquad\qquad (3.9)$$

This expression is equivalent to method of area estimation but benefit of this method is that permeability ordering is not required. Although, value from this method shows negative bias for system having small sample size (n<40), high heterogeneity distributions, and gives under-estimated value of reservoir heterogeneity, it is reportedly more precise when compared with Dykstra-Parsons estimation [23].

3.6   Average Permeability Calculation

Regarding objectives of this work, heterogeneous models are developed with various degree of heterogeneity while average and median value of absolute permeability are still constant for all cases. Practical way to average absolute permeability is dependent upon how permeability is distributed. There are three commonly used techniques in averaging absolute permeability value including (1) weighted-average, (2) harmonic-average, and (3) geometric-average permeability [24]. However, in this work, only first two mentioned techniques are discussed.

3.6.1 Weighted-Average Permeability

In this case, flow through layered-parallel beds is considered and all layers have the same width (W) and length (L) as shown in Figure 3.12. Flow from layer j can be calculated by utilizing Darcy's equation as:

$$Q_j \quad = \quad \frac{k_j W h_j \Delta P}{\mu L} \qquad\qquad (3.10),$$

where $\qquad Q_j \qquad = \qquad$ flow rate through layer j,

K_j =   permeability of layer j,

W =   formation width,

H_j =   thickness of layer j,

ΔP =   pressure difference between inflow and outflow,

μ =   viscosity,

L =   formation length.
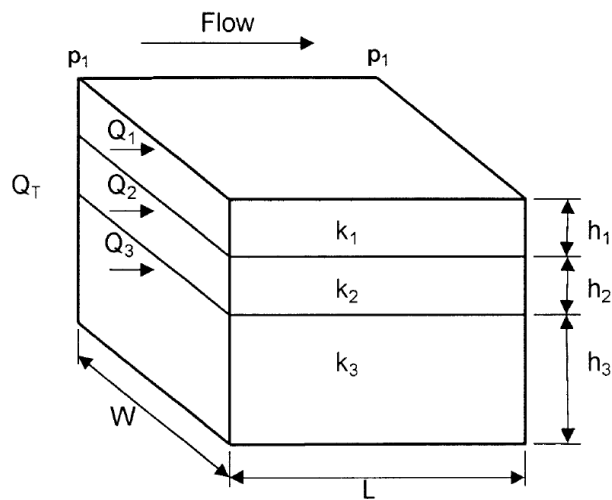
Figure 3.12 Flow through layered reservoir

The total flow rate (Q_t) from all layers can be expressed as:

$$Q_t = \frac{k_{avg} W h_t \Delta P}{\mu L} \qquad (3.11),$$

and the total flow rate also is equal to the sum of flow rate from all layers

$$Q_t = \sum_{j=1}^{n} Q_j = Q_1 + Q_2 + Q_3 \qquad (3.12),$$

combine the above terms, will get

$$\frac{k_{avg}Wh_t\Delta P}{\mu L} \quad = \quad \frac{k_1 Wh_1 \Delta P}{\mu L} + \frac{k_2 Wh_2 \Delta P}{\mu L} + \frac{k_3 Wh_3 \Delta P}{\mu L} \qquad (3.13),$$

or

$$k_{avg}h_t \quad = \quad k_1 h_1 + k_2 h_2 + k_3 h_3 \qquad (3.14),$$

$$k_{avg} \quad = \quad \frac{k_1 h_1 + k_2 h_2 + k_3 h_3}{h_t} \qquad (3.15).$$

Therefore, average permeability of layered-parallel reservoir can be expressed in the form:

$$k_{avg} \quad = \quad \frac{\displaystyle\sum_{j=1}^{n} k_j h_j}{\displaystyle\sum_{j=1}^{n} h_j} \qquad (3.16).$$

3.6.2 Harmonic-Average Permeability

Permeability variation can be occurred in lateral form which is shown in Figure 13. Fluid flows through a series of beds with different permeability and it is assumed that total pressure drop is equal to the combined pressure drop in each section.
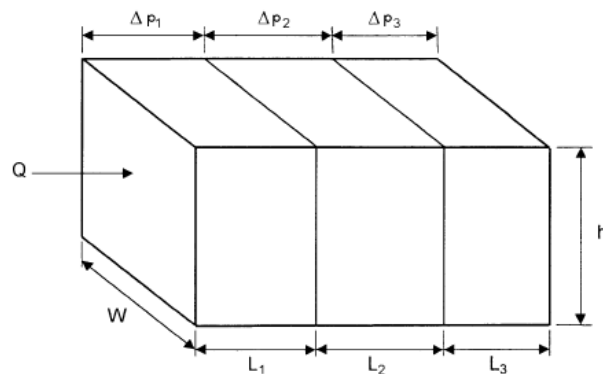
Figure 3.13 Flow through a series of bed with different permeability

$$\Delta p_t \quad = \quad \Delta p_1 + \Delta p_2 + \Delta p_3 \qquad (3.17).$$

Darcy's law is applied for the above equation and gives;

$$\frac{Q\mu L}{Ak_{avg}} \quad = \quad \frac{Q\mu L_1}{Ak_1} + \frac{Q\mu L_2}{Ak_2} + \frac{Q\mu L_3}{Ak_3} \qquad (3.18).$$

Cancel Q and μ which have equal value along the beds, then, average permeability is

$$k_{avg} \quad = \quad \frac{L}{\left(\dfrac{L}{k}\right)_1 + \left(\dfrac{L}{k}\right)_2 + \left(\dfrac{L}{k}\right)_3} \qquad (3.19).$$

Therefore, it can be expressed as

$$k_{avg} \quad = \quad \frac{\displaystyle\sum_{i=1}^{n} L_i}{\displaystyle\sum_{i=1}^{n} \left(\dfrac{L}{k}\right)_i} \qquad (3.20),$$

where L_i =   length of each bed,

               k_i =   absolute permeability of each bed.

3.7   Viscosity Calculation

A reduction on oil viscosity is one of the mechanisms encountered when CO_2 vaporizes some light to intermediate hydrocarbons from original reservoir oil during miscibility mechanism. In compositional ECLIPSE simulator, the default method used to evaluate value of crude oil-gas mixture viscosity is The Lorentz-Bray-Clark correlation [25]. It is widely used due to availability of required data. Following is the given estimation of liquid mixture viscosity [26].

$$[\mu - \mu^*)\varsigma + 10^{-4}]^{1/4} \quad = \quad 0.1023 + 0.023364\rho_r + 0.058533\rho_r^2 -$$

$$0.040758\rho_r^3 + 0.0093324\rho_r^4 \qquad (3.21)$$

Where

$$\mu^* \quad = \quad \frac{\sum\limits_{i=1}^{n} x_i \mu_i^* M_i^{1/2}}{\sum\limits_{i=1}^{n} x_i M_i^{1/2}} \qquad (3.22)$$

$$\varsigma \quad = \quad \frac{\left(\sum\limits_{i=1}^{n} x_i T_{c_i}\right)^{1/8}}{\left(\sum\limits_{i=1}^{n} x_i M_i\right)^{1/2}\left(\sum\limits_{i=1}^{n} x_i P_{c_i}\right)^{2/3}} \qquad (3.23)$$

x_i = mole fraction of component i

m_i = molecular weight of component i

T_{ci} = absolute critical temperature of component i

P_{ci} = critical pressure of component i

μ_i^* = low-pressure gas viscosity of component i

The low-pressure gas viscosity of component i is given by

$$\mu_i^* \varsigma_i \quad = \quad \begin{cases} 34.0 \times 10^{-5} T_{r_i}^{0.94} & T_{r_i} < 1.5 \\ 17.78 \times 10^{-5}(4.58 T_{r_i} - 1.67)^{5/8}, & T_{r_i} > 1.5 \end{cases} \qquad (3.24)$$

Where

$$T_{r_i} \quad = \quad \frac{T}{T_{c_i}} \qquad (3.25)$$

and

$$\varsigma_i \quad = \quad \frac{T_{c_i}^{1/6}}{M_i^{1/2} P_{c_i}^{2/3}} \qquad (3.26)$$

The pseudo-critical mixture density is calculated from

$$\rho_c^{'} \quad = \quad \frac{1}{V_{c_i}^{'}} \tag{3.27}$$

$$V_c^{'} \quad = \quad \sum_{i=1}^{n} V_{c_i} + x_{C_{7+}} V_{c_{C_{7+}}} \tag{3.28}$$

Where

V_{ci} =   critical molar volume of component i

$V_{c_{C_{7+}}}$ =   pseudo-critical molar volume of the C7+ fraction

Lohrenz et al. [27] published a correlation to approximate the C7+ pseudo-critical molar volume as follows:

$$V_{c_{C_{7+}}} \quad = \quad 21.573 + 0.015122 M_{C7+} - 27.656 \gamma_{C7+}$$

$$+ 0.070615 \, M_{C7+} \gamma_{C7+} \tag{3.29}$$

Where

γ_{C7+} =   specific gravity of C7+ fraction

M_{C7+} =   average molecular weight of C7+ fraction

The reduced mixture density in then obtained from

$$\rho_r \quad = \quad \frac{\rho}{\rho_c^{'}}$$

Where

ρ =   mixture density

CHAPTER IV

RESERVOIR SIMULATION MODEL

Reservoir models are constructed by using reservoir simulator to evaluate both reservoir and operational parameters, specified to meet the objectives of this study. Furthermore, these constructed models are utilized to determine performance of CO_2 miscible injection in reservoir containing heterogeneity that would give a guideline for any field intended to perform CO_2 flooding. Detail of constructed model is described in the following sections of this chapter and simulation. The models are developed by exploiting compositional oil reservoir simulator **ECLIPSE®300** as fluid composition is dynamically changed during displacement mechanism and oil recovery process.

4.1 Grid Section

For an initial base case model, homogeneous reservoir is modeled to compose of ten layers in which properties are kept constant. Employed grid type is Cartesian coordinate with block centered geometry and reservoir dimension is 840×5,000×200 ft in the *x*-, *y*- and *z*- direction, respectively. However, for further study cases after optimization section, heterogeneous reservoir is developed by means of varying absolute permeability in horizontal direction in each layer in a range between 20 to 300 mD. Each heterogeneous model is quantified by reservoir heterogeneity index. Lorenz coefficient (L_c) is calculated to represent heterogeneous index in this study. In addition, the approach used to express heterogeneity index is to keep all reservoir models with average and median permeability of 150 mD. The top of reservoir is located at depth of 5,000 ft. Porosity is constant at 20 percent as this is typical value for sandstone reservoir. Additional properties of reservoir model in this study are summarized in Table 4.1. Figures 4.1, 4.2 and 4.3 illustrate top, side and three dimension views of base case reservoir model and Figure 4.4 shows heterogeneity of reservoir models as variation of absolute permeability in both fining upward and coarsening upward sequences.

Table 4.1 Summary of reservoir properties

Parameter	Value	Unit
Grid dimension	21×50×40	Block
Grid size	40×100×5	ft
Effective porosity	20	%
Horizontal permeability	Varied in each layer (ranging from 20-300)	mD
Vertical permeability	0.1 k_h	mD
Average permeability	150	mD
Top of reservoir	5,000	ft
Reservoir thickness	200	ft
Initial water saturation	28	%
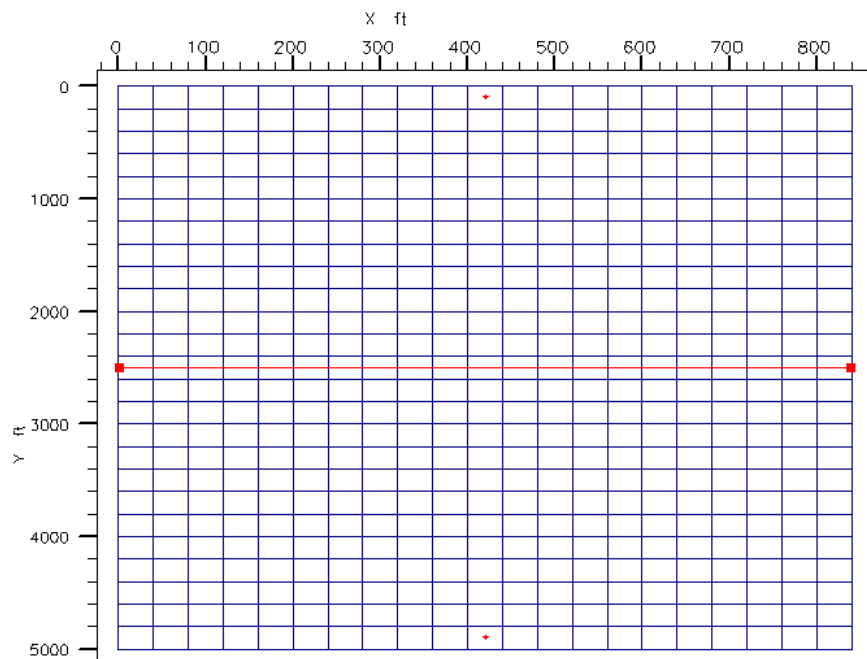
Figure 4.1 Top view of base case reservoir model
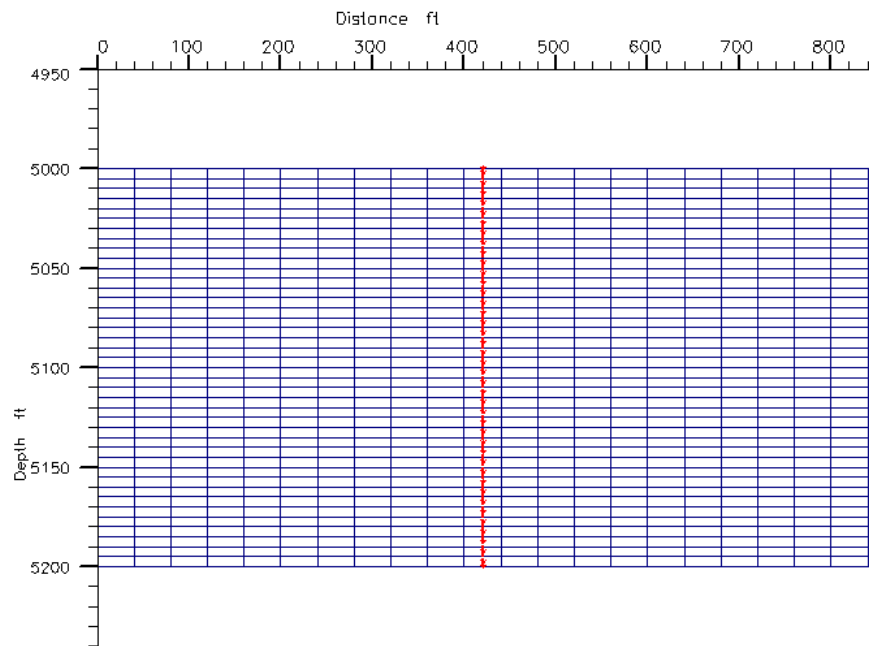
Figure 4.2 Side view of base case reservoir model
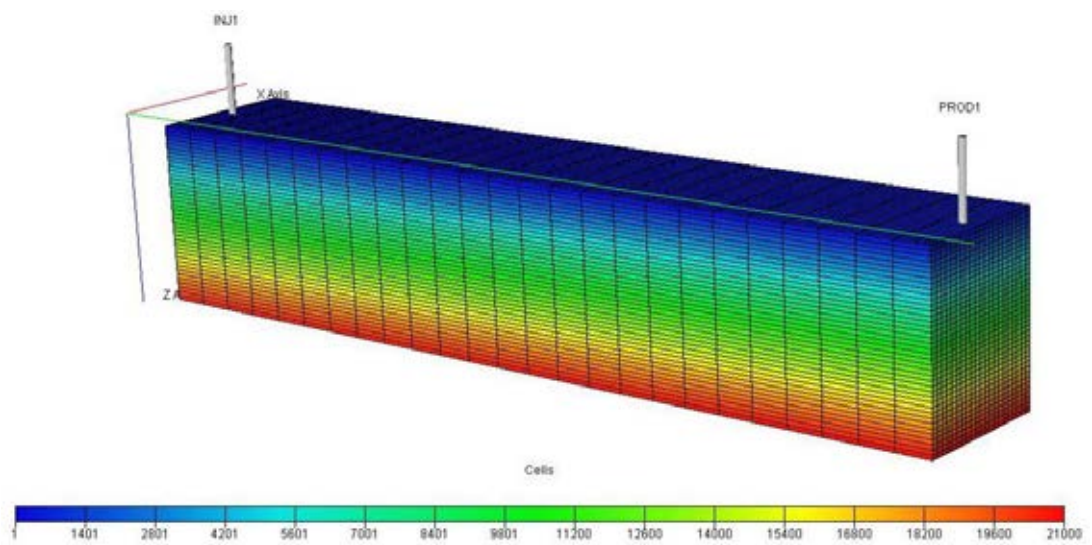
Figure 4.3 Three dimension view of base case reservoir model illustrated in color

scale ranging by number of cell
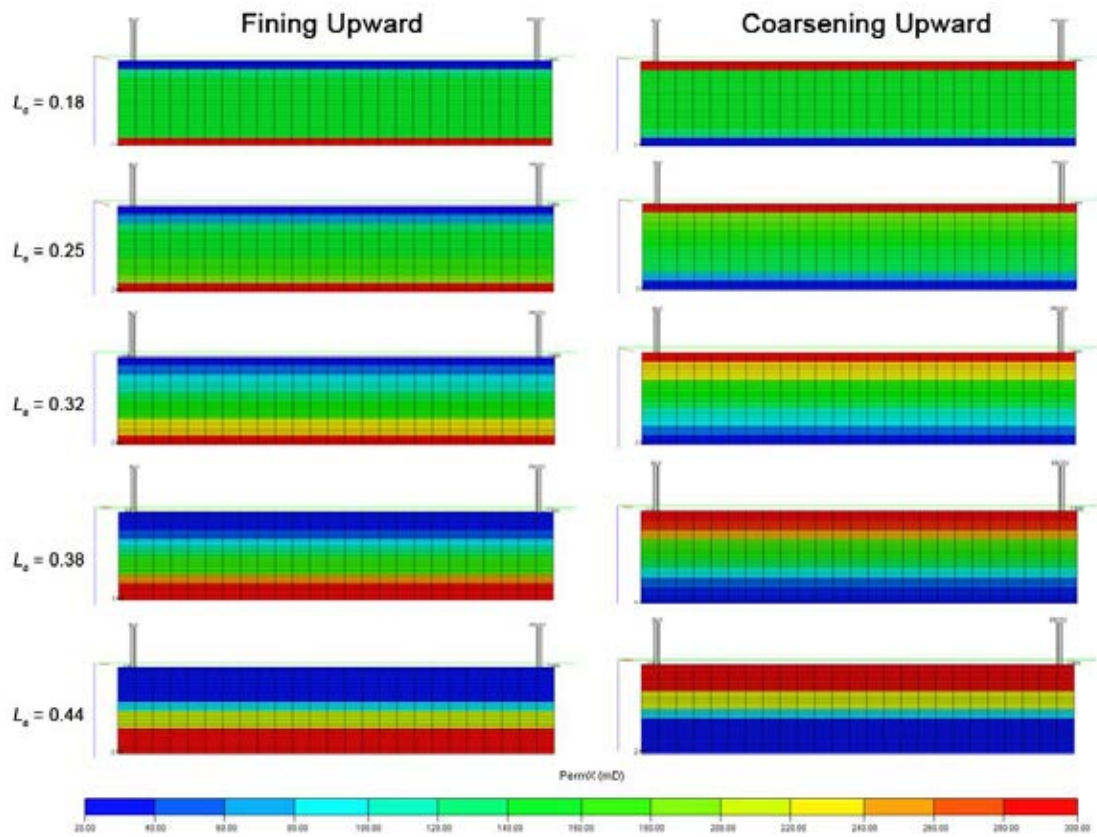
Figure 4.4 Reservoir models containing heterogeneity with different value of Lorenz coefficient (L_c) illustrated by horizontal permeability scale

In study cases where reservoir inclination is involved, corner point geometry is applied in order to attain models with required inclination degree. Reservoir thickness, length and datum depth remain equal, even though reservoir dip angle is changed. Figure 4.5 shows reservoir model with different dip angles which are 15°, 30° and 45°.
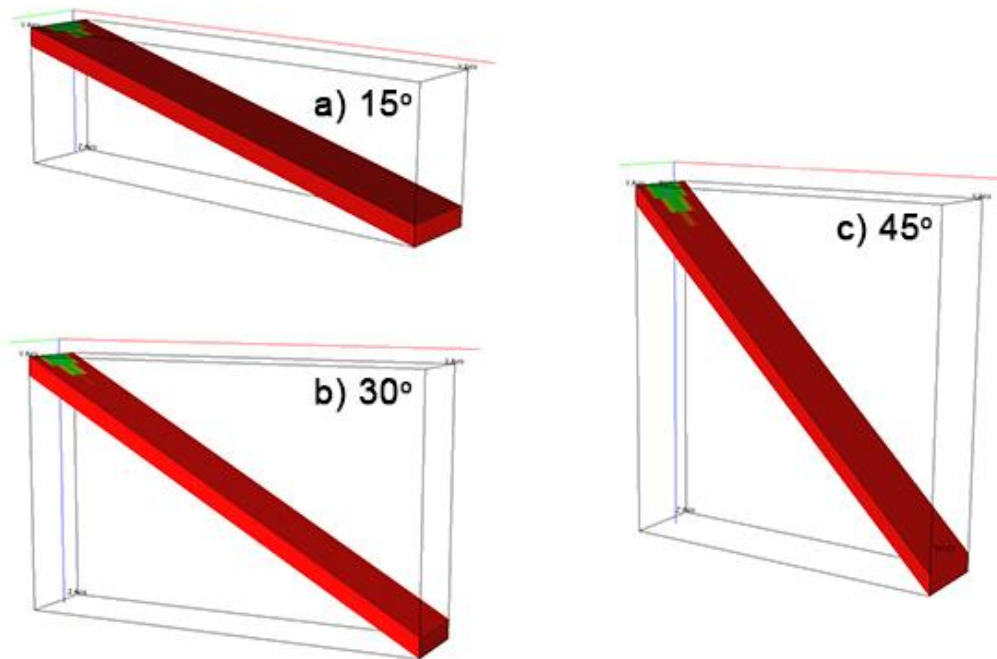
Figure 4.5 Reservoir models with different dip angles

4.2 Fluid Property Section

Parameters related to initial fluid condition such as datum depth, datum depth pressure and Oil-Water Contact (OWC) are defined inside Equilibration Data Specification (EQUIL) in INITIALIZATION section in the ECLIPSE software. Initial reservoir fluid composition applied in this study is shown in Table 4.2 and injected fluid is purified CO_2. Equation of state used in this study is Peng-Robinson.

Table 4.2 Initial composition of reservoir fluid

Component		Mole fraction (%)
Carbon dioxide	CO_2	0.91
Nitrogen	N_2	0.06
Methane	C_1	33.83
Ethane	C_2	9.04
Propane	C_3	7.99
iso-Butane	$i\text{-}C_4$	1.97
normal-Butane	$n\text{-}C_4$	4.69
iso-Pentane	$i\text{-}C_5$	3.6
normal-Pentane	$n\text{-}C_5$	1.78
Hexane	C_6	5.01
Heptane plus	C_{7+}	31.12
Specific gravity of C_{7+}		0.8615
Molecular weight of C_{7+}		267

Physical properties of each component as well as binary interaction coefficient can be found from PVTi, the add-on software of ECLIPSE®300. Properties of fluid components are summarized in Table 4.3a and 4.3b and binary interaction coefficients are listed in Table 4.4.

Table 4.3a Physical properties of components in reservoir fluid

Component	Boiling point (°R)	Critical pressure (psia)	Critical temp. (°R)	Critical volume (ft³/lb-mole)	Molecular weight
CO_2	350.46	1071.33	548.46	1.5057	44.01
N_2	139.32	492.31	227.16	1.4417	28.01
C_1	200.88	667.78	343.08	1.5698	16.04
C_2	332.28	708.34	549.77	2.3707	30.07
C_3	415.98	615.76	665.64	3.2037	44.10
$i\text{-}C_4$	470.34	529.05	734.58	4.2129	58.12
$n\text{-}C_4$	490.86	550.66	765.36	4.0847	58.12
$i\text{-}C_5$	541.80	491.58	828.72	4.9337	72.15
$n\text{-}C_5$	556.56	488.79	845.28	4.9817	72.15
C_6	606.69	436.62	913.50	5.6225	84.00
C_{7+}	1345.20	124.23	1597.00	24.1208	267.00

Table 4.3b Physical properties of component (continued)

Component	Acentric factor	Critical Z-factor	Component Parachor	EOS volume shift
CO_2	0.225	0.2741	78.0	-0.0427
N_2	0.040	0.2912	41.0	-0.1313
C_1	0.013	0.2847	77.0	-0.1443
C_2	0.099	0.2846	108.0	-0.1033
C_3	0.152	0.2762	150.3	-0.0775
$i\text{-}C_4$	0.185	0.2827	181.5	-0.0620
$n\text{-}C_4$	0.201	0.2739	189.9	-0.0542
$i\text{-}C_5$	0.227	0.2727	225.0	-0.0418
$n\text{-}C_5$	0.251	0.2684	231.5	-0.0303
C_6	0.299	0.2504	271.0	-0.0073
C_{7+}	1.184	0.1755	965.2	0.2396

Table 4.4 Binary interaction coefficients between components

	CO_2	N_2	C_1	C_2	C_3	i-C4	$n-C_4$	$i-C_5$	$n-C_5$	C_6	C_{7+}
CO_2	0	-0.012	0.1	0.1	0.1	0.1	0.1	0.1	0.1	0.1	0.1
N_2	-0.012	0	0.1	0.1	0.1	0.1	0.1	0.1	0.1	0.1	0.1
C_1	0.1	0.1	0	0	0	0	0	0	0	0.0279	0.0526
C_2	0.1	0.1	0	0	0	0	0	0	0	0.01	0.01
C_3	0.1	0.1	0	0	0	0	0	0	0	0.01	0.01
$i-C_4$	0.1	0.1	0	0	0	0	0	0	0	0	0
$n-C_4$	0.1	0.1	0	0	0	0	0	0	0	0	0
$i-C_5$	0.1	0.1	0	0	0	0	0	0	0	0	0
$n-C_5$	0.1	0.1	0	0	0	0	0	0	0	0	0
C_6	0.1	0.1	0.0279	0.01	0.01	0	0	0	0	0	0
C_{7+}	0.1	0.1	0.0526	0.01	0.01	0	0	0	0	0	0

In this study, reservoir temperature is assumed to be constant at $172^{o}F$ and initial reservoir pressure is 2,512 psia. Bubble point pressure is 2,375 psia which creates initial condition as an undersaturated reservoir.

4.3 SCAL (Special Core Analysis) Section

In this section, two sets of relative permeability data, which are oil-water relative permeability curves and oil-gas relative permeability curves, are required. The curves are generated with default Corey's exponents together with end-point data. Relationship between fluid saturation and relative permeability in oil-water and oil-gas systems are tabulated in Tables 4.5 and 4.6, respectively. Consecutively, tabulated data are plotted as functions of fluid saturation and illustrated in Figures 4.6 and 4.7. The constructed reservoir model is considered as a water-wet system and asreservoir temperature is constant, rock expansion is neglected. Besides, no capillary pressure is applied in this study.

Table 4.5 Relative permeability to water and oil as a function of water saturation

No.	S_w	k_{rw}	k_{ro}
1	0.28	0.0000	0.4100
2	0.31	0.0000	0.3378
3	0.34	0.0000	0.2747
4	0.37	0.0002	0.2199
5	0.40	0.0005	0.1730
6	0.43	0.0012	0.1332
7	0.46	0.0026	0.1001
8	0.49	0.0048	0.0730
9	0.52	0.0081	0.0513
10	0.55	0.0130	0.0343
11	0.58	0.0198	0.0216
12	0.61	0.0290	0.0125
13	0.64	0.0411	0.0064
14	0.67	0.0567	0.0027
15	0.7	0.0762	0.0008
16	0.73	0.1004	0.0001
17	0.76	0.1300	0.0000
18	1.00	1.0000	0.0000

Table 4.6 Relative permeability to gas and oil as a function of gas saturation

No.	S_g	k_{rg}	k_{ro}
1	0	0.0000	0.4100
2	0.15	0.0000	0.1786
3	0.18	0.0002	0.1452
4	0.21	0.0014	0.1163
5	0.24	0.0048	0.0914
6	0.28	0.0114	0.0704
7	0.31	0.0222	0.0529
8	0.34	0.0384	0.0386
9	0.37	0.0610	0.0271
10	0.40	0.0910	0.0182
11	0.43	0.1296	0.0114
12	0.46	0.1778	0.0066
13	0.49	0.2366	0.0034
14	0.53	0.3072	0.0014
15	0.56	0.3906	0.0004
16	0.59	0.4878	0.0001
17	0.62	0.6000	0.0000
18	0.72	1.0000	0.0000

Figure 4.6 Relative permeability to water and oil as a function of water saturation
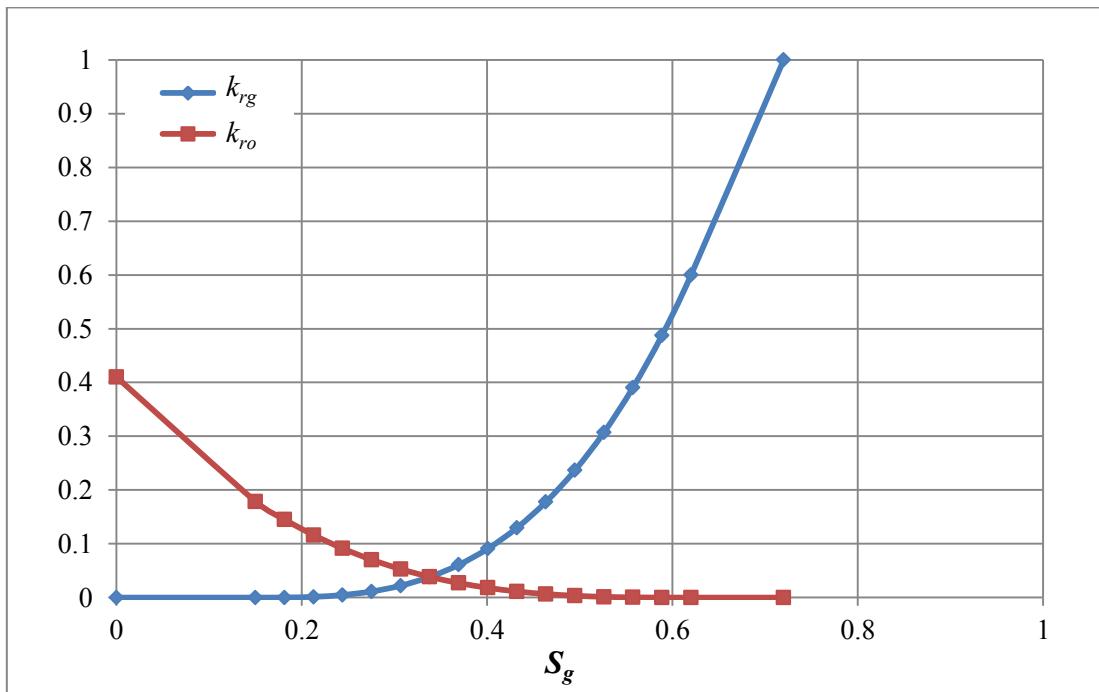
Figure 4.7 Relative permeability to gas and oil as a function of gas saturation

4.4 Schedule Section

Specification and location of both injection and production wells and also production schedule are set up and described in this section. These two wells appear to have equal in size of conventional 8-1/2 inch wellbore diameter for oil reservoir and located at the middle of reservoir according to *x*-axis, opposite to each other, as illustrated in Figure 4.8. This draws the distance between these two well at 5,000 ft. They are totally perforated at full reservoir thickness as no presence of fluid contact is assumed.

In this study, a flooding sequence is divided into three steps of injection. Firstly, water is injected, and secondly a slug of CO_2 is followed. Chasing water is injected until production is terminated. Constraints of injection well and production well are listed in Table 4.7 and 4.8, respectively.
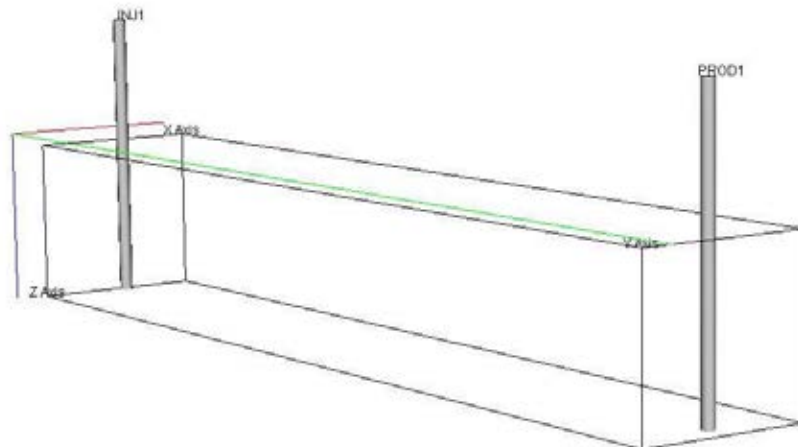
Figure 4.8 Location of injection well and production well

Table 4.7 Production well specification and constraints

Parameter	Value	Unit
Location	I = 11, J = 25	block
Perforation (Base case)	K=1-40	block
Maximum oil production rate	2,000	STB/day
Cut-off oil production rate	100	STB/day
Maximum well water cut	95	percent
Minimum bottom hole pressure	400	psia
Maximum gas production rate	8	MMSCFD

Table 4.8 Injection well specification and constraints

Parameter	Value	Unit
Location	I = 11, J = 1	block
Perforation (Base case)	K=1-40	block
1st step and 3rd step – water injection		
Maximum water injection rate	3,000	STB/day
Maximum bottom hole pressure	3,800	psia
2nd step – CO_2 injection		
Maximum CO_2 injection rate (Base case)	8	MMSCFD
Maximum bottom hole pressure	3,800	psia

4.5   Reservoir Heterogeneity Construction

Heterogeneity of reservoir models is quantified by Lorenz coefficient (L_c) proposed by Schmalz-Rahme [22]. Even though, obtaining the coefficient can be done by applying the simple mathematical relationship between Lorenz coefficient and Gini's coefficient of concentration [23], the relationship is more suitable to be applied with system having a number of samples (permeability) higher than 40, and also when the variation shows a significant contrast. Therefore, the original method of plotting curve and calculating area under curve should be able to provide more accuracy as the study system consist only ten layers with a directional variation of permeability. The plot which is described in section 3.5, called flow capacity distribution is to be used to

get heterogeneity indexes. Two parameters including fraction of flow capacity (F_j) and fraction of total storage capacity (C_j) are involved referring to equation 3.6 and 3.7.

$$F_j \quad = \quad \frac{\sum_{j=1}^{j=n} k_j h_j}{\sum_{j=1}^{j=N} k_j h_j} \tag{4.1},$$

and

$$C_j \quad = \quad \frac{\sum_{j=1}^{j=n} \phi_j h_j}{\sum_{j=1}^{j=N} \phi_j h_j} \tag{4.2}.$$

Due to the lack of actual information of permeability, permeability is then presumed, ranging between 20 to 300 mD, as a minimum-maximum boundary, within its 10 layers of formation. Estimated heterogeneity indexes keep the average value of permeability data set at 150 mD and median of permeability data set is kept at 150 mD as well. Tables 4.9 to 4.14 summarize permeability value employed in each layer of reservoir and the sequence has to be arranged in descending order of permeability value. Moreover, the value shown in the following tables can be implied as a coarsening upward sequence as well.

Table 4.9 Permeability data for each layer of model and flow capacity distribution calculation for the case applying heterogeneity index of 0 ($L_c = 0$)

Layer	k (mD)	h (ft)	kh	ϕh	Σkh	$\Sigma \phi h$	C_j (X)	F_j (Y)
							0.0	0.0
1	150	20	3,000	4	3,000	4	0.1	0.1
2	150	20	3,000	4	6,000	8	0.2	0.2
3	150	20	3,000	4	9,000	12	0.3	0.3
4	150	20	3,000	4	12,000	16	0.4	0.4
5	150	20	3,000	4	15,000	20	0.5	0.5
6	150	20	3,000	4	18,000	24	0.6	0.6
7	150	20	3,000	4	21,000	28	0.7	0.7
8	150	20	3,000	4	24,000	32	0.8	0.8
9	150	20	3,000	4	27,000	36	0.9	0.9
10	150	20	3,000	4	30,000	40	1.0	1.0
k_{avg}	150	Sum	30,000	40				

Table 4.10 Permeability data for each layer of model and flow capacity distribution calculation for the case applying heterogeneity index of 0.18 ($L_c = 0.18$)

Layer	k (mD)	h (ft)	kh	ϕh	Σkh	$\Sigma \phi h$	C_j (X)	F_j (Y)
							0.0	0.000
1	300	20	6,000	4	6,000	4	0.1	0.200
2	150	20	3,000	4	9,000	8	0.2	0.300
3	150	20	3,000	4	12,000	12	0.3	0.400
4	150	20	3,000	4	15,000	16	0.4	0.500
5	150	20	3,000	4	18,000	20	0.5	0.600
6	150	20	3,000	4	21,000	24	0.6	0.700
7	150	20	3,000	4	24,000	28	0.7	0.800
8	150	20	3,000	4	27,000	32	0.8	0.900
9	130	20	2,600	4	29,600	36	0.9	0.987
10	20	20	400	4	30,000	40	1.0	1.000
k_{avg}	150	Sum	30,000	40				

Table 4.11 Permeability data for each layer of model and flow capacity distribution calculation for the case applying heterogeneity index of 0.25 ($L_c = 0.25$)

Layer	k (mD)	h (ft)	kh	ϕh	Σkh	$\Sigma\phi h$	C_j (X)	F_j (Y)
							0.0	0.000
1	300	20	6,000	4	6,000	4	0.1	0.200
2	190	20	3,800	4	9,800	8	0.2	0.327
3	180	20	3,600	4	13,400	12	0.3	0.447
4	165	20	3,300	4	16,700	16	0.4	0.557
5	155	20	3,100	4	19,800	20	0.5	0.660
6	145	20	2,900	4	22,700	24	0.6	0.757
7	140	20	2,800	4	25,500	28	0.7	0.850
8	135	20	2,700	4	28,200	32	0.8	0.940
9	70	20	1,400	4	29,600	36	0.9	0.987
10	20	20	400	4	30,000	40	1.0	1.000
k_{avg}	150	**Sum**	30,000	40				

Table 4.12 Permeability data for each layer of model and flow capacity distribution calculation for the case applying heterogeneity index of 0.32 ($L_c = 0.32$)

Layer	k (mD)	h (ft)	kh	ϕh	Σkh	$\Sigma\phi h$	C_j (X)	F_j (Y)
							0.0	0.000
1	300	20	6,000	4	6,000	4	0.1	0.200
2	240	20	4,800	4	10,800	8	0.2	0.360
3	230	20	4,600	4	15,400	12	0.3	0.513
4	165	20	3,300	4	18,700	16	0.4	0.623
5	160	20	3,200	4	21,900	20	0.5	0.730
6	140	20	2,800	4	24,700	24	0.6	0.823
7	105	20	2,100	4	26,800	28	0.7	0.893
8	90	20	1,800	4	28,600	32	0.8	0.953
9	50	20	1,000	4	29,600	36	0.9	0.987
10	20	20	400	4	30,000	40	1.0	1.000
k_{avg}	150	**Sum**	30,000	40				

Table 4.13 Permeability data for each layer of model and flow capacity distribution
calculation for the case applying heterogeneity index of 0.38 ($L_c = 0.38$)

Layer	k (mD)	h (ft)	kh	ϕh	Σkh	$\Sigma \phi h$	$C_j (X)$	$F_j (Y)$
							0.0	0.000
1	300	20	6,000	4	6,000	4	0.1	0.200
2	290	20	5,800	4	11,800	8	0.2	0.393
3	250	20	5,000	4	16,800	12	0.3	0.560
4	175	20	3,500	4	20,300	16	0.4	0.677
5	165	20	3,300	4	23,600	20	0.5	0.787
6	135	20	2,700	4	26,300	24	0.6	0.877
7	95	20	1,900	4	28,200	28	0.7	0.940
8	45	20	900	4	29,100	32	0.8	0.970
9	25	20	500	4	29,600	36	0.9	0.987
10	20	20	400	4	30,000	40	1.0	1.000
k_{avg}	150	**Sum**	30,000	40				

Table 4.14 Permeability data for each layer of model and flow capacity distribution
calculation for the case applying heterogeneity index of 0.44 ($L_c = 0.44$)

Layer	k (mD)	h (ft)	kh	ϕh	Σkh	$\Sigma \phi h$	$C_j (X)$	$F_j (Y)$
							0.0	0.000
1	300.0	20	6,000	4	6,000	4	0.1	0.200
2	299.9	20	5,998	4	11,998	8	0.2	0.400
3	299.8	20	5,996	4	17,994	12	0.3	0.600
4	219.7	20	4,394	4	22,388	16	0.4	0.746
5	218.0	20	4,360	4	26,748	20	0.5	0.892
6	82.0	20	1,640	4	28,388	24	0.6	0.946
7	20.3	20	406	4	28,794	28	0.7	0.960
8	20.2	20	404	4	29,198	32	0.8	0.973
9	20.1	20	402	4	29,600	36	0.9	0.987
10	20.0	20	400	4	30,000	40	1.0	1.000
k_{avg}	150	**Sum**	30,000	40				

As stated earlier, parameters C_j and F_j are inserted into x and y axis respectively. The distribution of permeability can be made up to five different Lorenz coefficients entailing the number of 0.18, 0.25, 0.32, 0.38 and 0.44, respectively. The number is calculated from the ratio between area above straight line and under straight line, in which straight line ($L_c = 0$) implies characteristic of homogeneous reservoir model. Additionally, trapezoidal rule is applied for an approximation of area under the curve. Complete plot between C_j and F_j is also shown in Figure 4.9.
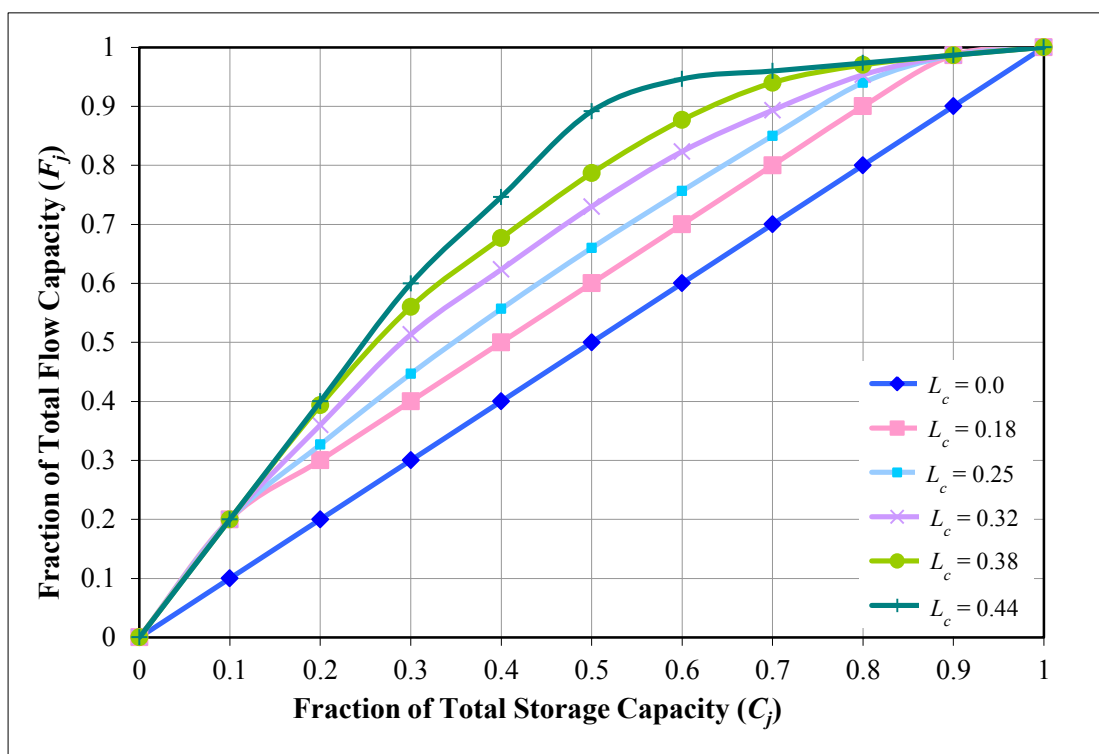
Figure 4.9 Flow capacity distributions of all study cases

4.6 Thesis Methodology

Thesis is divided into three main parts including an optimization of CO_2 miscible flooding in homogeneous reservoir base case, a comparison of water flooding case and CO_2 base case and an investigation of both controllable and uncontrollable parameters. These major parts can be described in details as following steps and schematically summarized in Figure 4.10.

1. Develop a base case homogeneous reservoir model without reservoir dip angle. A CO_2 flooding sequence consists of pre-flushed water slug, CO_2 slug, and then chasing water slug. Determining of optimum pre-flushed water slug size includes 0.05, 0.1, 0.15, 0.2 and 0.25 PV, whereas CO_2 slug size remains constant for all cases at recommended 0.4 Hydrocarbon Pore Volume (HCPV). Pre-flushed water slug aims to sweep movable oil from reservoir. Outcome from this optimization is kept as a base case model for comparison with other study parameters.

2. Construct heterogeneous reservoir models to represent fining upward lithofacies having absolute permeability in order from the smallest permeability on top to the highest permeability at bottom. Constructed models are prepared to have Lorenz coefficient (L_c), used to determine heterogeneity degree in this study. The values of this coefficient comprise of 0.18, 0.25, 0.32, 0.38 and 0.44.

3. Simulate heterogeneous models (all heterogeneous values) with different reservoir dip angles, ranging from 0°, 15°, 30° and 45°.

4. Repeat simulation per step 2 and 3 by replacing fining upward lithofacies with coarsening upward lithofacies. Absolute permeability in each layer is therefore in order from the highest permeability on top to the smallest permeability at bottom.

5. Simulate heterogeneous models with operational parameters by repeating step 2 to 4, starting with CO_2 injection rate. The additional rates to be varied cover 6, 10, 12 and 14 MMSCFD (injection rate used in previous steps is fixed at 8 MMSCFD).

6. Simulate variation of CO_2 injection perforation interval by reducing its length to 75% and 50% of total injection interval. Reduced injection zone is located away from high permeability streak zone in order to avoid gas channeling effect.

7. Compare and discuss results using oil recovery factor as a major criterion. The CO_2 flooding performance is also judged by accompaniment simulation outcomes which are oil production rate, water production rate, water cut, CO_2 injection rate and reservoir pressure. Judging parameters are plotted as a function of heterogeneity index.

8. Summarize results of each parameter as appropriate value to be applied for CO_2 miscible flooding in the multi-layered heterogeneous reservoir.
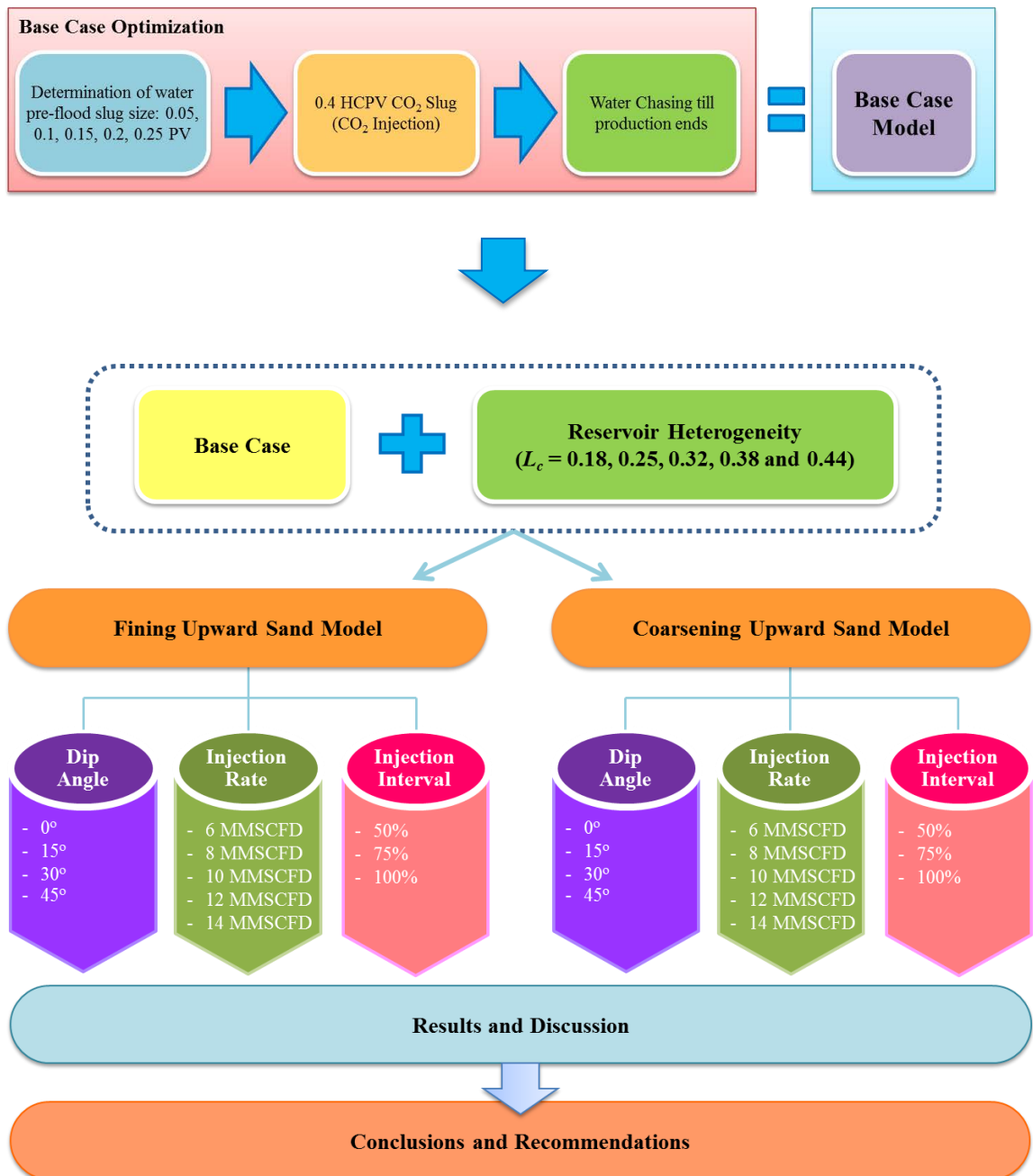
Figure 4.10 Schematic diagram of thesis methodology

CHAPTER V

RESULTS AND DISCUSSION

This chapter discusses results obtained from models executed using compositional reservoir simulator ECLIPSE®300 by following details in Chapter 4 and based on 30 years of production period as per a given concessionaire period.

Sequence of discussion will start from optimization of CO_2 miscible flooding base case in homogeneous reservoir, which is applied with pre-flushing water and also chasing water. Hence, determination of optimal slug size of pre-flushed water will be discussed in order to obtain base case for further study. Then, in a comparison purpose, waterflooding case will also be shown to emphasize the result that base case shows a better performance than only waterflooding. Finally, each study parameter will be applied into heterogeneous models and their effects will be discussed. Summary list below indicates cases and parameters in accordance with objectives for this study:

1. Optimization for CO_2 miscible flooding base case
2. Waterflood case
3. Effect of reservoir dip angle
4. Effect of CO_2 injection rate
5. Effect of CO_2 injection interval

5.1 Optimization for CO_2 Miscible Flooding Base Case

5.1.1 Determination of Pre-Flushed Water Slug Size

The model in this part is considered to attain CO_2 miscible flooding base case. Proposed package of CO_2 miscible flooding scheme in this study includes initial water pre-flushing aiming at displacing moveable hydrocarbon from reservoir because water is abundant as well as it is considered as a lower cost medium compared to CO_2. Hence, this optimization emphasizes on determining slug size of pre-flushed water.

Reservoir model is, thereafter, flooded by injected CO_2 equal to 0.4 Hydrocarbon Pore Volume (HCPV) in order to create in-situ miscible bank. Number of hydrocarbon pore volume used in this study is obtained from recommendation of National Petroleum Council for CO_2 flooding in U.S. oil fields chosen as a practical value to avoid gas preceded production. Calculate amount of injected CO_2 is therefore equivalent to 8.62 million reservoir barrel (MMRB) and is considered as a chosen slug size when alternating injection between water and CO_2 [14]. Reservoir is lastly chased with water again to sweep created miscible bank ahead, displacing residual hydrocarbon.

Reservoir pressure is also a concerned parameter as occurrence of miscible bank requires it to be above Minimum Miscibility Pressure (MMP). According to four published formulations mentioned in Section 3.3, MMP is averagely calculated based on reservoir and fluid properties and the predicted MMP is found to be 3,067 psia.

Homogeneous reservoir model is used for identifying optimal slug size of pre-flushed water (zero heterogeneity index, L_c =0), consisting one injection well and one production well located at center on each side of reservoir, opposite to each other. Production well is set to produce oil at 2,000 STB/D maximum, while injection well begins with water injection followed by CO_2 injection and then chased with water. Water injection rate is preferably fixed at maximum value of 3,000 STB/D on both period of pre-flushed and chasing. CO_2 is injected from surface through injector at maximum rate of 8 MMSCFD. Actual injection rate is also controlled by reservoir fracture pressure at injector which is approximately around 3,800 psia, estimated based on Ben Eaton's method. Besides, producer is shut in once water cut ratio is larger than 95%.

Model is varied with water slug size containing 0.05, 0.1, 0.15, 0.2 and 0.25 reservoir Pore Volume (PV), respectively. Table 5.1 summarizes simulated cases for determination of optimal pre-flushed water slug size.

Table 5.1 Summary of simulated case for determination of optimal pre-flushed water slug size

Case no.	Pre-flushed Water Slug Size	CO$_2$ Injection Slug Size	Chasing Water
1	0.05 PV		
2	0.10 PV		Continuous injection until production meets criteria
3	0.15 PV	0.4 HCPV	
4	0.20 PV		
5	0.25 PV		

Oil recovery factor versus pre-flushed water slug size is plotted in Figure 5.1. Oil recovery factor is found at 64.56% for 0.05 PV and it increases significantly from slug size of 0.10 PV to 0.20 PV. The slug size of 0.05 PV is likely to be too small to flush oil from reservoir; therefore, relatively small amount of oil could be produced. On the other hand, slug size of 0.25 PV seems to be too big as movable oil is already flushed, so an incremental of water slug size does not contribute better oil recovery. In fact, slug size of 0.25 should be able to maintain the longest oil production but there is a significant amount of water arrives at producer as shown in Figure 5.2. Therefore, a dropping period of oil production rate can also be noticed in Figure 5.3. It can be seen that production period before the well shut off for first three cases is quite close to each other which is around 6,440 days, whereas production periods for case 4 and 5 are approximately 6,640 days and 6,800 days, respectively. This longer production period is due to pressure supporting from injected water and also a later gas breakthrough (Figure 5.4), resulting in higher cumulative oil production for last two cases. Though 0.25 PV gives the highest oil recovery factor, it requires higher amount of water to be injected and if compared cases of 0.20 PV with 0.25 PV, oil recovery is not meaningfully different. Table 5.2 concludes simulation results for case 1 to case 5. Consequently, case 4 is selected as an optimum base case to be exploited for next steps.
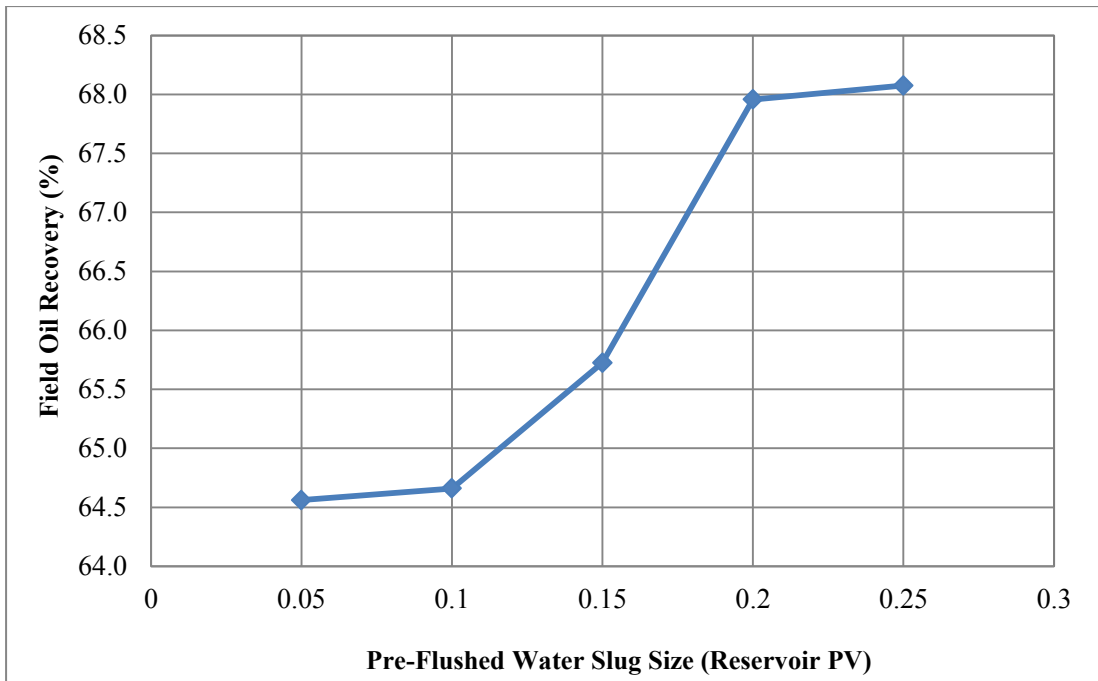
Figure 5.1 Oil recovery as a function of pre-flushed water slug size
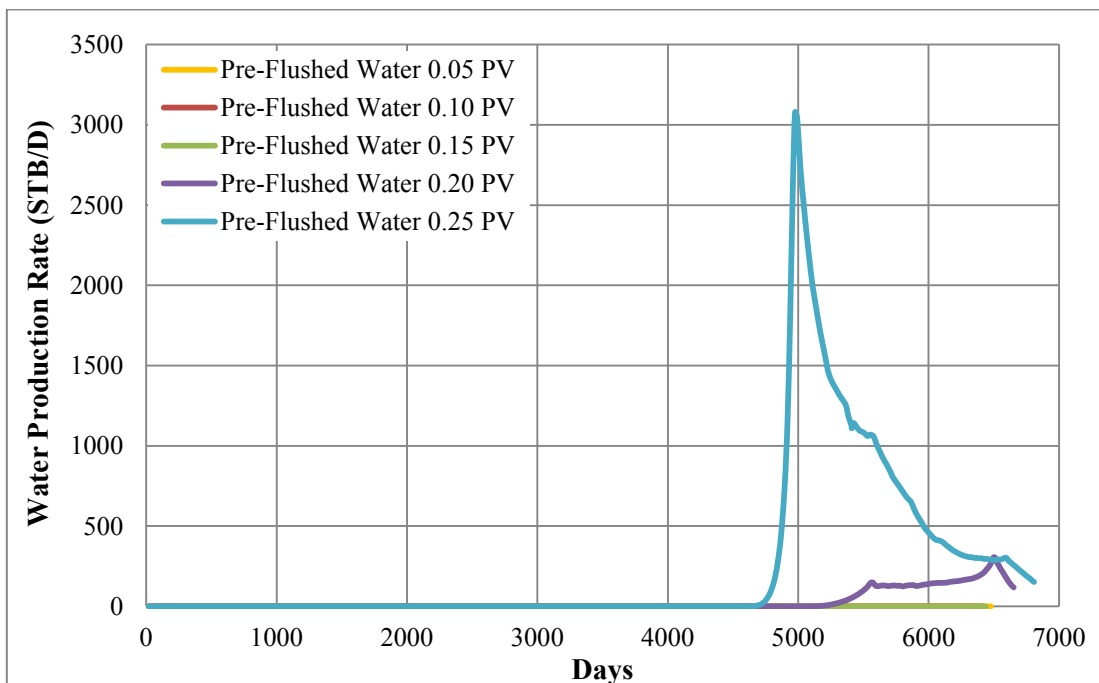
Figure 5.2 Water production rates as functions of time for determination of optimal slug size of pre-flushed water
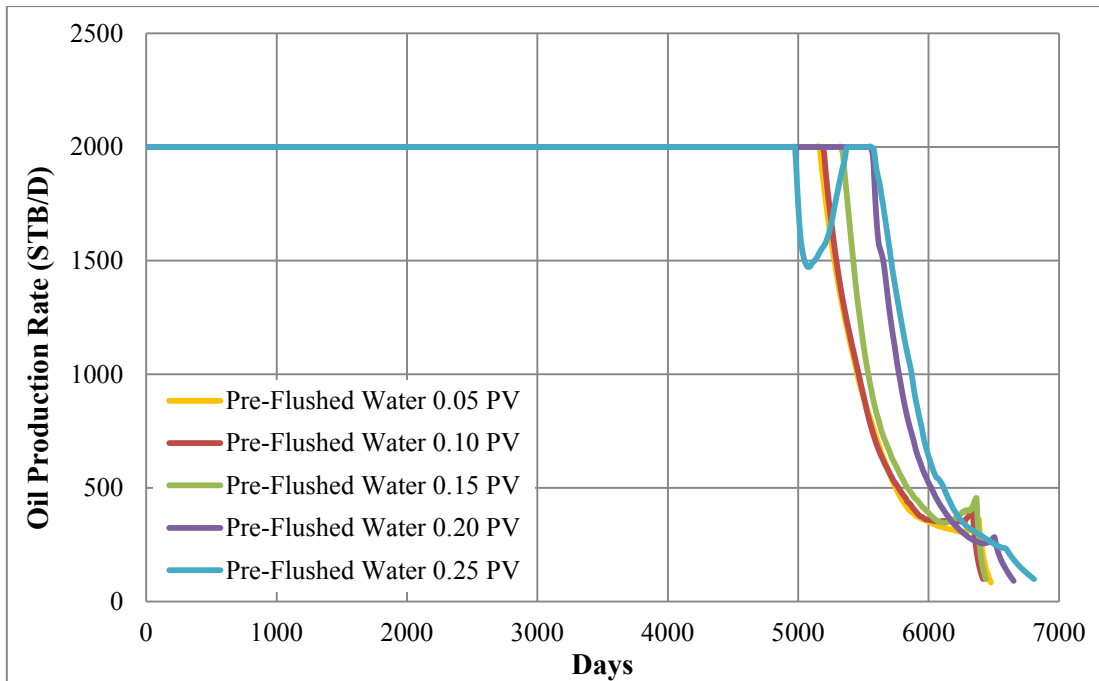
Figure 5.3 Oil production rates as functions of time for determination of optimal slug size of pre-flushed water
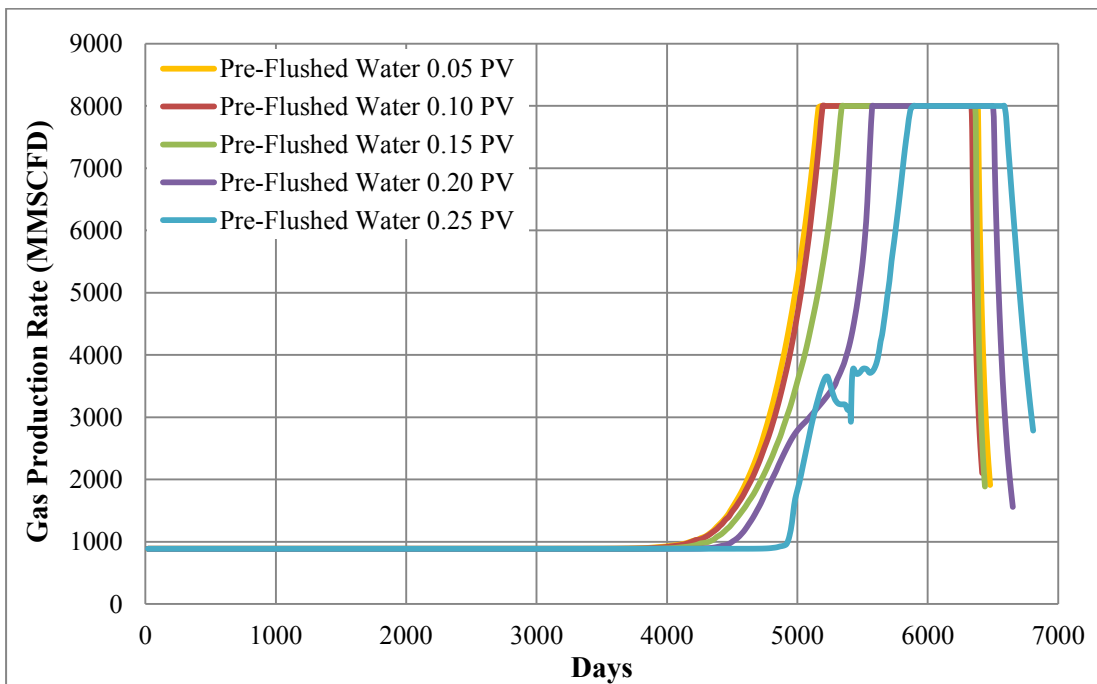
Figure 5.4 Gas production rates as functions of time for determination of optimal slug size of pre-flushed water

Table 5.2 Summary of simulation results from a determination of optimal slug size of pre-flushed water

Case no.	Pre-Flushed Water Slug Size	Amount of Water Injected for Pre-Flushing (MMSTB)	Amount of CO_2 Injected (BSCF)	Amount of Water Injected for Chasing (MMSTB)	Total Production Time (days)	Oil Recovery (%)
1	0.05 PV	1.51	17.2	6.10	6,461	64.56
2	0.10 PV	3.02	16.7	5.04	6,424	64.66
3	0.15 PV	4.53	16.2	4.20	6,424	65.73
4	0.20 PV	6.04	15.8	3.92	6,643	67.96
5	0.25 PV	7.55	15.4	3.75	6,789	68.07

5.1.2 Performance of Optimized Base Case

Following designed flooding scheme, water injection rate which is initially set at 3,000 STB/D cannot be constantly maintained at this rate due to preset maximum bottomhole pressure that is related to fracture pressure limit at 3,800 psia. At beginning, water is injected at maximum rate as bottomhole pressure at injector is much different from fracture pressure. After bottomhole pressure reaches its limitation, injection rate is automatically reduced to avoid creating fractures around wellbore. This event occurs at day 570, as shown in Figures 5.5 and 5.6. Similarly, injected chasing water is also controlled by this constraint. CO_2 injection is also in line with the previously mentioned control structure. Slug size of CO_2 meets equivalent of 0.4 HCPV as per requirement after injecting for 2,897 days as displayed in Figure 5.7.
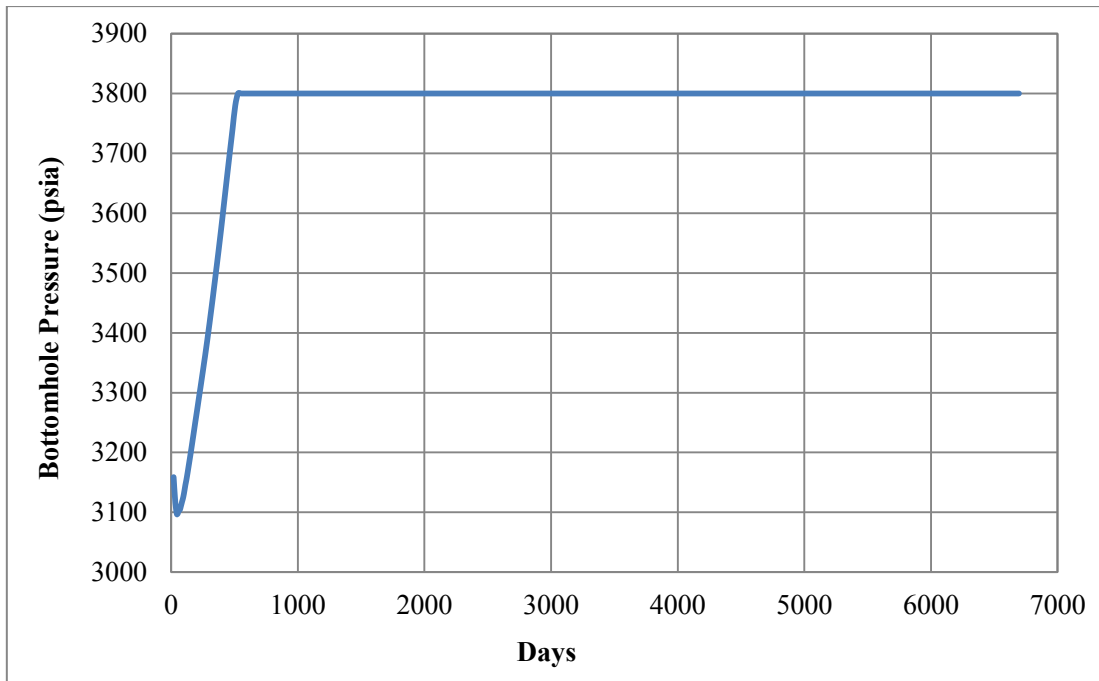
Figure 5.5 Bottomhole pressure at injector of selected base case as a function of time
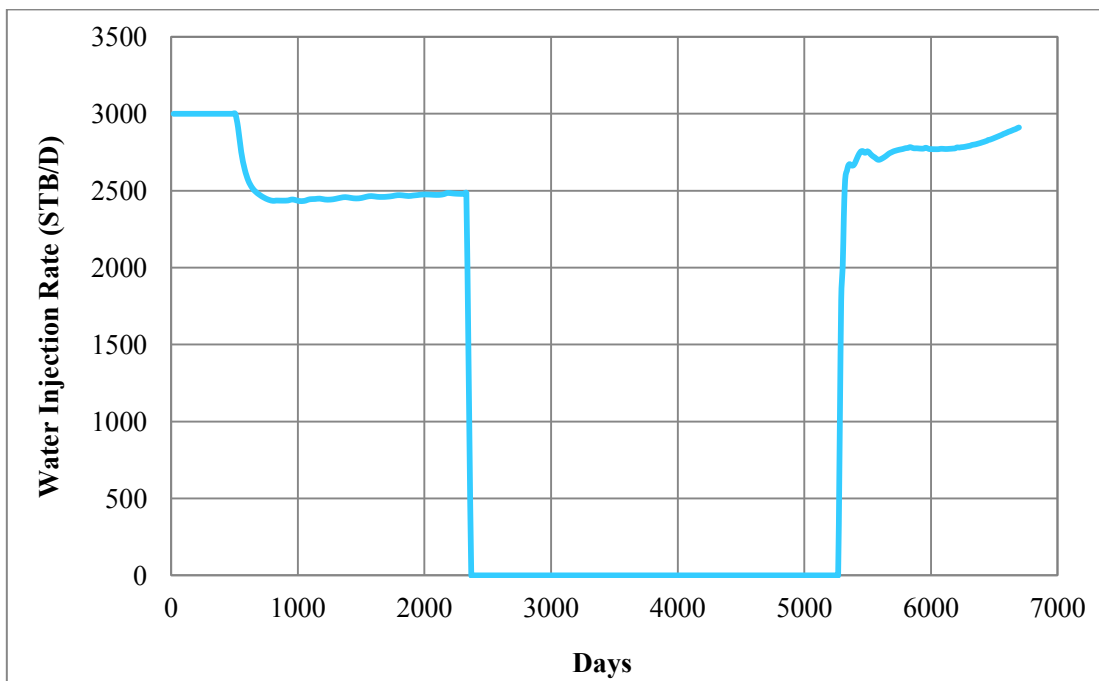
Figure 5.6 Water injection rate of selected base case as a function of time
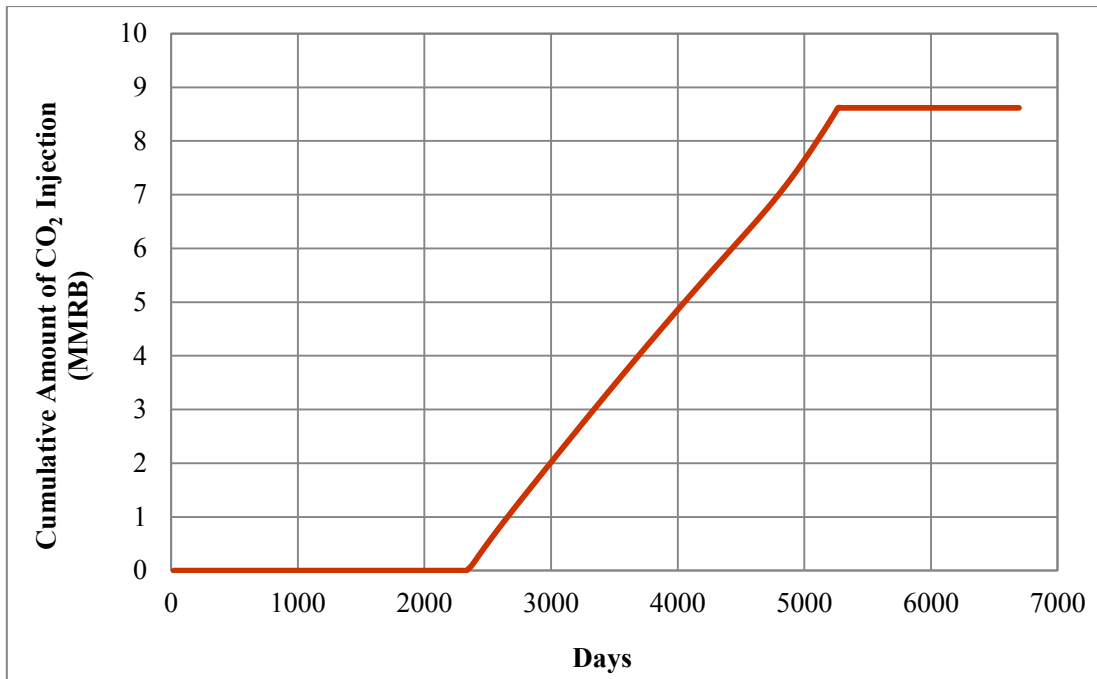
Figure 5.7 Cumulative amount of CO_2 injected of selected base case

as a function of time

From Figure 5.8, oil production from selected base case can be maintained at maximum rate for 5,560 days. Meanwhile, gas starts breaking through the producer at around day 4,500. Gas production rate keeps rising up, affecting permeability to oil due to an increase in gas saturation in reservoir. Therefore, to avoid declining of production, bottomhole pressure of producer is reduced as seen in Figure 5.9. However, as gas production rate reaches the maximum constraint, oil production rate and bottomhole pressure at producer sharply drops because production well is switched control mode to gas production rate. Gas production rate can be monitored stable at early stage because reservoir pressure is still higher than bubble point pressure and an increase in gas production rate at around 4,500 day is on account of gas breakthrough at producer. It is also noted that production abandonment is due to oil production rate is lower than minimum limit.
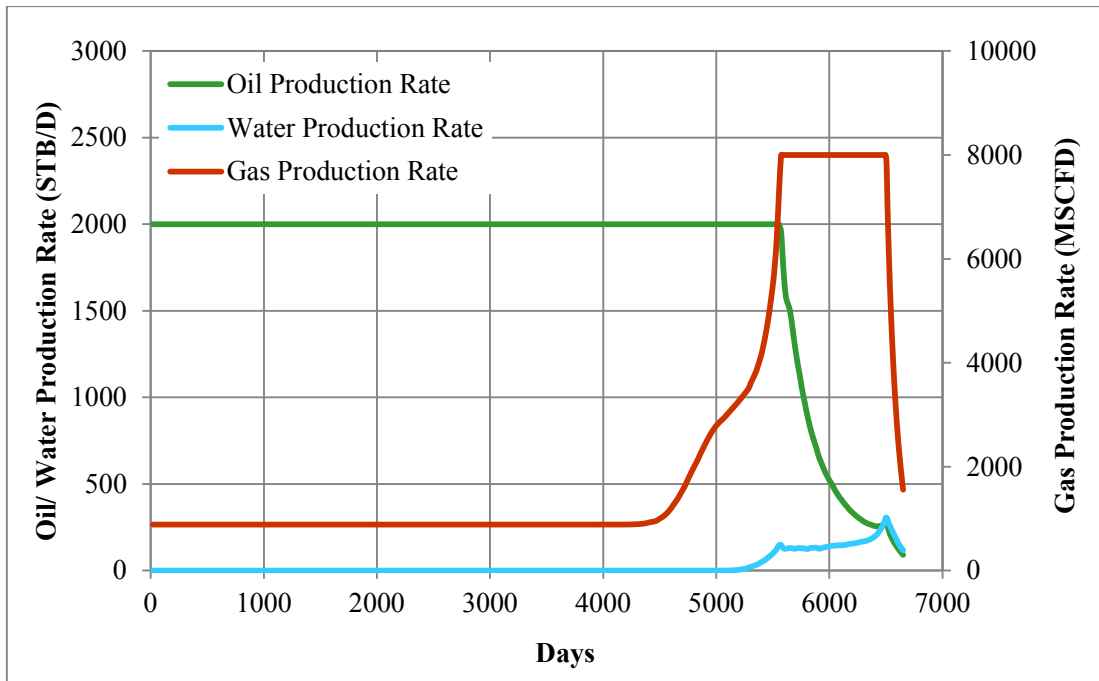
Figure 5.8 Oil, water and gas production rates of selected base case
as functions of time
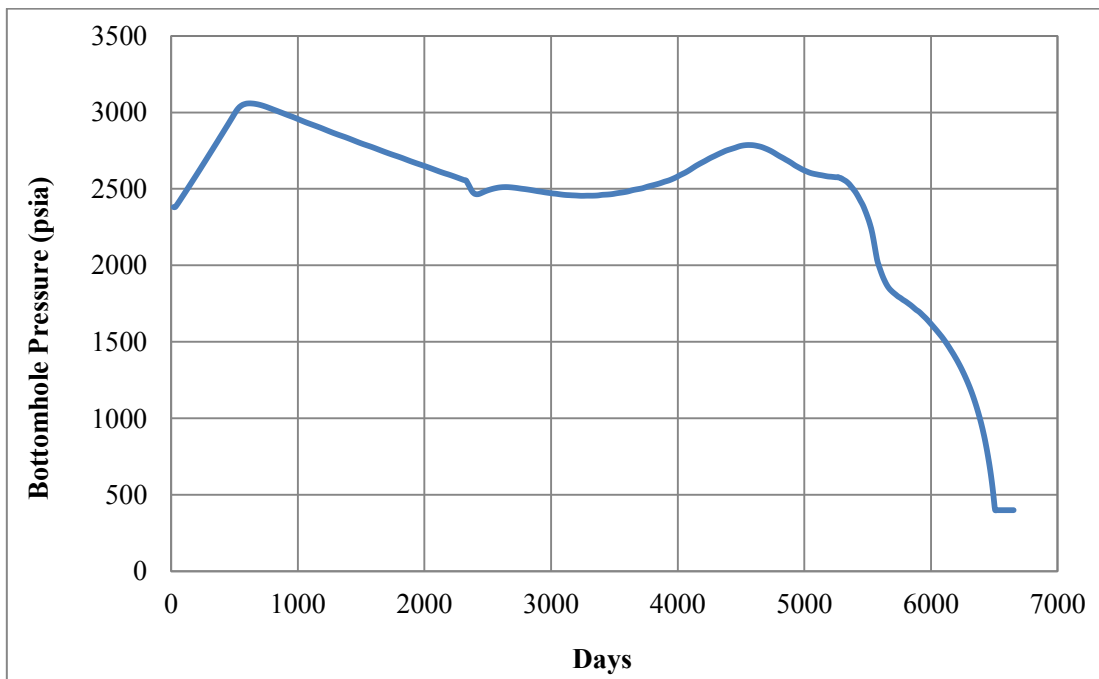
Figure 5.9 Bottomhole pressure of producer of selected base case
as a function of time

Theoretically, CO_2 is able to vaporize light to intermediate portions of hydrocarbon from reservoir by multi-contact miscibility mechanism. As pressure during CO_2 injection is greater than MMP, miscible bank can be formed. This bank could extract a significant amount of trapped oil as seen from lower oil saturation after miscible bank moves pass pore spaces. To observe effect from miscibility mechanism, oil viscosity reduction is considered. Figure 5.10 shows three-dimension models illustrating scale of oil viscosity and oil saturation in order of injection period. When reservoir is displaced by water, oil viscosity is remained the same through that period, but, when CO_2 is injected, it vaporizes light hydrocarbon from oil into gaseous phase, leaving heavy compounds in oil phase, causing oil to be more viscous. According to this oil recovery mechanism, the front of an in-situ miscible bank could be tracked through viscosity map and this is displayed in Figure 5.10a. Later on, this bank is pushed ahead by chasing water, providing an additional recovery.
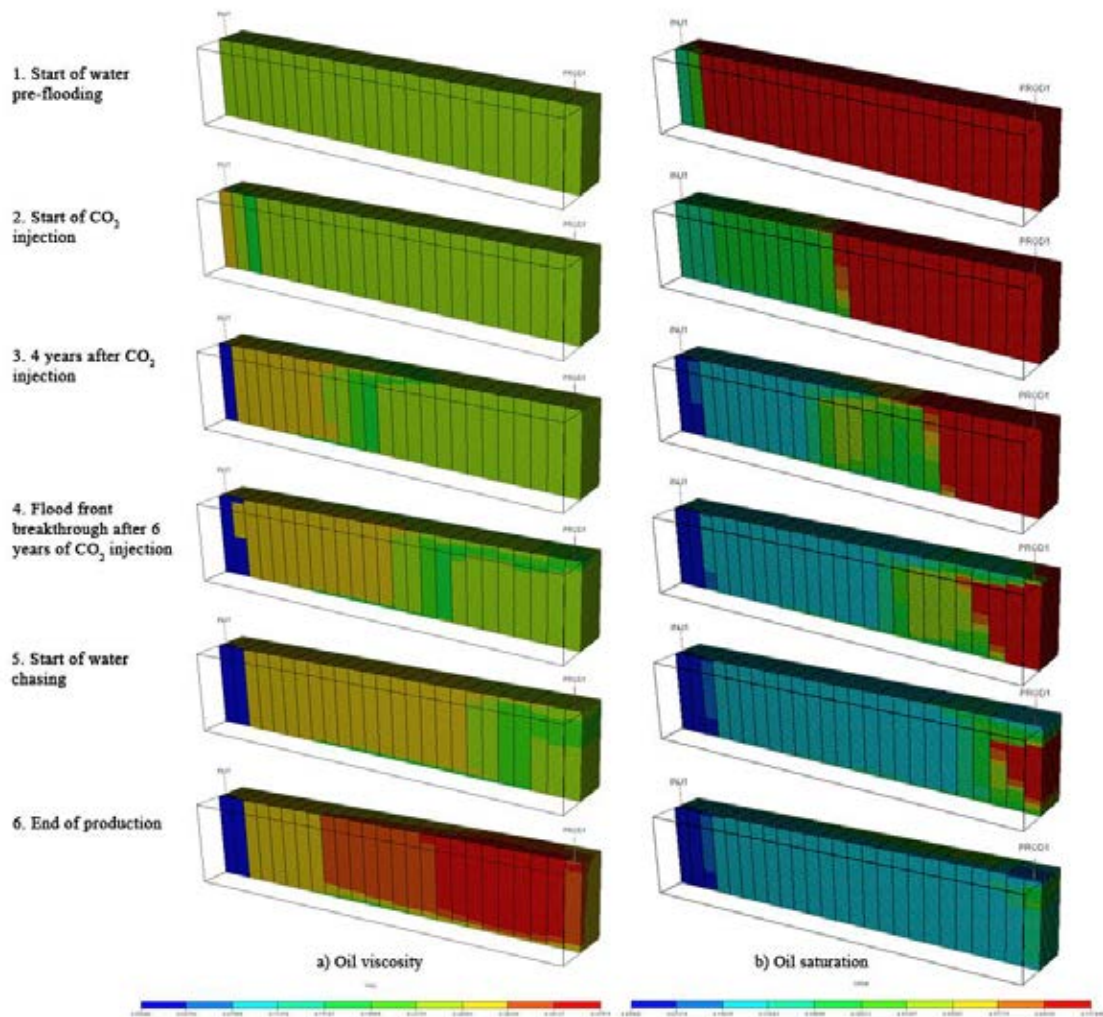
Figure 5.10 Reservoir profile as displayed by a) oil viscosity and
b) oil saturation at different time steps of selected base case

At first stage, reservoir is initially filled with oil having just one value viscosity of 0.24 cP illustrated by green color in Figure 5.10a and saturation around 0.72 illustrated by red color in Figure 5.10b. Once the field starts producing, water injection decreases oil saturation that means oil is removed from pore space. Average oil saturation in flooded zone is deducted to 0.33 with the same viscosity. Subsequently, injected CO_2 helps vaporize intermediates. In microscopic point of view, this emerges by diffusion of CO_2 through water and eventually reaches oil globules, trapped in pore spaces, as reservoir is water-wet where surface is

preferentially covered by water from previous injection. Vaporized hydrocarbon which is obtained from contacting with CO_2 goes into gaseous phase together with injected CO_2 which becomes less viscosity. Technically, at particular temperature and pressure, viscosity of gas phase reduces as composition of paraffinic hydrocarbons increases. Figure 5.11 represents gas viscosity after CO_2 is injected into the reservoir for several years and after chasing water is injected. From figure, red color indicates viscosity of CO_2 which mainly occupies pore spaces while yellow color represents light hydrocarbon such as methane which is vaporized by means of CO_2. Vaporized hydrocarbon possesses both lower viscosity and density compared to pure CO_2, thus; it moves faster than CO_2 and is located at very front location. Additionally, zone combining between CO_2 and vaporized hydrocarbon is considered as a miscible bank and this zone has medium gas viscosity around 0.048 cP. It is noted that after chasing water is injected, it sweeps the bank toward producer, leaving heavy molecular weight hydrocarbons behind. This results in existing of lower gas viscosity inside reservoir as seen in Figure 5.11b.

a)   b)
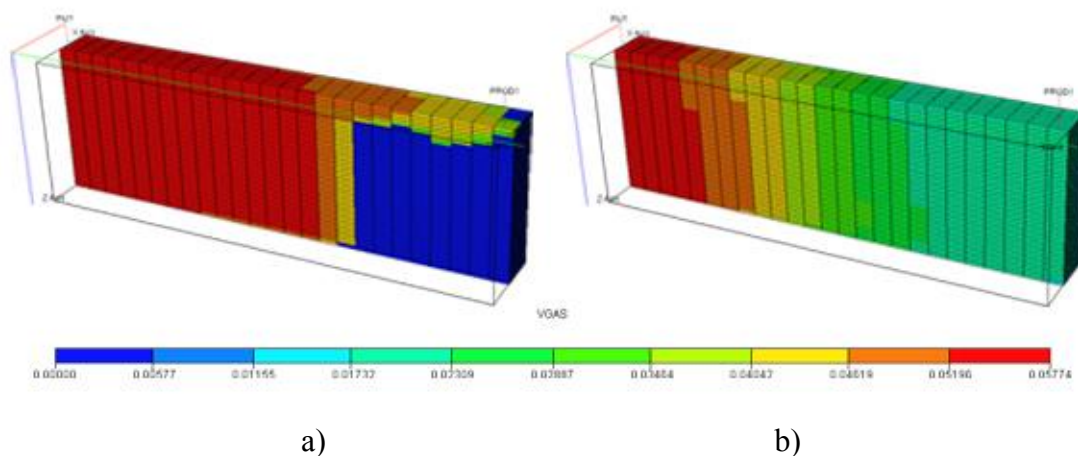
Figure 5.11 Gas viscosity of selected base case at a) six years after CO_2 injection
b) four years after chasing water is injected

Approximately 4,500 days, the front of miscible bank arrives to production well, gas production rate increases obviously as shown in Figure 5.8. In addition, from Figure 5.10, it is noticed that shock front before breakthrough is unstable

because reservoir is assumed as homogeneous having equal permeability in all layers. Flood front goes mainly on upper part rather than lower of reservoir model according to effect from low density of gas.

Injected CO_2 does not only raise reservoir pressure which declines by means of injecting only water seen in Figure 5.12, but also increases additional oil production by means of extracting residual oil from pore spaces which is considered as an effect from miscibility with CO_2 as discussed previously. Figure 5.12 also shows that during the period of CO_2 injection, reservoir pressure is greater than MMP, indicating that miscibility could be found. Though, at late production period, reservoir pressure falls under this MMP, the monitored oil viscosity in Figure 5.10 supports that miscibility could be maintained until it arrives to the producer before disappearance of miscible bank might occur.
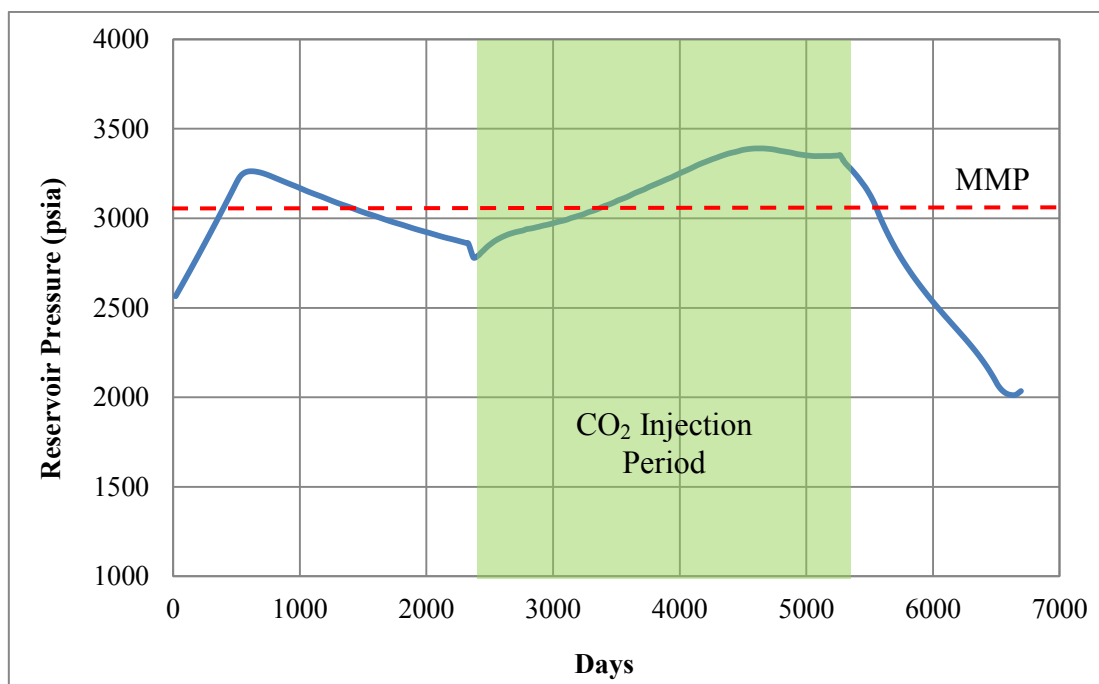
Figure 5.12 Reservoir pressure of selected base case as a function of time

5.2   Waterflood Case

In waterflood scenario, likewise, homogeneous model from optimized CO_2 flooding scenario is employed. The only exception is that injection rate at injector is fixed at the maximum 3,000 STB/D from beginning until production reaches one of the constraints. Production well is also preset to produce oil at maximum rate of 2,000 STB/D and this rate can be sustained for approximately 4,860 days as shown in Figure 5.13. After that, an oil production rate declines which is coincident with reduction in reservoir pressure as seen in Figure 5.14.

It is clearly seen that amount of water can be injected at its maximum rate for long since bottomhole pressure of injector is not greater than fracture pressure at 3,800 psia, indicating injection well is initially controlled by injection rate before switching to bottomhole pressure and finally controlled by injection rate again. Figures 5.15 and 5.16 illustrate water injection rate and bottomhole pressure at injection well. It can be seen that water breakthrough occurs at day 4,660 and this flooding scenario can totally last for 6,900 days approximately before water cut at producer reaches limitation at 95% as shown in Figure 5.17.

Cumulative oil production from total period of water flooding case is 10.32 MMSTB, yielding recovery factor of 59.56% which is illustrated in Figure 5.18. To display hydrocarbon distribution inside reservoir, initial and final oil saturations of are compared in Figure 5.19. Initial oil saturation is uniformly distributed around 0.72, while final oil saturation is distributed around 0.24 nearby injection well, 0.40 in upper part and 0.26 in lower part of reservoir. This is due to the fact that water possesses higher density than oil, so it usually under-runs the reservoir. Table 5.3 summarizes study outcomes of water flooding case.
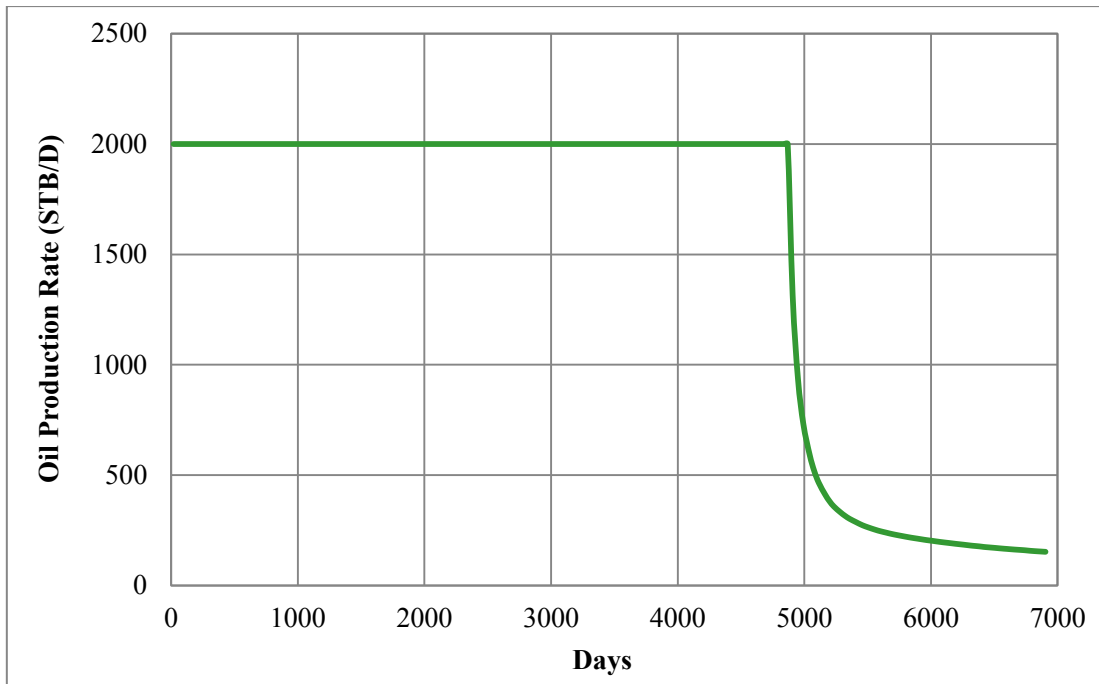
Figure 5.13 Oil production rate of waterflood case as a function of time
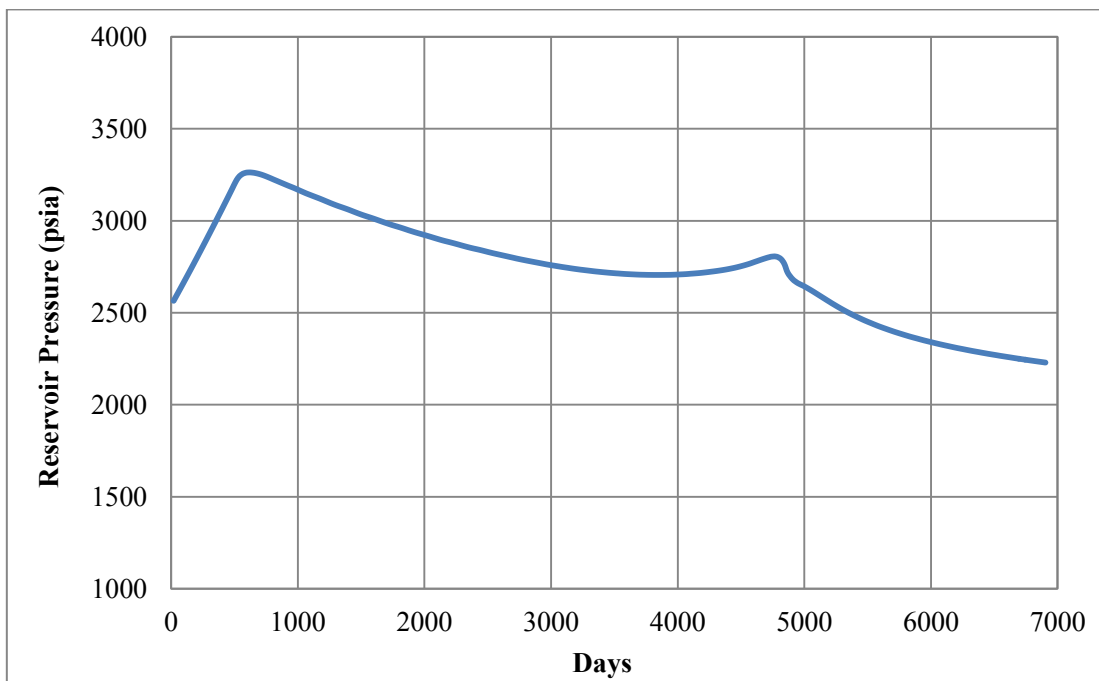
Figure 5.14 Reservoir pressure of waterflood case as a function of time
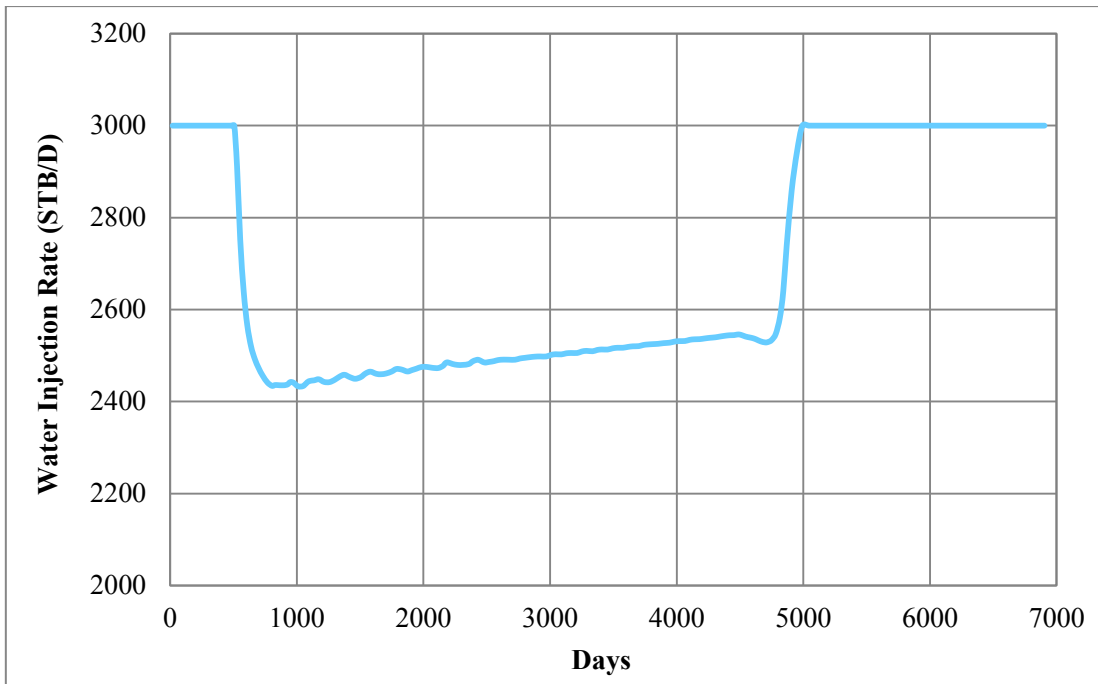
Figure 5.15 Water injection rate of waterflood case as a function of time
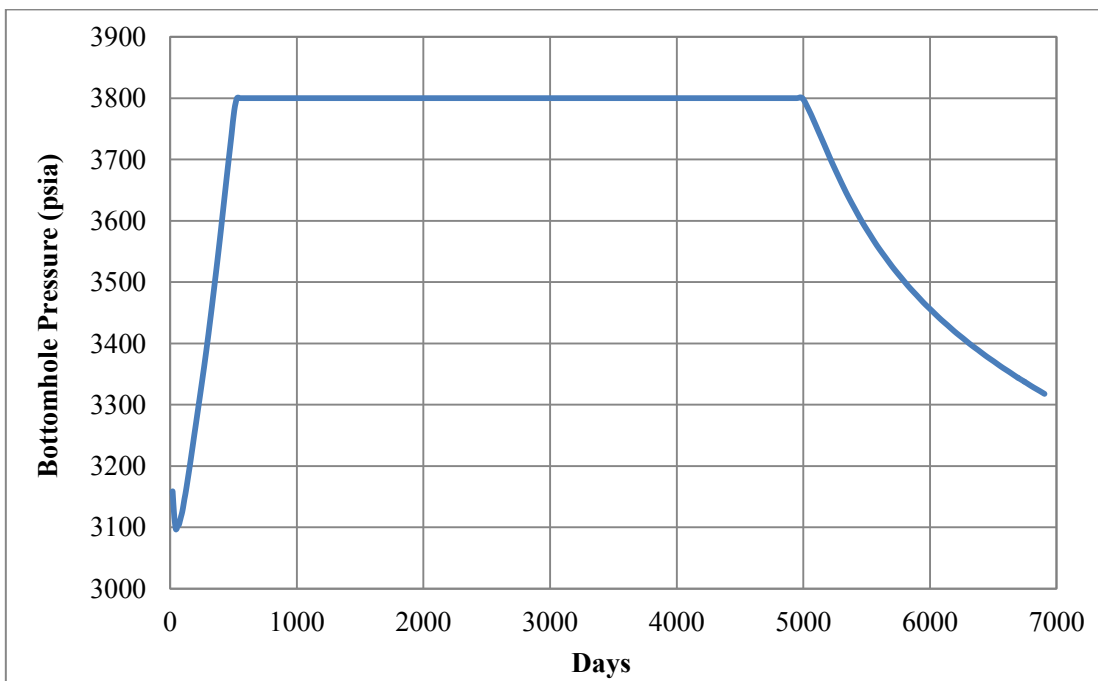
Figure 5.16 Bottomhole pressure of injection well of waterflood case

as a function of time
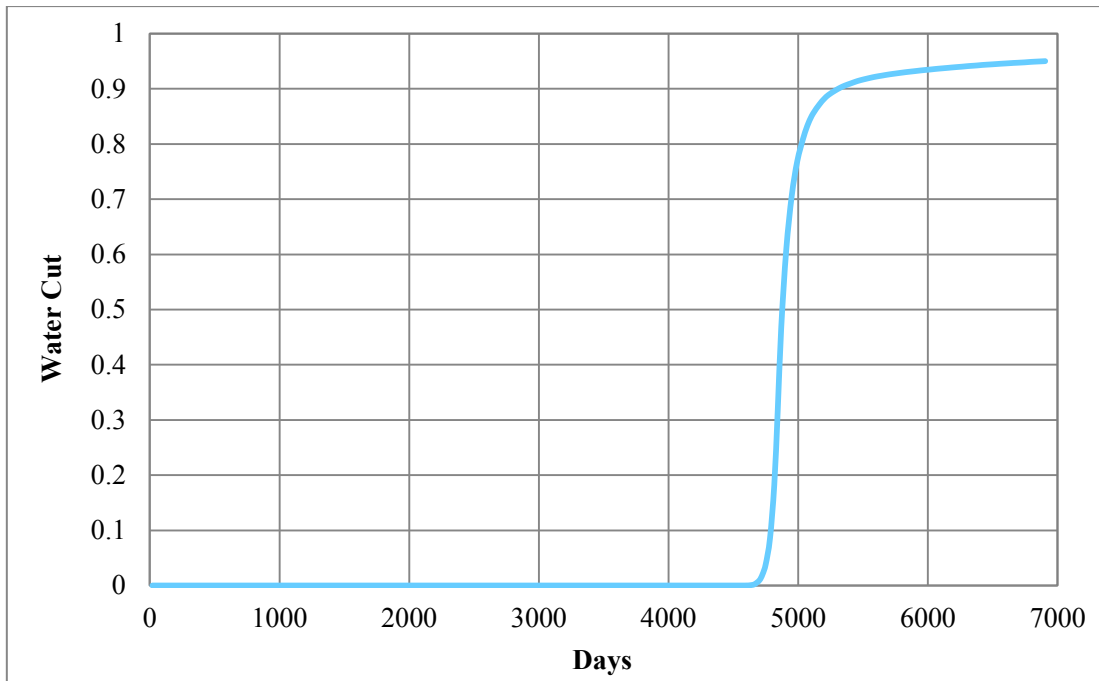
Figure 5.17 Water cut at producer of waterflood case as a function of time
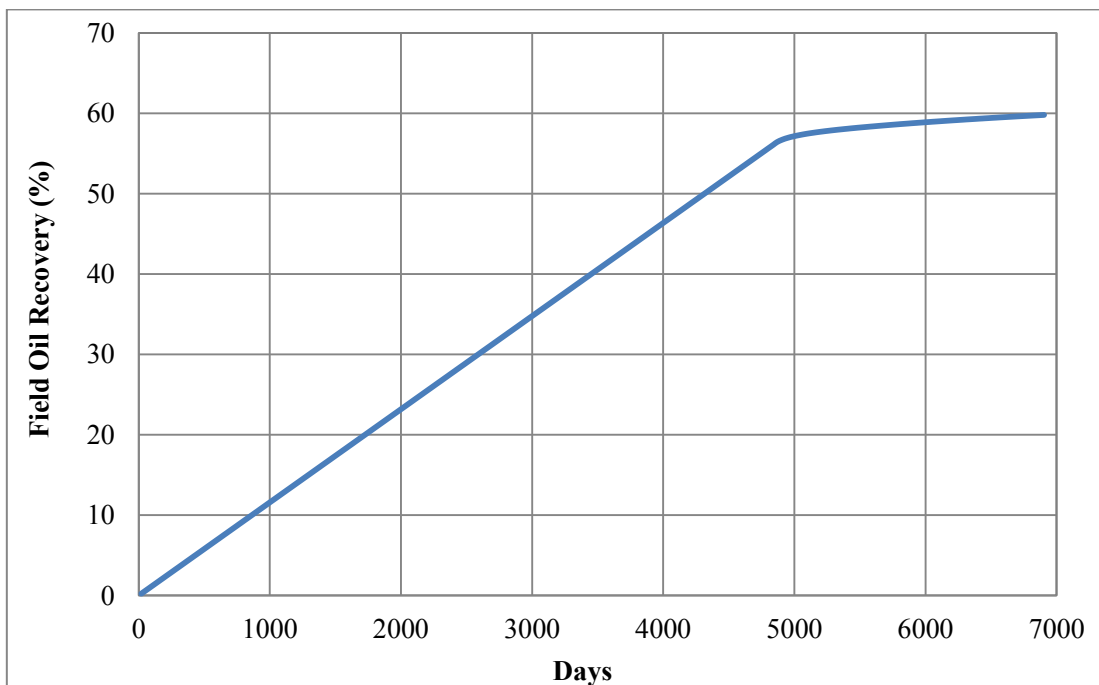
Figure 5.18 Oil recovery factor of waterflood case as a function of time
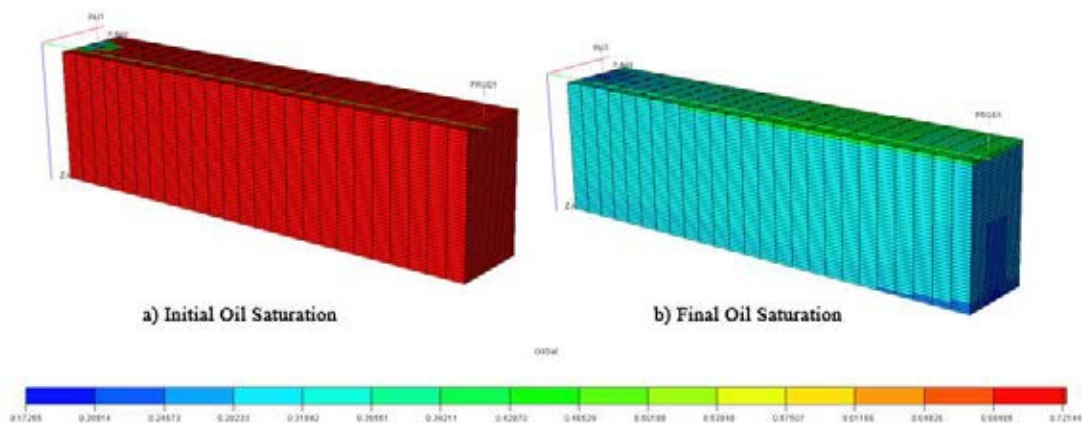
Figure 5.19 Initial and final oil saturation distribution of waterflood case

Table 5.3 Summary of simulation parameters for waterflood case

Scenario	Amount of Water Injected (MMSTB)	Cumulative Oil Production (MMSTB)	Oil Recovery (%)	Total Production Time (days)
Water Flooding	18.58	10.27	59.56	6,899

5.3 Performance Comparison between CO_2 Flooding Base Case and Waterflood Case

Performance between CO_2 miscible flooding base case and waterflood case is compared in this section, regarding mainly on a matter of oil recovery factors as functions of time. The plot is shown in Figure 5.20. CO_2 miscible flooding base case visibly yields higher oil recovery factor. Even a shorter total production period, eight percent enhancement in oil recovery from CO_2 base case compared to waterflood case is achieved through miscibility between CO_2 and reservoir fluid. It is clearly seen that enhanced oil production comes from longer maximum production period as seen in Figure 5.21 and this is because injected CO_2 can increase reservoir pressure, as illustrated in Figure 5.22, and can sweep additional residual oil from reservoir. Table 5.4 summarizes simulation results from these two cases in order to confirm that the study CO_2 flooding base case yields a better performance than only waterflooding scenario.
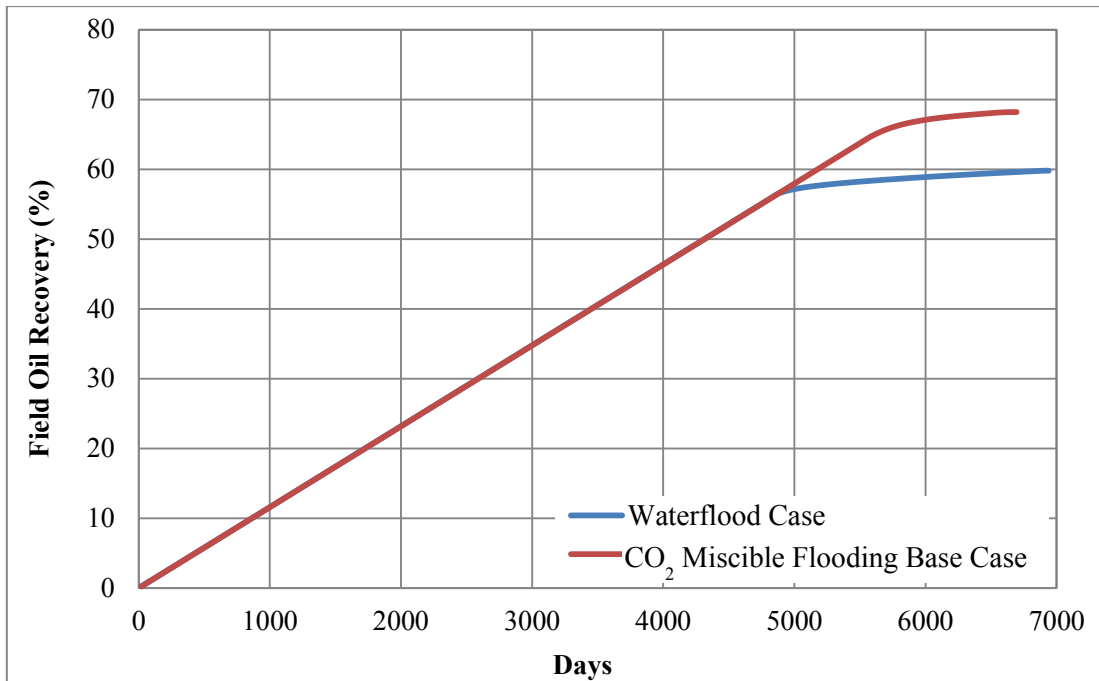
Figure 5.20 Comparison of oil recovery factor between CO_2 flooding base case and
waterflood case
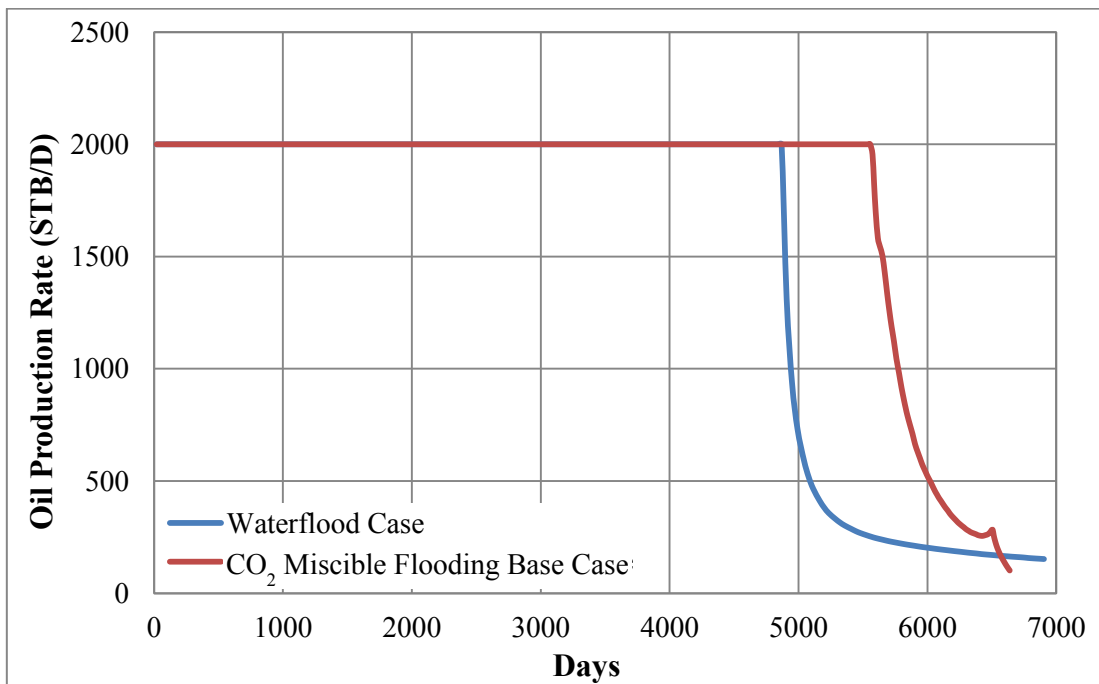
Figure 5.21 Comparison of oil production rate between CO_2 flooding base case and
waterflood case
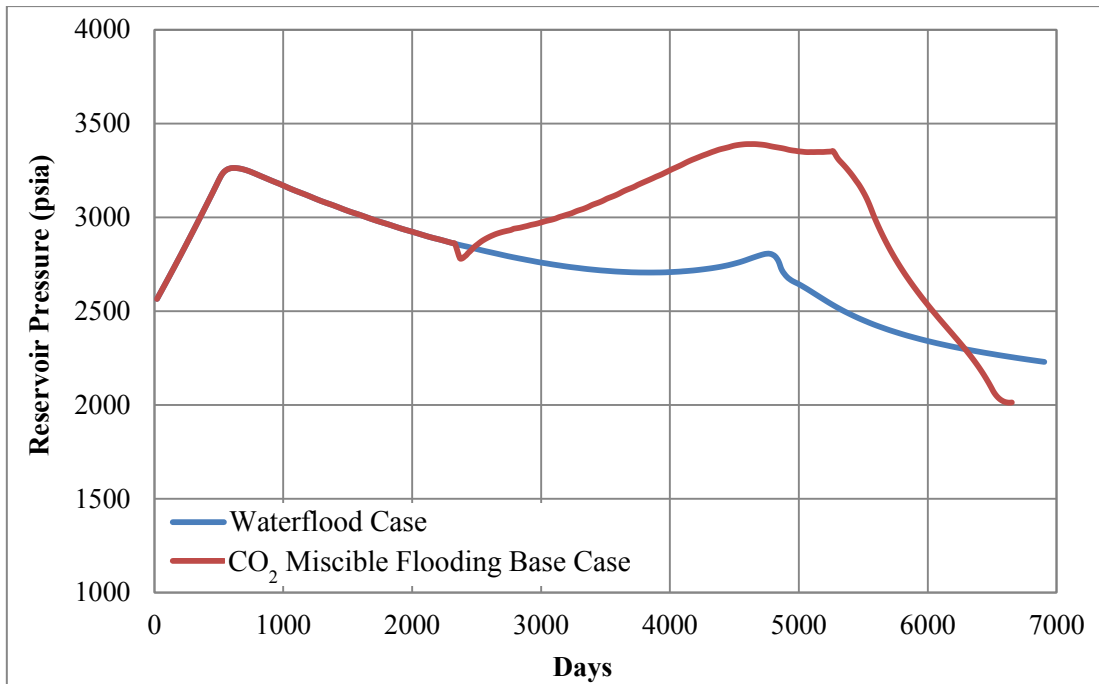
Figure 5.22 Comparison of reservoir pressure between CO_2 flooding case and waterflood case

Table 5.4 Comparison of simulation results on performance of CO_2 miscible flooding base case and waterflood case

Scenario	Cumulative Gas Production (BSCF)	Cumulative Water Production (MMSTB)	Oil Recovery (%)	Total Production Time (days)
CO_2 miscible flooding	15.24	0.20	67.96	6,643
Waterflood	4.48	5.89	59.56	6,899

5.4 Effect of Study Parameters on the CO_2 Miscible Flooding Base Case

The impact of reservoir heterogeneity is one of concerns for production from reservoir as it affects flow behavior, resulting in poor flooding performance, especially when reservoir is flooded with low gravity injectant like gas. To achieve objectives of this study, effect of reservoir heterogeneity and its lithofacies on study parameters is to be discussed. Reservoir heterogeneity model is created, based on the approach demonstrated on section 4.5. Each model is assigned with different value of heterogeneity index or Lorenz coefficient to represent a variation of permeability on stratified reservoir, while other model configurations and controls are remained the same as base case.

5.4.1 Effect of Reservoir Dip Angle

Reservoir dip angle is one of the most important uncontrollable parameters because it might aid stability of displacement mechanism due to gravity segregation effect when displacement mechanism is performed by injecting gas at updip location. In this section, heterogeneous reservoir models including heterogeneity index of 0.18, 0.25, 0.32, 0.38 and 0.44 employed with reservoir dip angle of 0, 15, 30 and 45 degree are studied. Total amount of the cases simulated in this section is 40 and cases are grouped into ten as shown in Table 5.5.

Table 5.5 Summary of simulated cases on the study of reservoir dip angle

Group No.	Depositional Sequence	Heterogeneity Index	Dip Angle (degree)
1		0.18	0, 15, 30 and 45
2		0.25	0, 15, 30 and 45
3	Fining Upward	0.32	0, 15, 30 and 45
4		0.38	0, 15, 30 and 45
5		0.44	0, 15, 30 and 45
6		0.18	0, 15, 30 and 45
7		0.25	0, 15, 30 and 45
8	Coarsening Upward	0.32	0, 15, 30 and 45
9		0.38	0, 15, 30 and 45
10		0.44	0, 15, 30 and 45

Oil recoveries as a function of reservoir heterogeneity index for the study of reservoir dip angle effect are plotted in Figure 5.23 and 5.24, respectively.
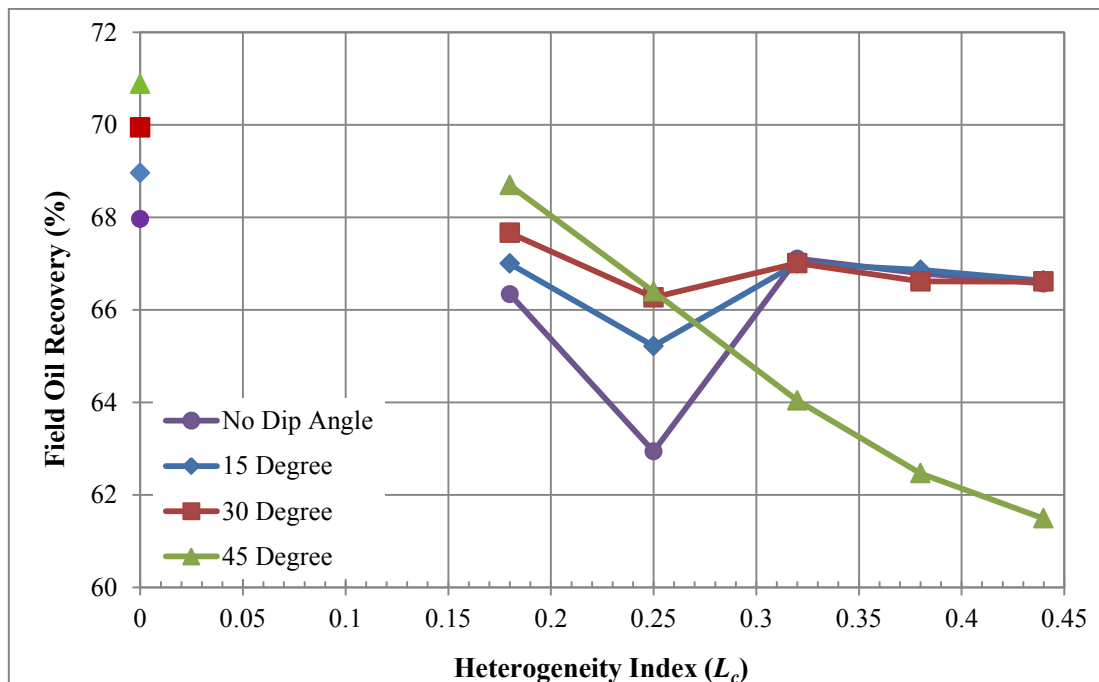
Figure 5.23 Relationship between field oil recovery and heterogeneity index on different reservoir dip angles on fining upward reservoir model
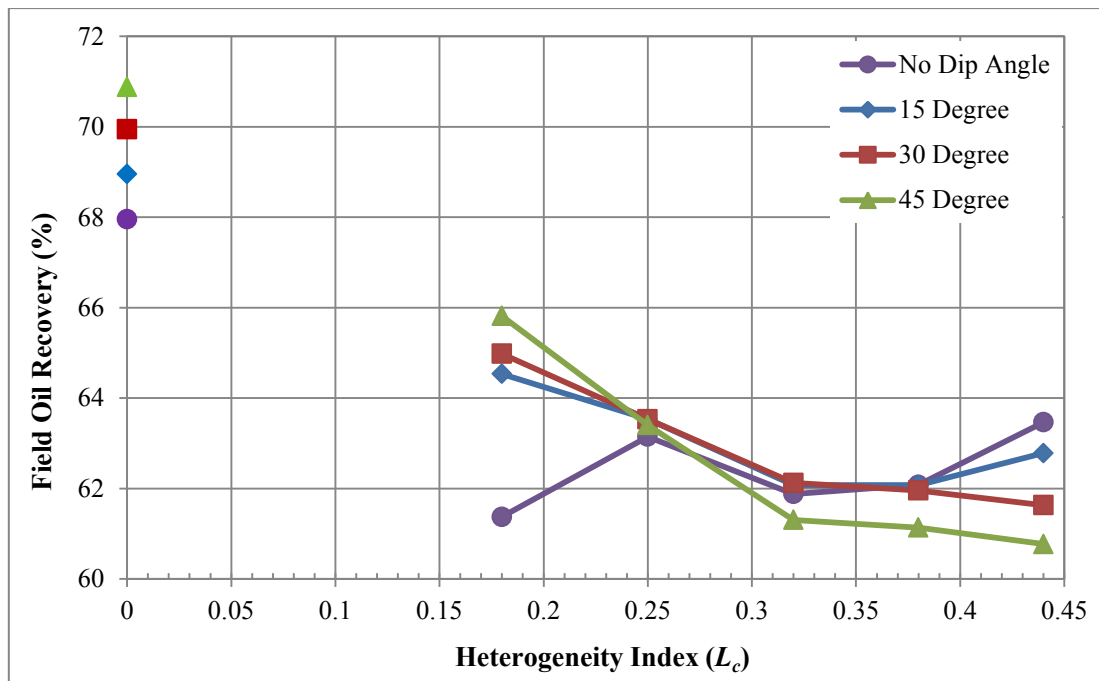
Figure 5.24 Relationship between field oil recovery and heterogeneity index on different reservoir dip angles on coarsening upward reservoir model

Initially, from Figures 5.23 and 5.24, oil recoveries obtained from fining upward tend to be slightly higher since this lithofacies tends to inhibit gas movement at top location, resulting in later breakthrough of gas. Also, when model has no effect from heterogeneity (L_c of 0), it shows the highest oil recovery compared within its dip angle. Nevertheless, discussion is subdivided for both lithofacies cases since results show remarkable difference. Fining upward models (group 1-5) is firstly considered and followed by cases of coarsening upward lithofacies (group 6-10).

From Figure 5.23, it can be seen that there are two different trends on plots between heterogeneity index and oil recovery factor. The first trend is found on plots obtained from reservoir dip angle of 0, 15 and 30 degree, while another trend is only observed from reservoir dip angle of 45.

For a first trend, result from horizontal model (reservoir dip angle of zero) is firstly chosen to determine effect from heterogeneity along with dip angle. There are three transition zones separated from a change on the trend line, consisting of zone 1 (L_c of 0.18 to 0.25), zone 2 (L_c of 0.25 to 0.32) and zone 3 (L_c of 0.32 to 0.44).

In zone 1 or a transition from heterogeneity index of 0.18 to 0.25, a reduction of oil recovery factor can be significantly found. This can be explained by using Figures 5.25 and 5.26.

Figure 5.25 Oil, water and gas production rates as functions of time for case L_c of 0.18 on fining upward reservoir model with zero degree dip angle

Figure 5.26 Bottomhole pressure at production well as a function of time for case
L_c of 0.18 on fining upward reservoir model with zero degree dip angle

From Figure 5.25 where production profiles for case L_c of 0.18 with zero dip angle case are illustrated, oil can be produced at constant rate of 2,000 STB/D for 5,370 days, whereas gas production also starts increasing on a day of 4,225. An increase of gas production indicates an arrival of injected gas at producer which leads to an increase in gas saturation and this consecutively impacts in reducing relative permeability to oil. However, oil is still produced at its maximum rate as a result from lowering bottomhole pressure as seen in Figure 5.26. Gas production rate keeps going up from the day that gas breakthroughs until it reaches the maximum limit. Production well then switches control mode to gas production rate in order to limit gas production at its maximum rate. As a result, oil production rate starts declining, whereas bottomhole pressure of production well continues falling. Bottomhole pressure keeps lowering until it reaches target bottomhole pressure, control mode now switches to bottomhole pressure. By means of maintaining bottomhole pressure, which prevents back flow of fluid from producer to reservoir, oil production rate is

continuously lowering and eventually oil production rate approaches lower limit of 100 STB/D, causing well to shut-in.

It is obviously seen from plot between oil recoveries versus heterogeneity in Figure 5.23 that, in the case L_c of 0.25, oil recovery is lower than the case L_c of 0.18. This can be described as gas in this case causes an earlier breakthrough at production well as seen in Figure 5.27 and it reaches maximum limit quickly, resulting in a shorter maximum oil production period. Hence, with the same reason mentioned above on reducing relative permeability to oil, it can be inferred that the faster gas arrival at production well, the earlier declining of oil production rate that also affects amount of oil recovered, accordingly.

Figure 5.27 Gas production rates as functions of time for all heterogeneity index cases on fining upward reservoir model with zero degree dip angle

Zone 2 is designated within a transition from heterogeneity index of 0.25 to 0.32. Even though gas breakthrough can be found at sooner time as shown in Figure 5.27, a rise of oil recovery is accomplished. This is a consequence from a large amount of water arrives at production well from the case L_c of 0.32 as seen in Figure 5.28.

During the middle production period of this case, around day 5,940, production well is controlled by its bottomhole pressure and a fall of oil production rate can still be seen in Figure 5.29. However, after a big slug of water arrives, oil production rate bounces up again for a little while as it pushes residual oil from pore space, before falling to its minimum limitation. Thus, this scenario yields an additional oil recovery.

Figure 5.28 Water production rates as functions of time for all heterogeneity index cases on fining upward reservoir model with zero degree dip angle

Figure 5.29 Oil, water production rate and bottomhole pressure at production well as functions of time for case L_c of 0.32 on fining upward reservoir model with zero degree dip angle

Remaining points on trend line from previous discussion are recognized as in Zone 3, where oil recovery from the case L_c of 0.44 is slightly lower than the case L_c of 0.32. As seen in Figure 5.27 for gas production rate, case L_c of 0.44 provides the earliest start of gas breakthrough and subsequently the earliest reaching of maximum production rate. This reaching of maximum gas production rate also causes a more rapid fall of oil production. Thus, it should give a poorer performance on oil recovery but a gradual arrival of water chasing slug at late period due to high heterogeneity is able to support a longer period during which oil production rate is above 100 STB/D as the same reason as previous case. So, oil recovery between these two cases is not much different.

Unlike previous discussed trend line in Figure 5.23, the case applying with 45 degree dip angle shows a continuous reduction of oil recovery as reservoir heterogeneity increases. It is similar to previous discussion that increasing heterogeneity reduces number of constant oil production period. However, this occurs

from water breakthrough at producer instead of CO_2. As reservoir is modeled with the highest inclination, effect from gravity segregation of water mainly plays a major role, leading to water tonguing downward quickly. As heterogeneity index increases, effect of water tonguing is more severe as water flows better in high permeability channel at bottom layers, leaving much oil un-swept at the top of reservoir and acquiring lesser oil recovery accordingly. A big slug of water can be monitored from the water production profile in Figure 5.30. It can be also seen on oil production profile for every case in Figure 5.31 that there is another peak happening after first oil rate declination. It is because water production declines and gas does not yet reach producer, so that relative permeability to oil is able to increase and oil rate starts going up as a result. An example from case L_c of 0.44 with 45 degree dip angle shows a clear mentioned phenomenon as in Figure 5.32.

Figure 5.30 Water production rates as functions of time for all heterogeneity index cases on fining upward reservoir model with 45 degree dip angle

Figure 5.31 Oil production rates as functions of time for all heterogeneity index cases
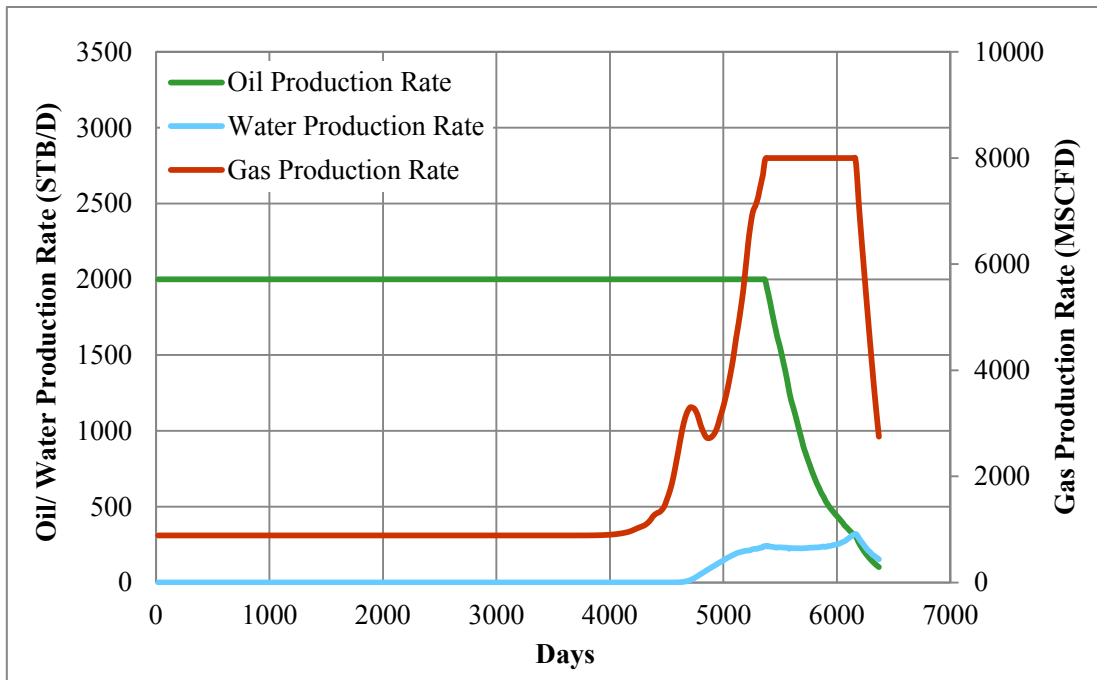on fining upward reservoir model with 45 degree dip angle

Figure 5.32 Oil, water and gas production rates as functions of time for case L_c of 0.44
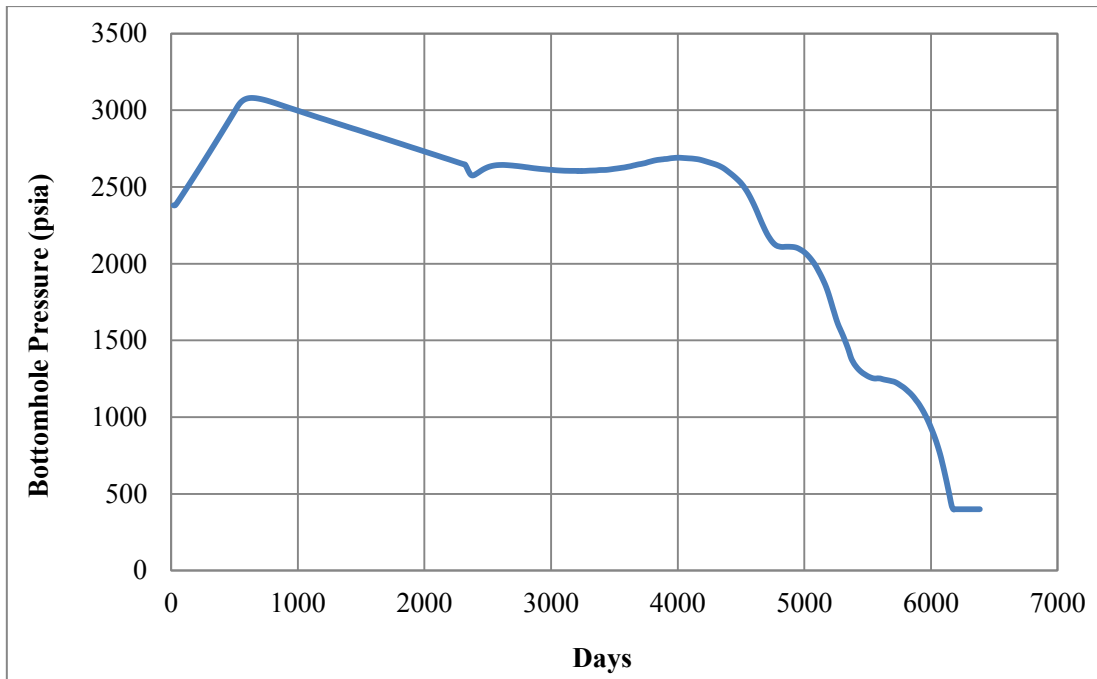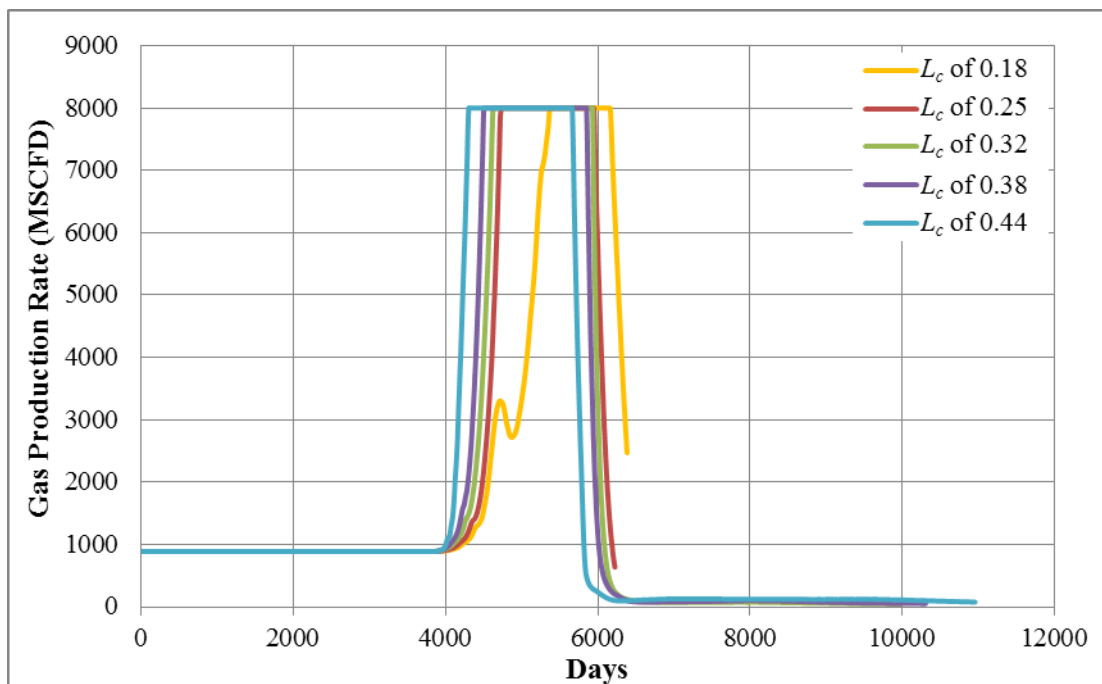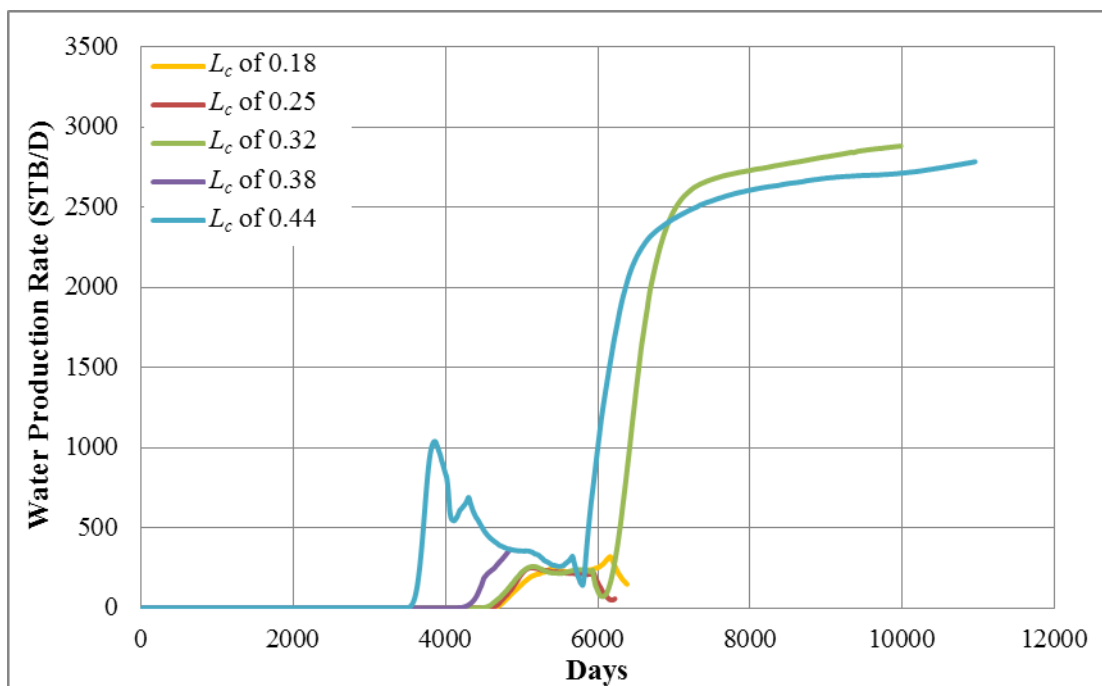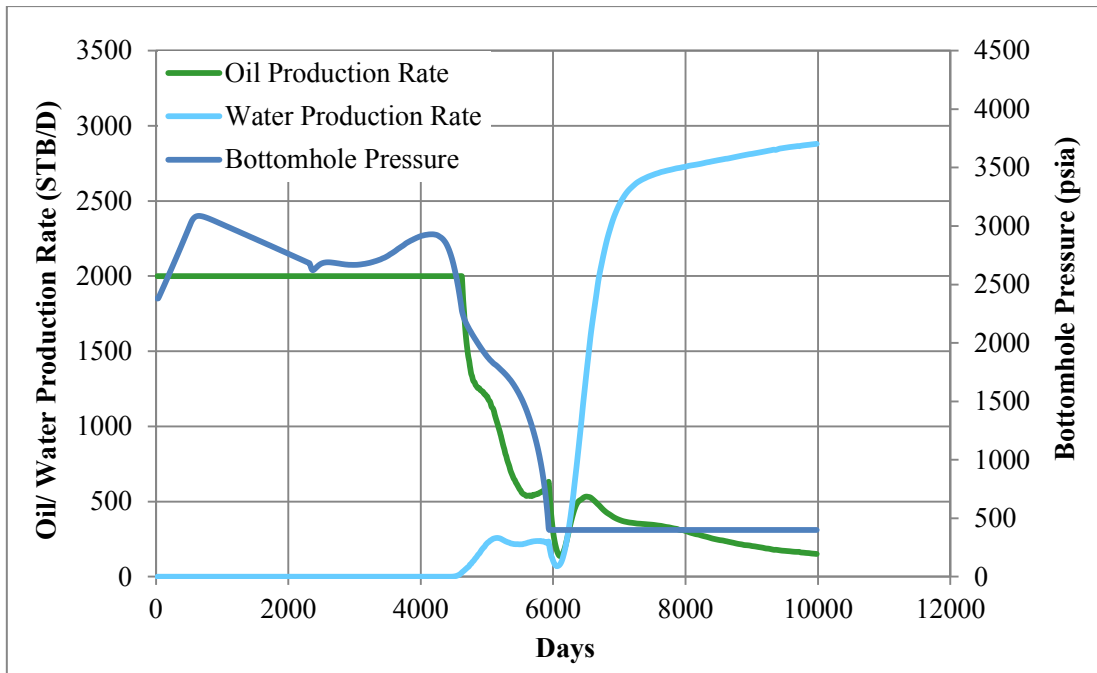on fining upward reservoir model with 45 degree dip angle

In summary for fining upward cases and 45 degree dip angle, increasing in heterogeneity index results in earlier water production and consequently oil production cannot be sustained at maximum target rate. However, with the case of low heterogeneity index, L_c of 0.18, production terminates earliest due to oil production is lower than minimum limit. In contrast, with the case of higher heterogeneity index, such as L_c of 0.25, 0.32, 0.38, production terminates from water production exceeding water cut limit, whereas, the case of L_c of 0.44, production can be extended up to end of concession period. Despite, increasing heterogeneity index can prolong a number of production days which is mainly by effect of water; it does not help in increasing oil recovery owing to earlier reduction in plateau oil production rate.

Second part of discussion in this section is based on Figure 5.24, where oil recoveries are plotted versus heterogeneity index. In this part, reservoir is constructed to have coarsening upward lithofacies and dip angle is also added. Cases are categorized as group 6-10 in Table 5.5.

It is observed that there are likely to get two trends on this figure. First trend is obtained from plots of no dip angle and 15 degree dip angle, whereas another different trend is can be seen from plots of 30 and 45 degrees dip angle.

From plots with first trend based on Figure 5.24, it looks like the lowest heterogeneity index yields the highest recovery compared to other values on the same line. Then, there is a fall of oil recovery when reservoir heterogeneity increases. Later, the highest heterogeneity bounces up oil recovery again. However, it is remarkable that, without dip angle, oil recovery at the lowest L_c of 0.18, is visibly dipped. This can be investigated based on oil production rate.

From this reservoir model without dip angle line and L_c of 0.18, even oil production rate can be sustained at maximum rate for the longest period compared to other heterogeneity indexes as seen in Figure 5.33, it obtains the lowest oil recovery. This occurs from production that terminates earliest at about day 5,800 due to oil production rate drops below minimum limit. Early termination of production in this case is caused by no pressure support from water displacing residual oil ahead to producer. Figure 5.34 shows water production profile of cases with no dip angle and it can be seen that only a trace amount of water can be produced from the case L_c of

0.18. This case is compared with the same heterogeneity value but with 15 degree dip degree. Oil production in this latter case can be achieved at highest amount compared to the same dip angle, as it can be maintained maximum for the longest period and a declination of this period is considered as affected from gas production. Although, total production period on the case L_c of 0.18 with 15 degree is finished earliest, difference from other heterogeneity values is not much different as seen in Figure 5.35. This similar result is caused by water production as shown in Figure 5.36. This water pushes an amount of residual oil inside pore space to production well. Therefore, oil production can be extended above minimum oil production constraint and it shows the best performance on this plot.

Figure 5.33 Oil production rates as functions of time for all heterogeneity index cases on coarsening upward reservoir model with zero dip angle
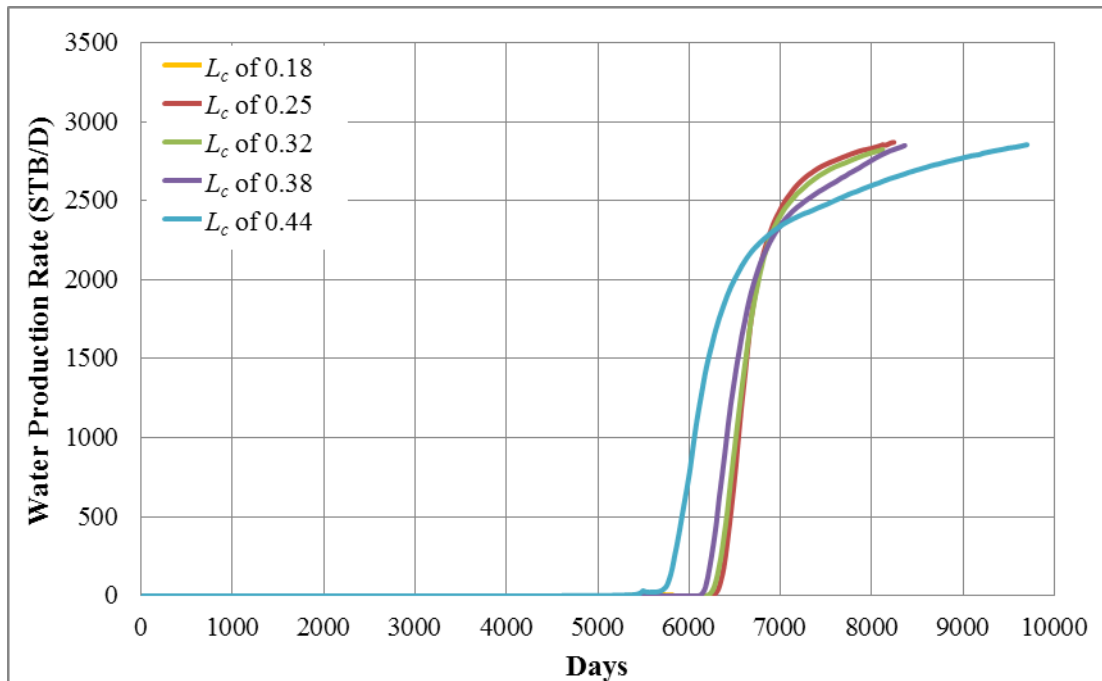
Figure 5.34 Water production rates as functions of time for all heterogeneity index cases on coarsening upward reservoir model with zero dip angle
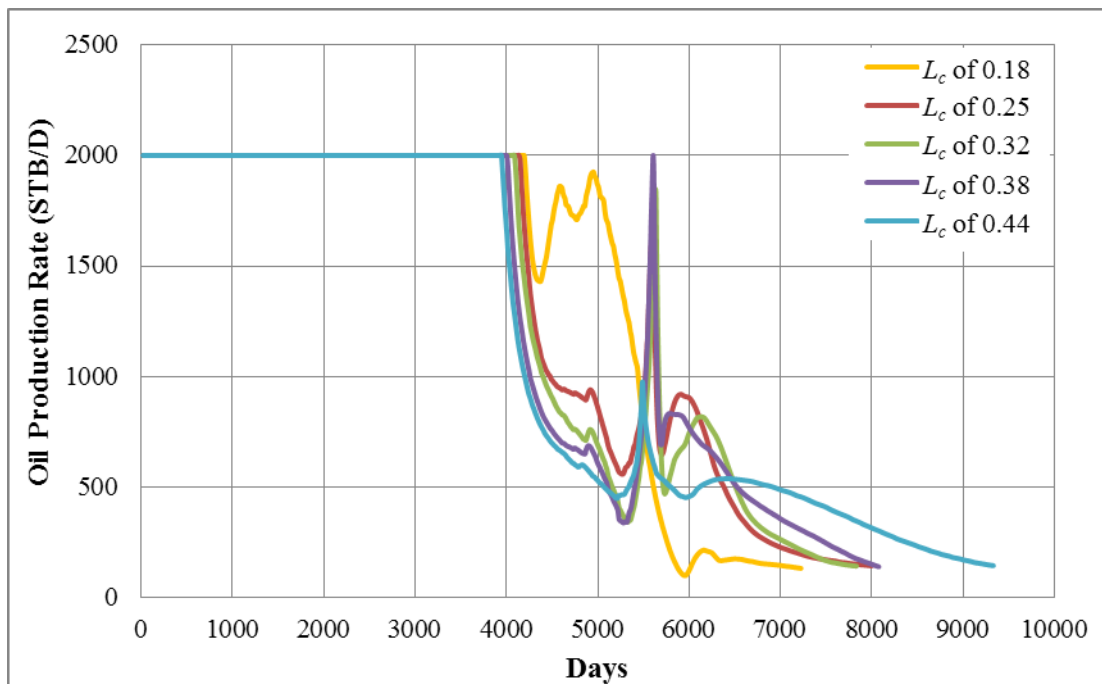
Figure 5.35 Oil production rates as functions of time for all heterogeneity index cases on coarsening upward reservoir model with 15 degree dip angle
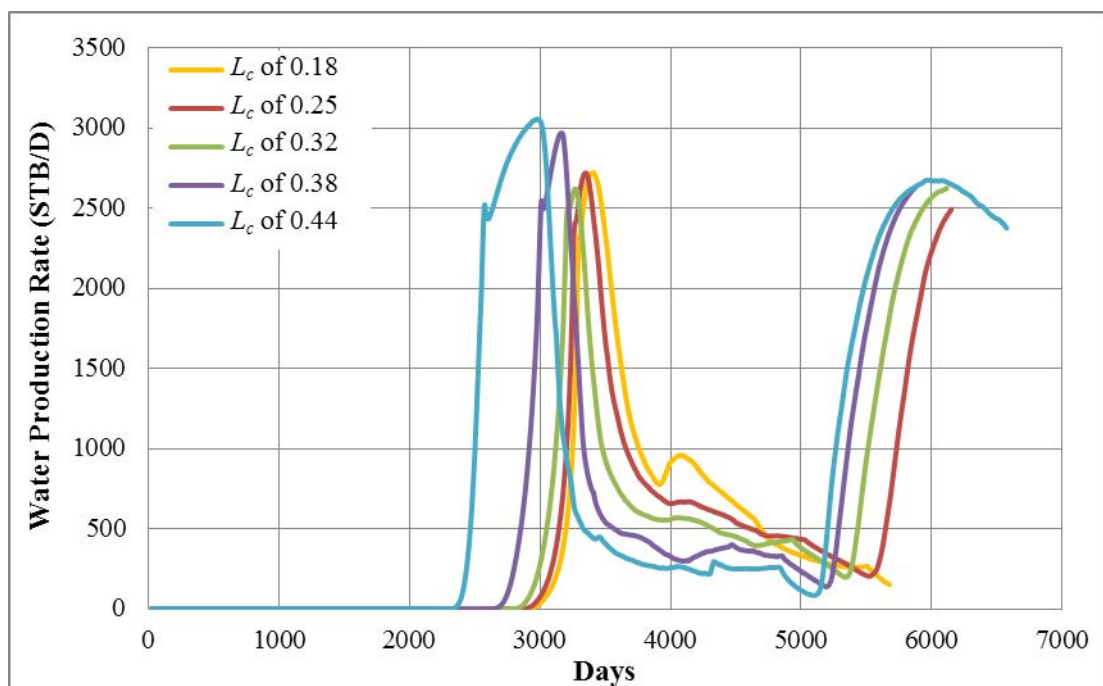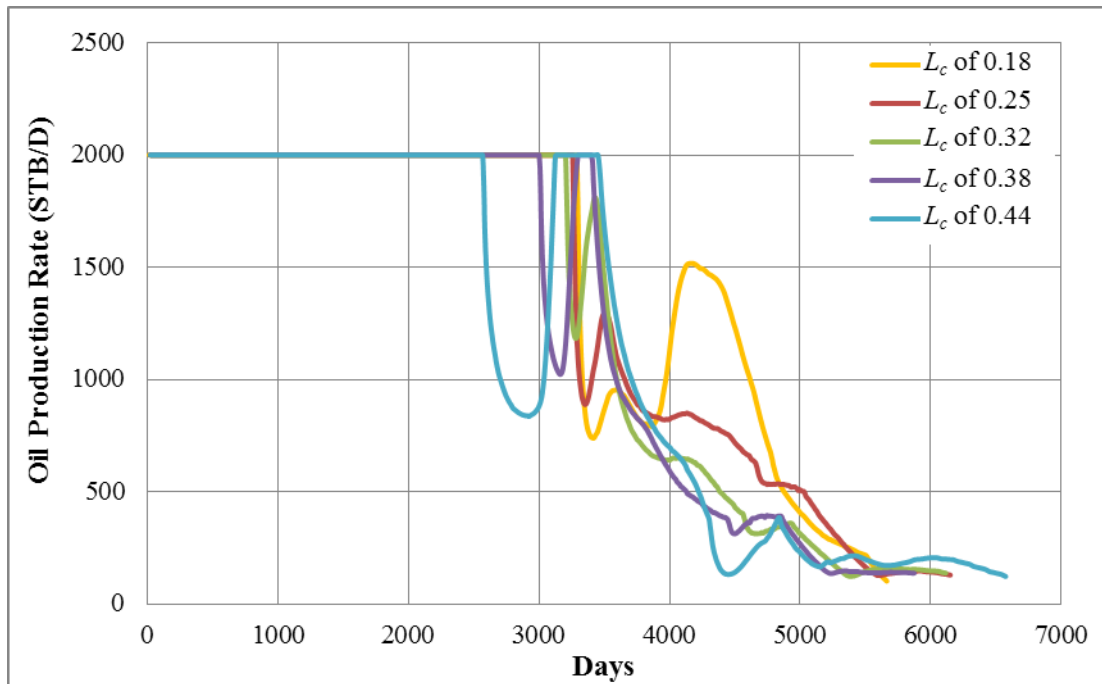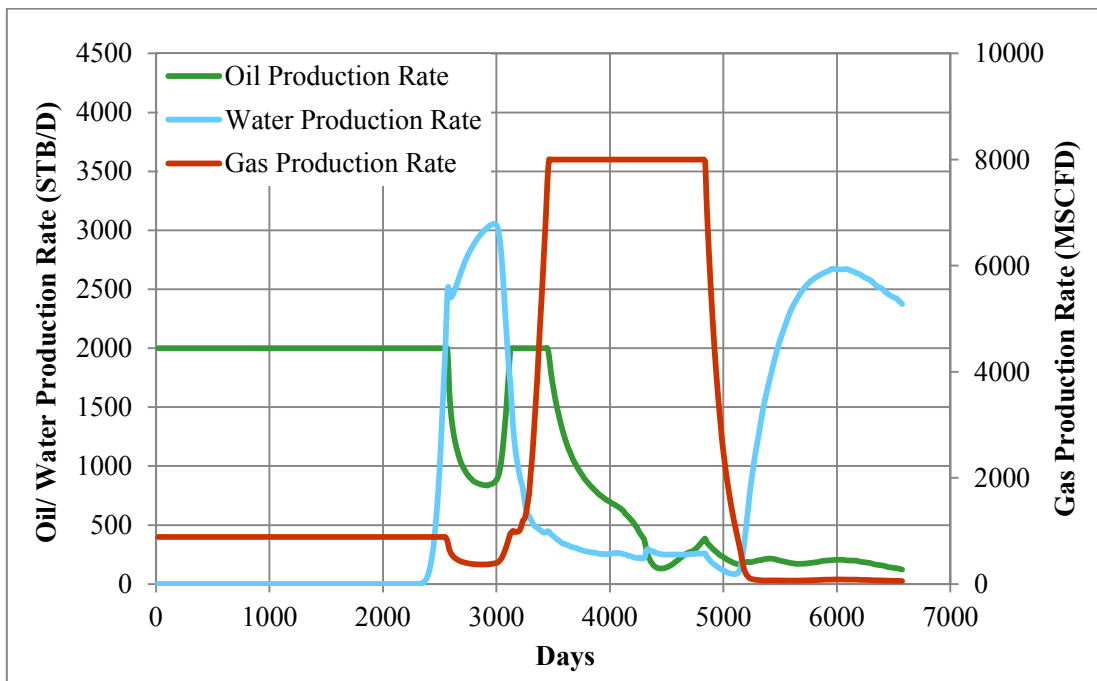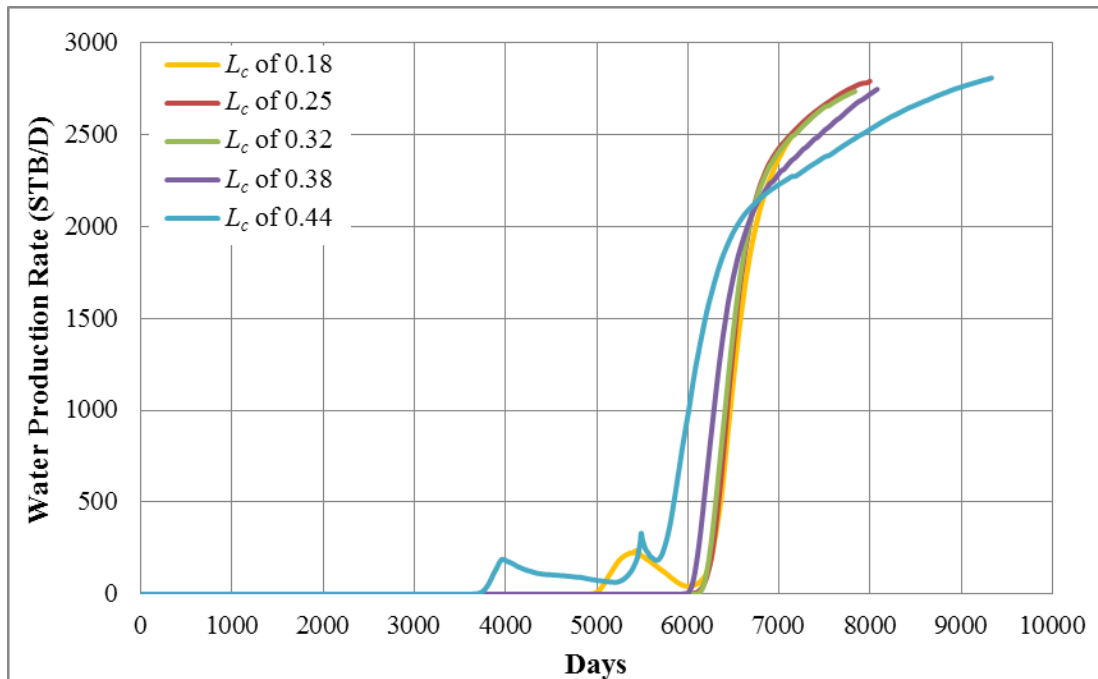
Figure 5.36 Water production rates as functions of time for all heterogeneity index cases of coarsening upward reservoir model with 15 degree dip angle

At heterogeneity index L_c of 0.25, on plot of reservoir without dip angle, oil recovery from this case increases from previous heterogeneity due to longer oil production period which is a result from breakthrough of injected water, sweeping oil forwards to producer. This helps to maintain oil production rate above minimum oil production constraint. Based on oil production profile in Figure 5.33, it can be seen that there are two other peaks from this profile. These two peaks are affected by gas and water production, respectively. For example, in the case of L_c of 0.25 as shown in Figure 5.37, oil is produced at plateau rate for 4,180 days. At the meantime, gas is produced at constant rate of 900 MSCFD, which is considered as solution gas because reservoir pressure is still higher than bubble point pressure. Gas production starts increasing due to gas breakthrough at day of 3,600 and it reaches to maximum production limit at day of 4,180. At this day, it is also coincident with decline rate of oil production which. This occurs from big amount of gas arrival at producer, together with production constraint of gas that is limited at maximum 8,000 MSCFD, so it prevents flow of oil by reducing relative permeability to oil. During maximum gas

production rate, it can be noted that there is a point where oil production rate increases again. It is likely to be a situation where gas located near wellbore is mostly produced. After retaining at maximum limit for a while, a substantial drop of gas production can be pointed out at around day 5,580. At this day, oil production rate is at the highest value of its first peak and then it falls again owing to minimum bottomhole pressure limitation at producer. Figure 5.38 illustrates gas saturation of this case at the days which gas breakthrough, gas reaching maximum production rate and declining of gas production rate. The second peak comes later on and it is responsible by injected water because this peak comes together with water at day of 6,200. In the case L_c of 0.44 where high permeability channels are mostly located at top section of reservoir, water production starts at the earliest day compared to lower heterogeneity cases but it is relatively slow in increasing, resulting in the longest production and yields higher oil recover again. Permeability variation in this heterogeneity index acts as a restriction at lower part of reservoir, so good water flow on top part is found in Figure 5.39.

Figure 5.37 Oil, water, gas production rates as functions of time for case L_c of 0.25 on coarsening upward reservoir model with zero dip angle
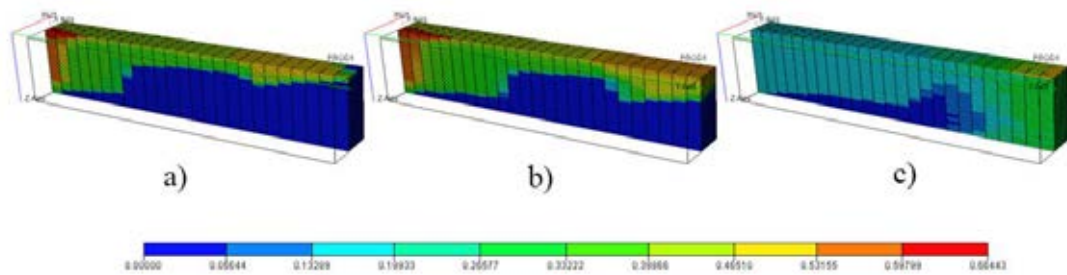
Figure 5.38 Evolution of gas saturation for case L_c of 0.25 on coarsening upward reservoir model with zero dip angle at a) gas breakthrough b) gas reaching maximum rate, and c) declining of gas production rate
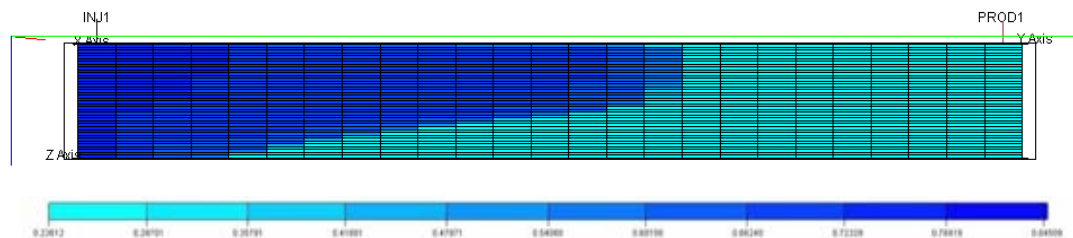
Figure 5.39 Water saturation profile for case L_c of 0.44 on coarsening upward reservoir model with zero dip angle

Second trend of oil recovery as a function of heterogeneity in coarsening upward lithofacies shown Figure 5.24 is considered by results obtained from models with 30 and 45 degrees dip angle. This trend shows a continuous deduction in oil recovery while increasing heterogeneity index.

First heterogeneity index for the case of 45 degree, L_c of 0.18 yields the highest oil recovery compared to other heterogeneity indexes. Similar to previous explanation, this is considered as low heterogeneity index that can help in maintaining the longest plateau oil production rate which is illustrated in Figure 5.40 due to a late coming of water and gas. It can be also noted that an extra oil production is from another huge peak coming up about day 3,800. In this case, water and gas reach production well relatively close as displayed in Figure 5.41. As water and gas are both produced for almost 200 days, they dramatically reduce relative permeability to oil and consequently oil production rate drops substantially. Furthermore, water and gas

productions also reduce bottomhole pressure to minimum value which switches production mode to control by bottomhole pressure as shown in Figure 5.42. The large peak of oil production rate which only occurs in this case improves oil recovery and this is a result from large water production in an early period, sweeping residual oil to producer, whereas this large water production peak does not exist in other cases. Furthermore, from Figure 5.24, increasing heterogeneity index in this highly inclination model results in decreasing of oil recovery. This reduction can be viewed as an impact from an arrival of both water and gas. Increasing heterogeneity index in high dip angle reservoir can cause an early breakthrough of water due to gravity segregation as seen in Figure 5.43. A big slug of pre-flushed water, which is early produced in the case of L_c 0.44, shortens plateau oil production rate as seen in Figure 5.44 and high permeability channels in the upper reservoir part also result in lower swept area by miscible bank, leaving higher oil saturation in reservoir. Figure 5.45 confirms impact of heterogeneity on oil saturation at the end of production, comparing between cases L_c of 0.18 and 0.44.
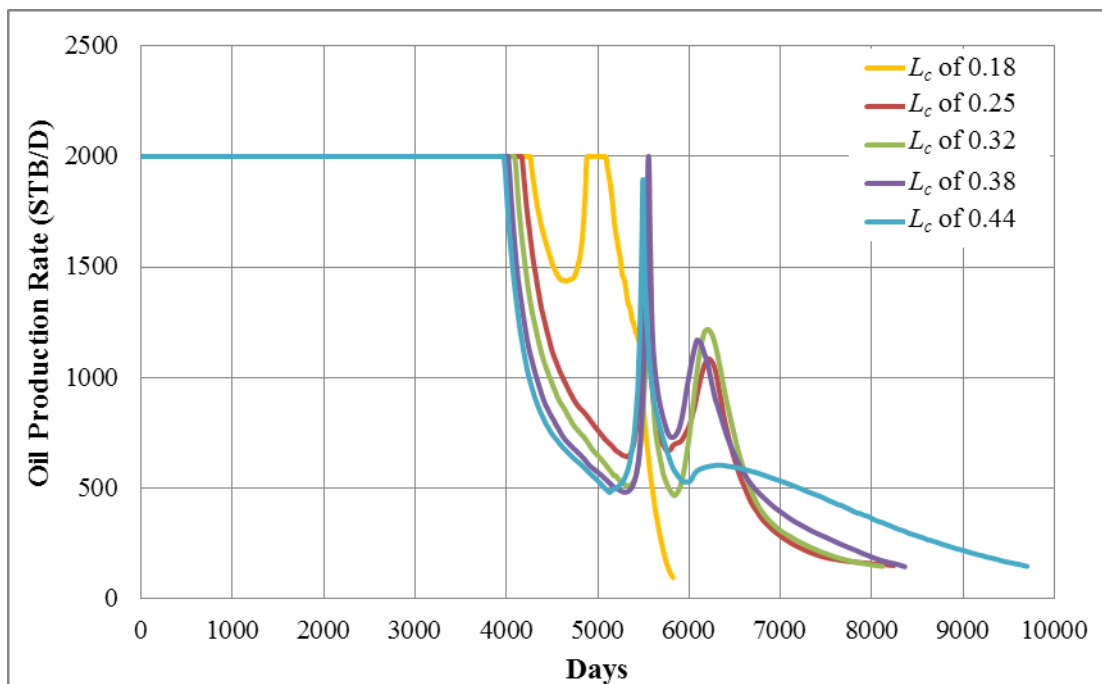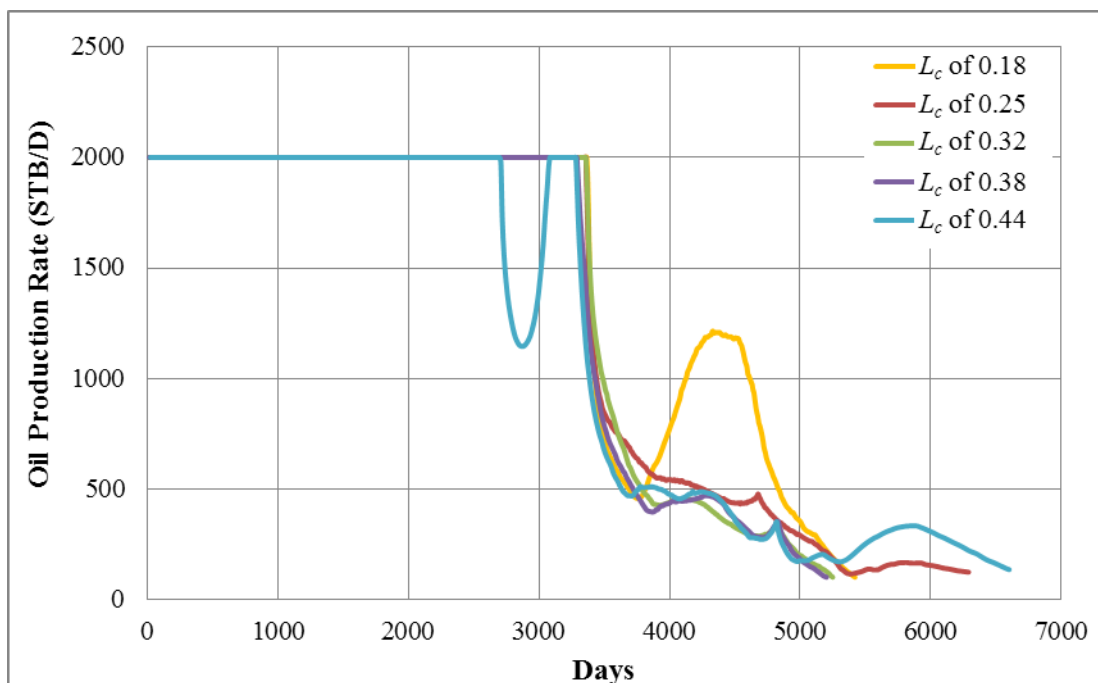

Figure 5.40 Oil production rates as functions of time for all heterogeneity index cases on coarsening upward reservoir model with 45 degree dip angle
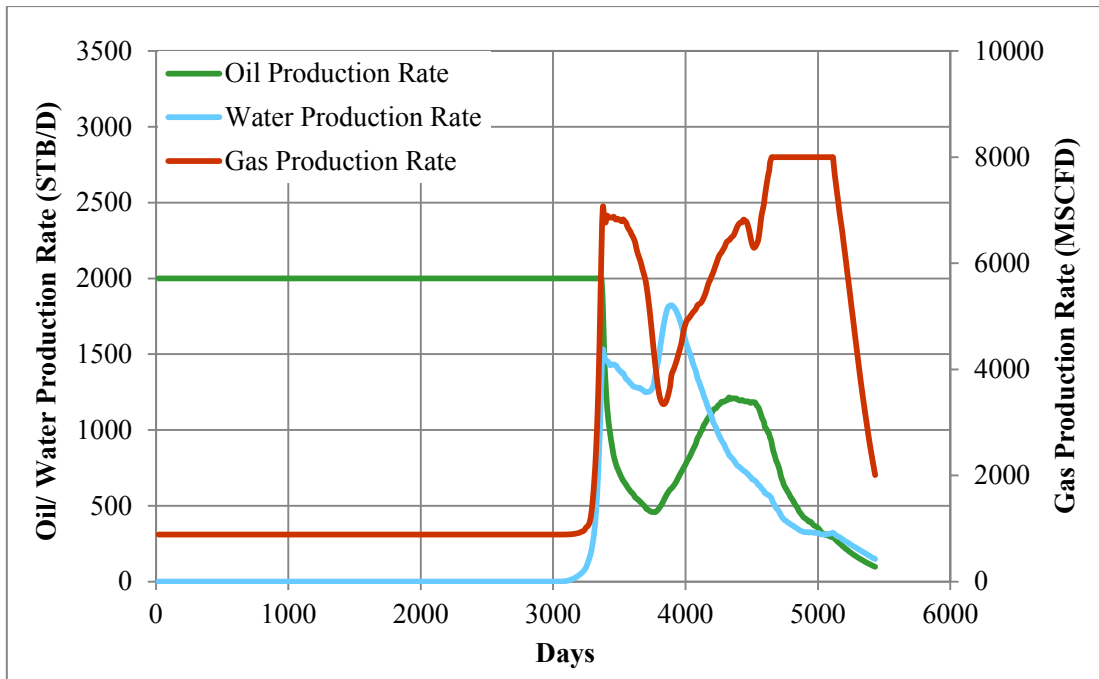
Figure 5.41 Oil, water and gas production rates as functions of time for case L_c of 0.18 on coarsening upward reservoir model with 45 degree dip angle
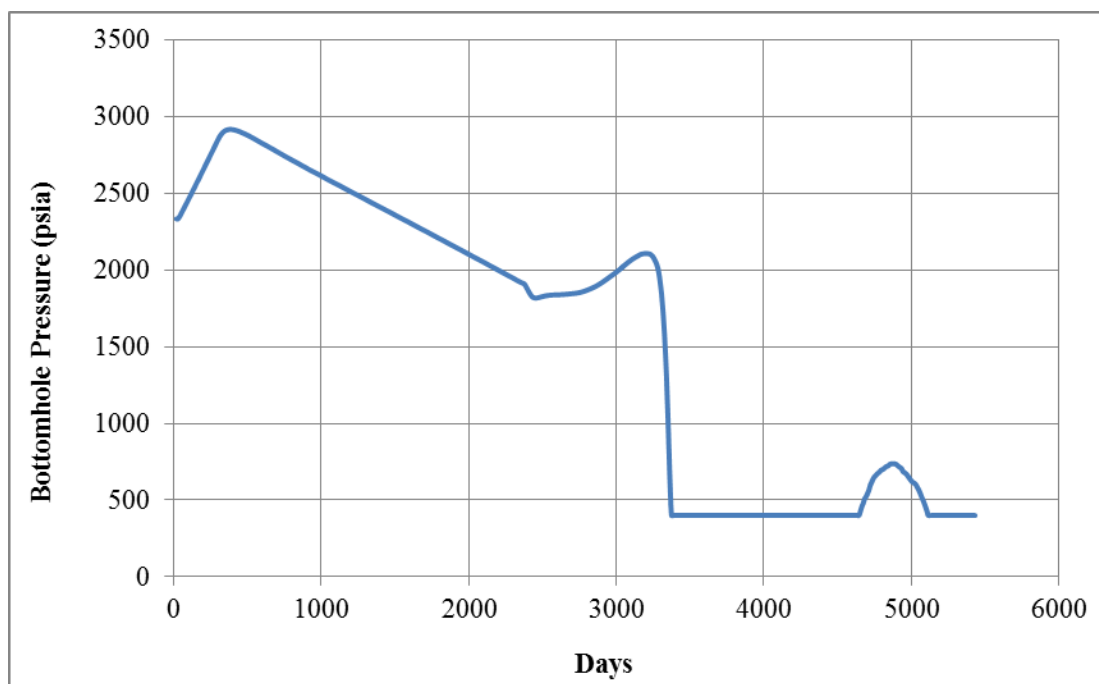
Figure 5.42 Bottomhole pressure as a function of time at production well for case L_c of 0.18 on coarsening upward reservoir model with 45 degree dip angle
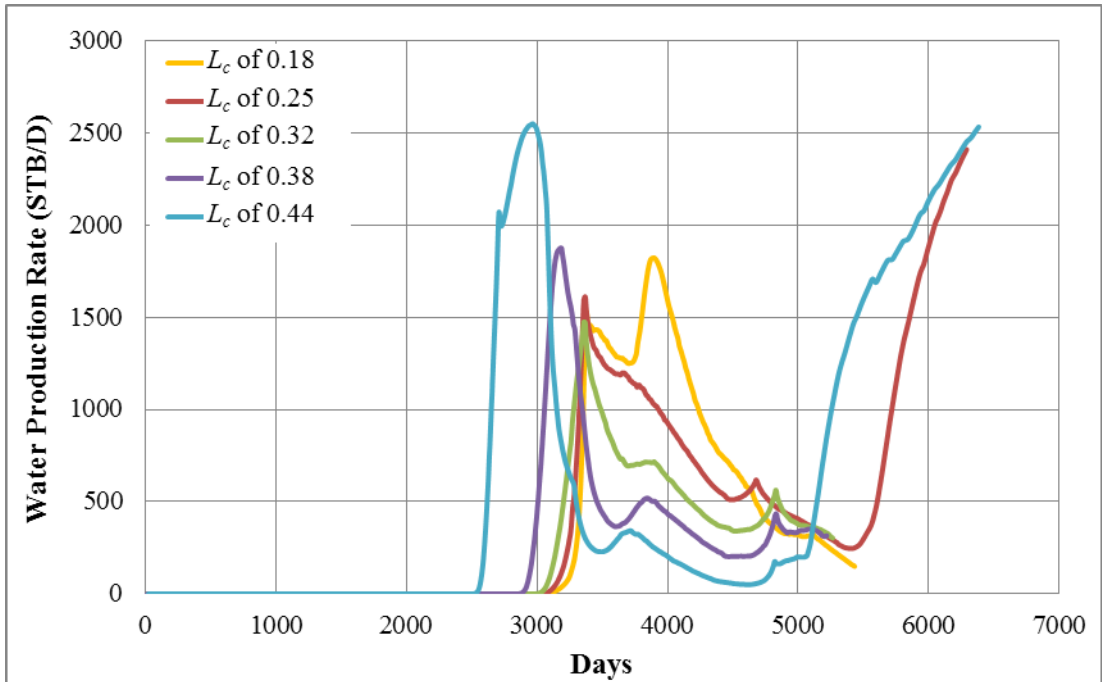
Figure 5.43 Water production rates as functions of time for all heterogeneity index

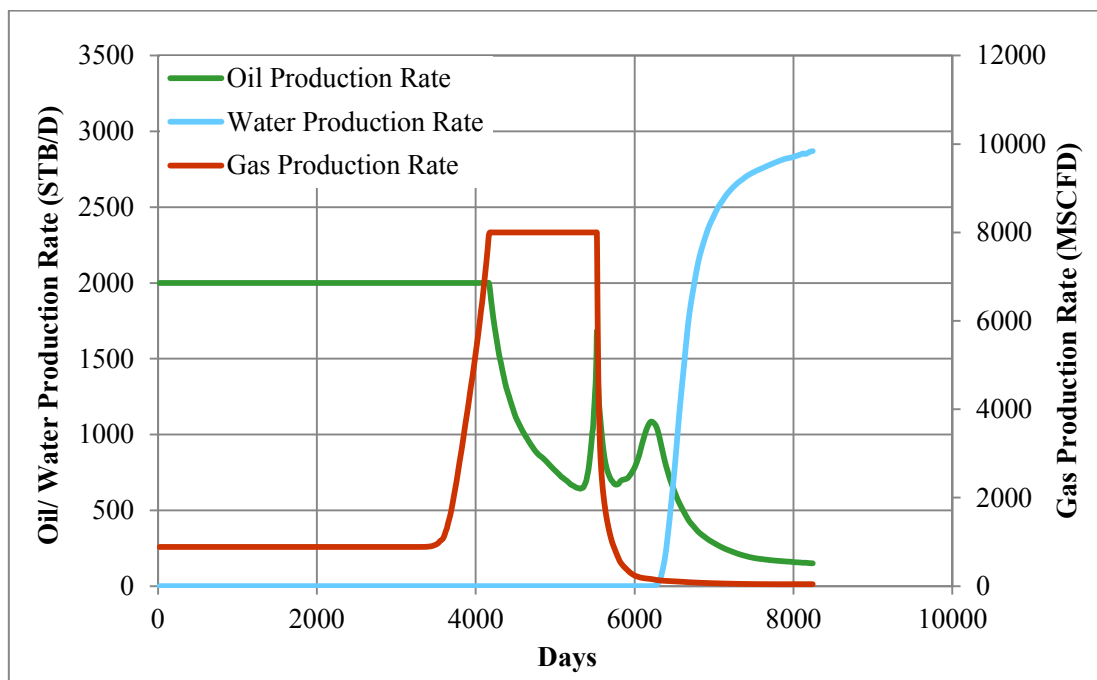cases on coarsening upward reservoir model with 45 degree dip angle
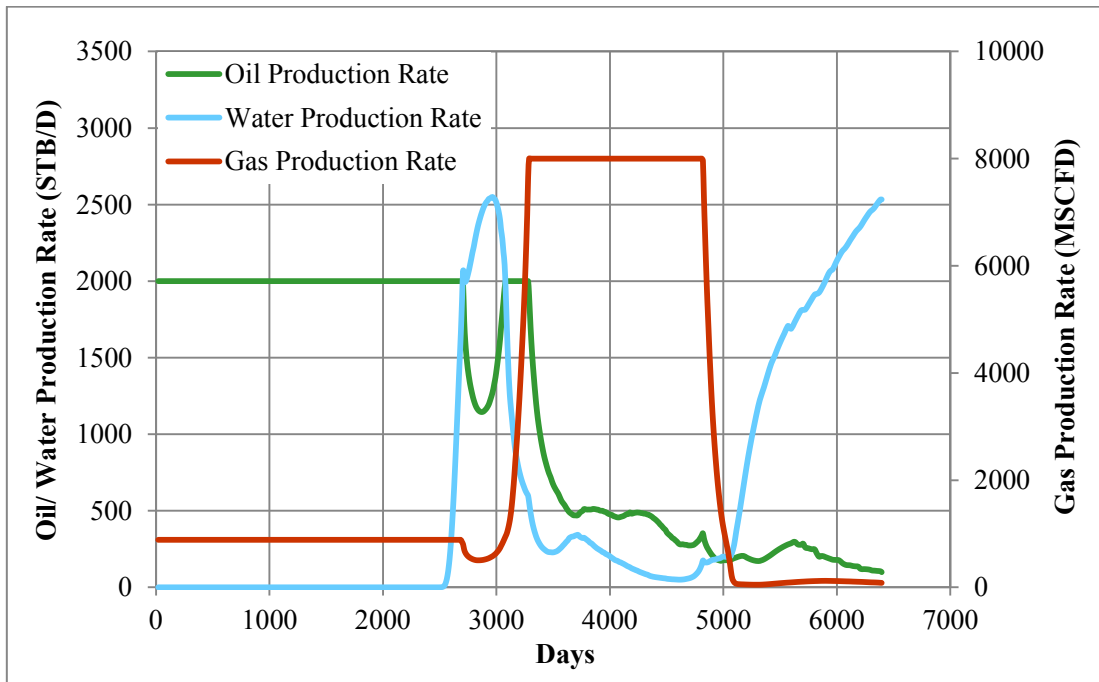
Figure 5.44 Oil, water and gas production rates as functions of time for

case L_c of 0.44 on coarsening upward reservoir model with 45 degree dip angle
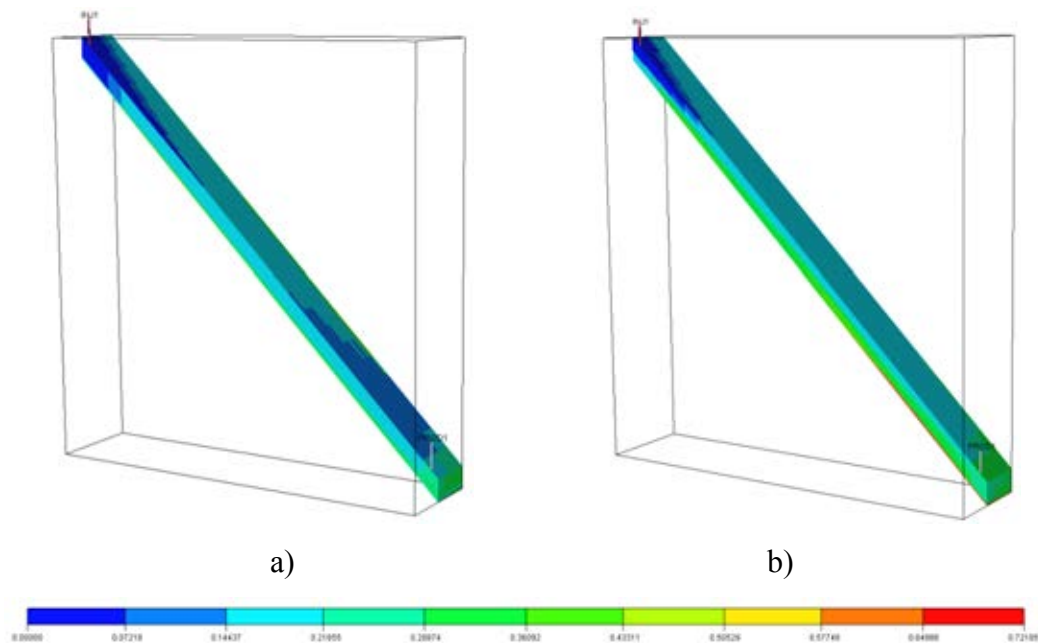
Figure 5.45 Oil saturation profile at the end of production on coarsening upward
reservoir model with 45 degree dip angle a) L_c of 0.18 and b) L_c of 0.44

In conclusion, for coarsening upward reservoir with zero dip angle, low heterogeneity index can help maintaining stable flood front. However, production is terminated earliest due to rapid drop of oil production below minimum limit as there is no water support on time which could help in sweeping additional oil and maintain oil production above minimum limit. This situation occurs only in horizontal reservoir case. When inclined reservoir is considered such as dip angle 15 degree, gravity segregates water to flow downward better than other fluids and so water breakthrough emerges earlier compared to case without inclination. Therefore, oil can be produced for longer period as a result of water which sweeps residual oil to producer. High heterogeneity index results in unstable flood front, showing gradual increase of water production. This retards maximum limit of water cut at producer compared to cases with lower heterogeneity, and since producer is maintained to produce for longer time, extra oil recovery is achieved accordingly. Although, increasing in dip angle at low heterogeneity index can prolong production period and can increase oil recovery, oil recovery gets continuously lowering when increasing heterogeneity index for case of 30 and 45 degree. It is a result from water which plays a major role impacting

performance because water which is injected from updip location flows downward quickly. Thus, the more increasing in heterogeneity index, the earlier water arrives to producer. Moreover, gas which is light material also flows easily to upper part of this coarsening upward model, leaving oil at the bottom part un-swept. Consequently, poorer oil recovery is obtained. All simulation results in this section are summarized in Table 5.6.

Table 5.6 Summary of simulation results on the study of reservoir dip angle when applied with reservoir heterogeneity for both fining and coarsening upward sequence

Case	Dip Angle (degree)	L_c	Cumulative Gas Production (BSCF)	Cumulative Water Production (MMSTB)	Oil Recovery (%)	Total Production Period (days)
Fining Upward Sand Model						
1A		0.18	15.07	0.34	66.33	6,376
1B		0.25	15.90	0.28	62.94	6,215
1C	0	0.32	16.42	9.81	67.10	9,982
1D		0.38	16.65	11.05	66.79	10,307
1E		0.44	16.71	13.71	66.57	10,958
2A		0.18	15.47	0.66	67.00	6,382
2B		0.25	16.50	8.57	68.24	9,578
2C	15	0.32	16.81	8.99	67.00	9,656
2D		0.38	16.93	10.51	66.86	10,062
2E		0.44	16.89	14.27	66.63	10,958
3A		0.18	15.99	1.28	67.66	6,125
3B		0.25	16.46	3.68	66.27	7,300
3C	30	0.32	16.86	9.34	67.01	9,410
3D		0.38	16.86	10.26	65.93	9,532
3E		0.44	16.42	14.78	64.72	10,688

Table 5.6 Summary of simulation results on the study of reservoir dip angle when applied with reservoir heterogeneity for both fining and coarsening upward sequence (continued)

Case	Dip Angle (degree)	L_c	Cumulative Gas Production (BSCF)	Cumulative Water Production (MMSTB)	Oil Recovery (%)	Total Production Period (days)
4A		0.18	15.64	2.10	68.69	5,664
4B		0.25	16.03	2.87	66.39	6,151
4C	45	0.32	16.02	3.07	64.04	6,116
4D		0.38	15.85	2.89	62.46	5,874
4E		0.44	15.62	5.52	61.49	6,575
Coarsening Upward Sand Model						
5A		0.18	16.81	Trace	61.37	5,817
5B		0.25	17.13	4.44	63.15	8,242
5C	0	0.32	17.52	4.08	61.88	8,118
5D		0.38	17.67	4.86	62.08	8,361
5E		0.44	17.63	9.16	63.47	9,700
6A		0.18	17.43	1.87	64.53	7,224
6B		0.25	17.49	3.92	63.54	7,998
6C	15	0.32	17.83	3.48	62.08	7,832
6D		0.38	17.98	4.24	62.08	8,050
6E		0.44	17.93	8.25	62.78	9,331
7A		0.18	16.78	0.82	64.60	5,844
7B		0.25	17.32	3.04	63.53	7,282
7C	30	0.32	17.55	2.96	62.12	7,219
7D		0.38	17.79	3.84	61.96	7,523
7E		0.44	17.62	6.29	61.63	8,182
8A		0.18	15.88	1.84	65.82	5,425
8B		0.25	15.62	2.82	63.40	6,291
8C	45	0.32	16.08	1.25	61.31	5,255
8D		0.38	16.25	1.19	60.14	5,210
8E		0.44	16.40	4.39	60.77	6,395

An occurrence of miscible bank is introduced again in this section in order to ensure whether the bank can be found and is actually formed by vaporizing mechanism between CO_2 and reservoir fluid. Similar to the previously mentioned occurrence in Section 5.1.2, a reduction in oil viscosity is used to monitor this matter. Figure 5.46 shows oil viscosity at each step during production from the case of heterogeneity index of L_c 0.18 without inclination. As miscible bank is considered as a zone where oil viscosity is deducted, it can be seen that after CO_2 is injected for only a couple of years, a miscible bank is formed. Deduction of viscosity found is a result from vaporizing mechanism of CO_2 which can vaporize intermediate hydrocarbon into its gaseous phase, leaving more viscous hydrocarbon behind. However, as model is heterogeneous in permeability, instability of flood front can be seen. Flood front mostly runs under the bottom part of reservoir for fining upward case, whereas it preferably goes to upper part for coarsening upward case. This is a result from values of permeability used to construct a heterogeneity index. Additionally, high mobility of gas causes an earlier breakthrough in the case of coarsening upward as seen from Figure 5.46. Flood front in this case can reach the producer only after four years of continuous CO_2 injection. Good mobility of gas in high permeability streak also lowers activity of contacting between CO_2 and reservoir oil. This reduces vaporization efficiency, leading to higher amount of intermediate hydrocarbon left in reservoir illustrated by green and orange color on oil saturation profile in Figure 5.47 at the end of production. It is also align with previous figure that higher amount of oil is not swept by miscible bank in the case of coarsening upward sequence colored by green near the bottom part of reservoir.
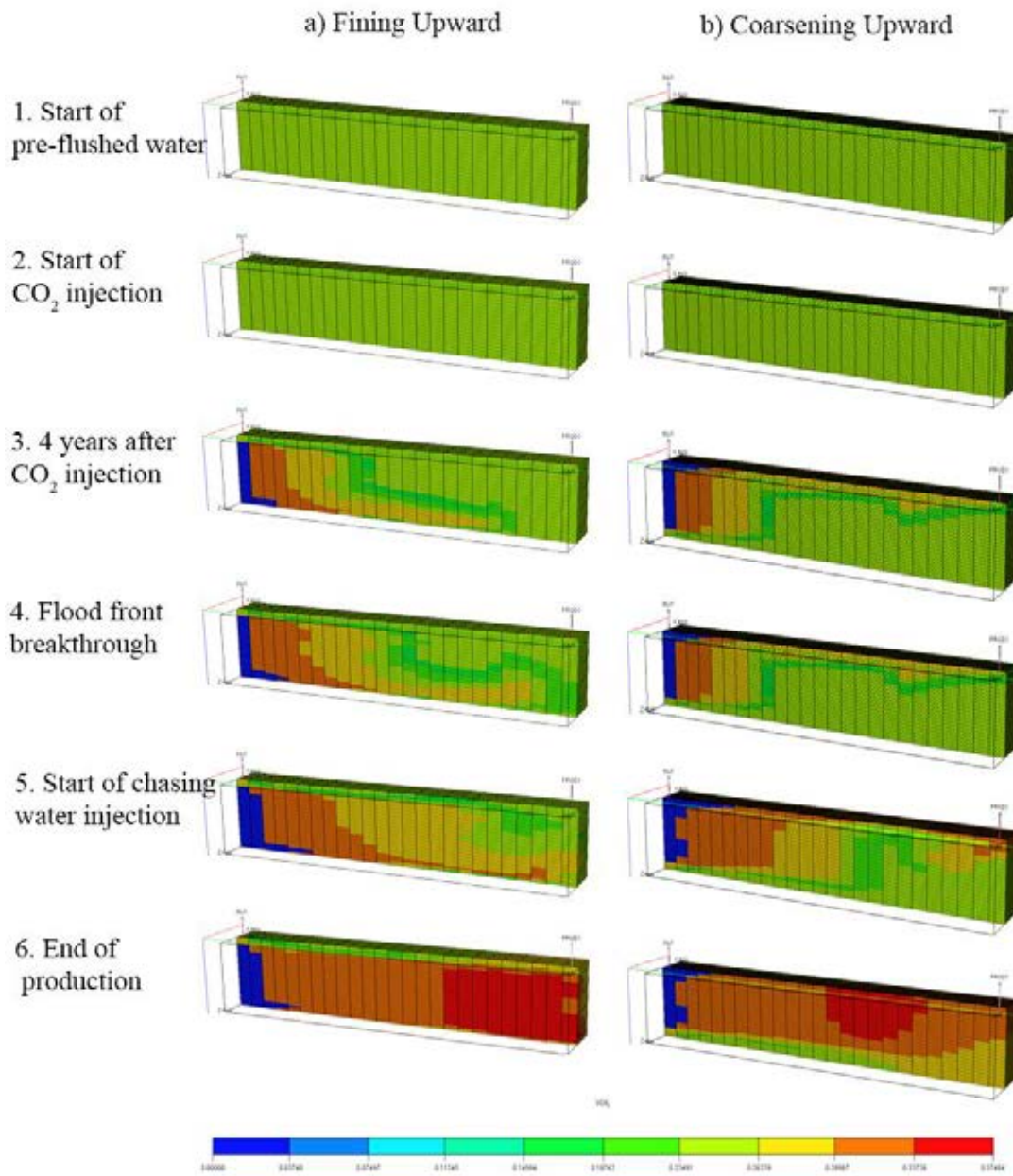
Figure 5.46 Oil viscosity profile at different production period between
a) fining upward b) coarsening upward with heterogeneity index L_c of 0.18
without reservoir dip angle
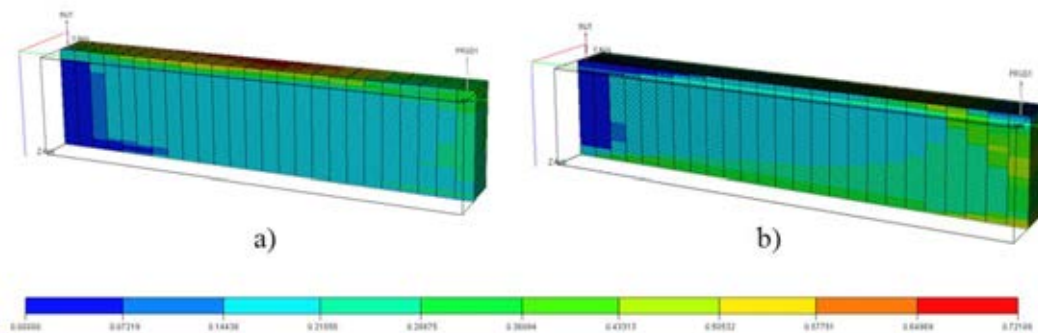
Figure 5.47 Oil saturation profile at the end of production compared between
a) fining upward b) coarsening upward with heterogeneity index L_c of 0.18
without reservoir dip angle

It should be concerned when performing CO_2 flooding in inclined reservoir that pre-flushed water injection from updip location can cause production problem from early water breakthrough which is impacted by gravity segregation. Consequently, oil recovery obtained might be lower than the case of injecting at downdip location. An additional waterflooding scenario with an injector located at downdip location is simulated and result is compared with the study CO_2 flooding case in order to ensure that an outcome from CO_2 flooding case is better. Models simulated with 45 degree dip angle on both fining upward and coarsening upward are selected to see this effect since these cases might yield boundary result. Table 5.7 summarizes additional cases where injector is located downdip and Figure 5.48 compares well location between original flooding scheme and additional waterflooding scheme.

Table 5.7 Summary of additional study cases when injector is located downdip

Case no.	Dip Angle	Depositional Sequence	Heterogeneity Index (L_c)	Injector Location
1		Fining Upward	0.18	I = 11, J = 25
2	45°		0.44	I = 11, J = 25
3		Coarsening Upward	0.18	I = 11, J = 25
4			0.44	I = 11, J = 25
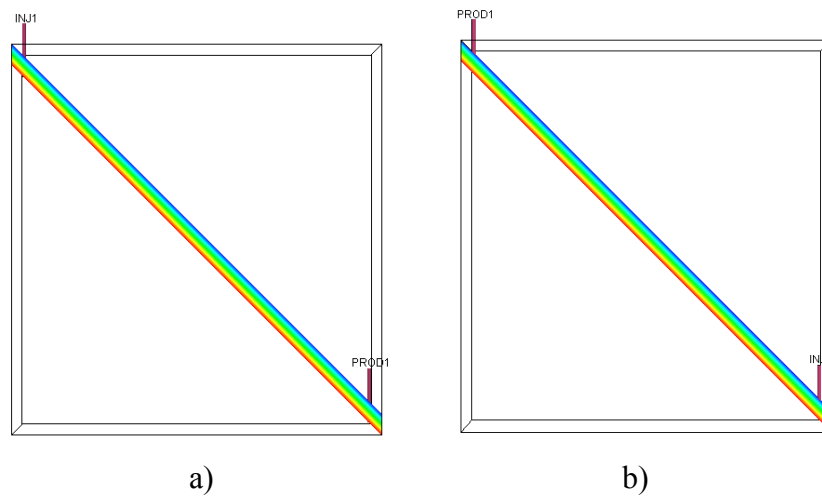
Figure 5.48 Side view of reservoir model showing location of injector in
a) original flooding scheme b) additional waterflooding case

Simulation results indicate that with original CO_2 flooding scheme where injector is located updip, the performance of this case is still better, yielding higher oil recovery. This higher oil recovery is a result of miscible displacement which is about eight percent relatively higher. Although, the selected cases are constructed with the highest value of dip angle, when applied CO_2 flooding with low heterogeneity index, this still show a good performance. However, there is an important notice that gravity segregation impacts flooding performance when reservoir is highly inclined together with high value of heterogeneity. Almost the same oil recovery is obtained from both scenarios as indicated in Table 5.8, but CO_2 miscible flooding can reach this recovery within a significantly shorter period, so it is still a good alternative in term of a number of oil recovery and without investment concern.

Table 5.8 Comparison of oil recovery obtained from waterflooding case when injector is located downdip and CO_2 miscible flooding case on 45 degree dip angle model

No.	Dip Angle	Depositional Sequence	Heterogeneity Index (L_c)	Waterflood from Downdip		CO_2 Miscible Flood	
				Oil recovery (%)	Total Production Period (days)	Oil recovery (%)	Total Production Period (days)
1		Fining Upward	0.18	59.80	5,649	68.69	5,664
2	45°		0.44	61.32	9,057	61.49	6,575
3		Coarsening Upward	0.18	59.88	5,649	66.21	5,425
4			0.44	61.67	8,451	61.23	6,395

5.4.2 Effect of CO_2 Injection Rate

Reservoir pressure can be raised by means of CO_2 injection due to its high compressibility. Reservoir pressure is one of the key parameters controlling displacement efficiency. Pressure must be higher than MMP in order to create miscibility. It might be said that the higher the reservoir pressure, the more chance of miscible bank to be formed. This considerably leads to an improved performance in oil recovery. CO_2 injection rate which is interrelated to injection pressure is therefore studied in this part.

Additional four injection rates covering 6, 10, 12 and 14 MMSCFD deviated from base case injection rate (8 MMSCFD) are chosen to simulate on the model without dip angle. Variation of heterogeneity index together with lithofacies is studied in this section. Although injection rate of CO_2 is changed, designed CO_2 slug size is fixed at 0.4 HCPV. All model configurations and controls are kept constant and reservoir pressure is higher than MMP in all cases to ensure that miscibility is occurred. The model is also varied with reservoir heterogeneity. Table 5.9 summarizes simulation cases on the study of CO_2 injection rate.

Table 5.9 Summary of simulated cases on the study of CO_2 injection rate

Group No.	Lithofacies	Heterogeneity Index	CO_2 Injection rate (MMSCFD)
1		0.18	6, 8, 10, 12 and 14
2		0.25	6, 8, 10, 12 and 14
3	Fining Upward	0.32	6, 8, 10, 12 and 14
4		0.38	6, 8, 10, 12 and 14
5		0.44	6, 8, 10, 12 and 14
6		0.18	6, 8, 10, 12 and 14
7		0.25	6, 8, 10, 12 and 14
8	Coarsening Upward	0.32	6, 8, 10, 12 and 14
9		0.38	6, 8, 10, 12 and 14
10		0.44	6, 8, 10, 12 and 14

The simulation results of oil recovery as a function of reservoir heterogeneity index for the study of CO_2 injection rate are plotted in Figure 5.49 and 5.50, respectively.
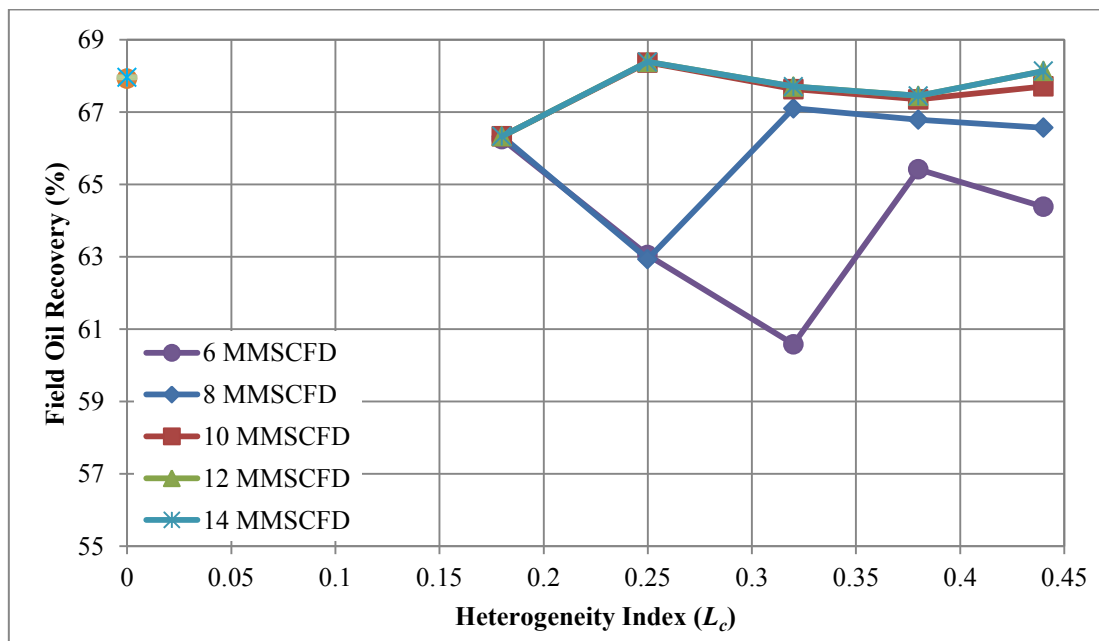
Figure 5.49 Field oil recoveries obtained from different injection rates as functions of heterogeneity index on fining upward reservoir model
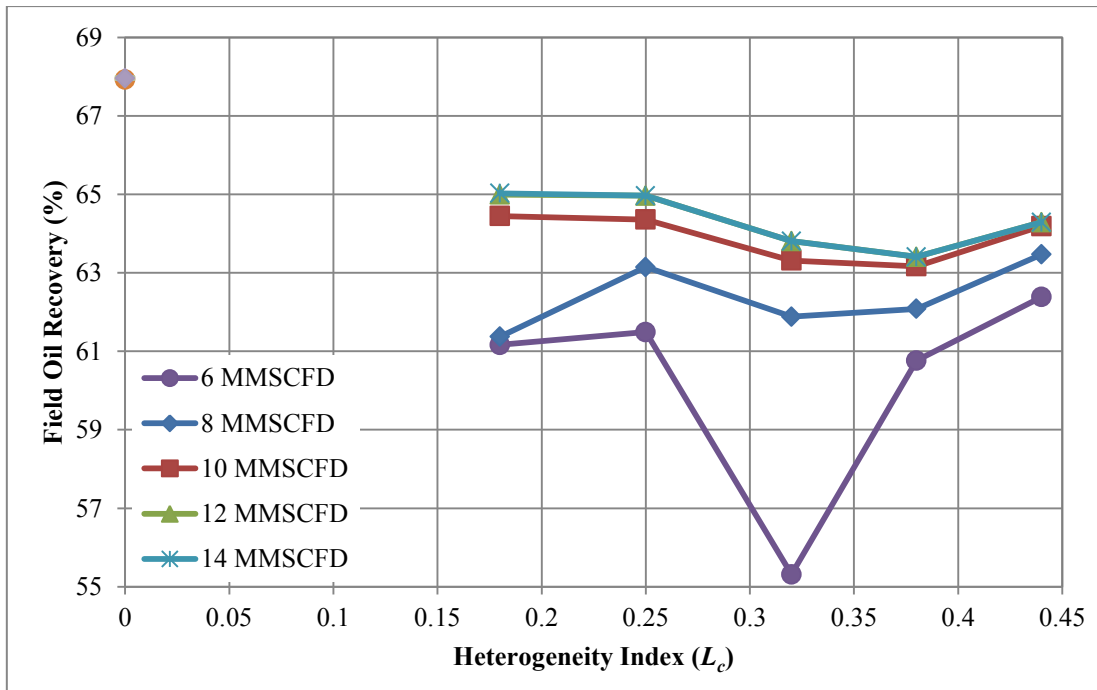
Figure 5.50 Field oil recoveries obtained from different injection rates as functions of heterogeneity index on coarsening upward reservoir model

Discussion on effect of injection rate is split into two parts divided from depositional sequence. The first part is on fining upward lithofacies (group 1-5), whereas the second part is on coarsening upward sequence (group 6-10).

From Figure 5.49 of fining upward model, oil recovery from CO_2 injection rate higher than 10 MMSCFD, can be yielded at greater value compared to lower injection rate and also variation from oil recovery when high heterogeneity index is applied is less than those of lower injection cases.

In fact, these five injection rates give a similar trend of oil recovery when heterogeneity index is varied and it is the same as per the trend on fining upward sequence described in the previous section where the trend is divided into three zones. The first zone drawn as a reduction of oil recovery is found before going up in the second zone and finally the last zone scarcely shows any difference on oil recovery. However, this mentioned trend is not clear for injection rates of 10,12 and 14 MMSCFD based on the studied heterogeneity indexes, because there is no point prior

to the drop as same as two lower injection rates. If the prior heterogeneity index is available in this case, clearly similar trend of these three injection rates may be seen.

With these lines plotted in Figure 5.49, they are quite similar but the lowest oil recovery of each is located on different value of heterogeneity index. This can be investigated by observing an oil production profile displayed in Figure 5.51. From the figure, a fall of oil recovery on the first three heterogeneity indexes in the case of 6 MMSCFD is from shutting in of producer in early period regarding that minimum limit of oil production rate is approached. This can be explained by similar reason from the previous discussion in section 5.4.1 that a slug of chasing water reaching producer can sweep residual oil as shown in water production profile in Figure 5.52. An arrival of this slug is likely to be an effect from instability of water flood front which helps water gradually arrive to producer, instead of stable flood front where there is not any significant amount of pre-flushed or chasing water arriving. Heterogeneity index of 0.38 shows a significant arrival of water, therefore, a longer production period is attained and this enhances oil recovery.
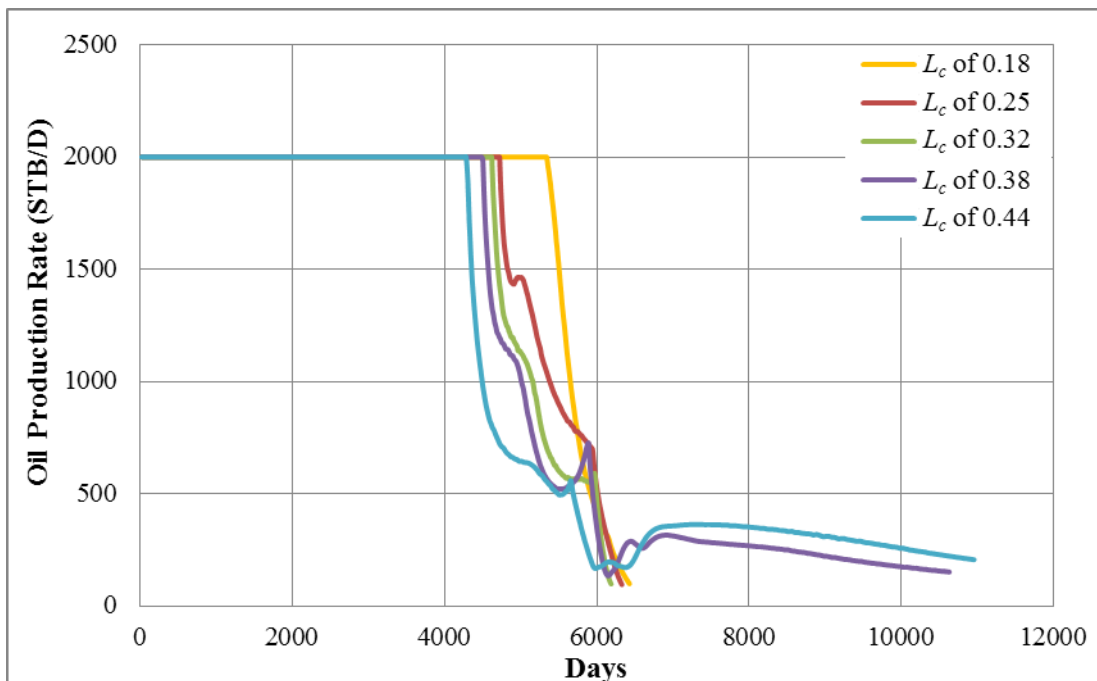
Figure 5.51 Oil production rates obtained from CO_2 injection rate of 6 MMSCFD as functions of time for all heterogeneity index cases on fining upward reservoir model
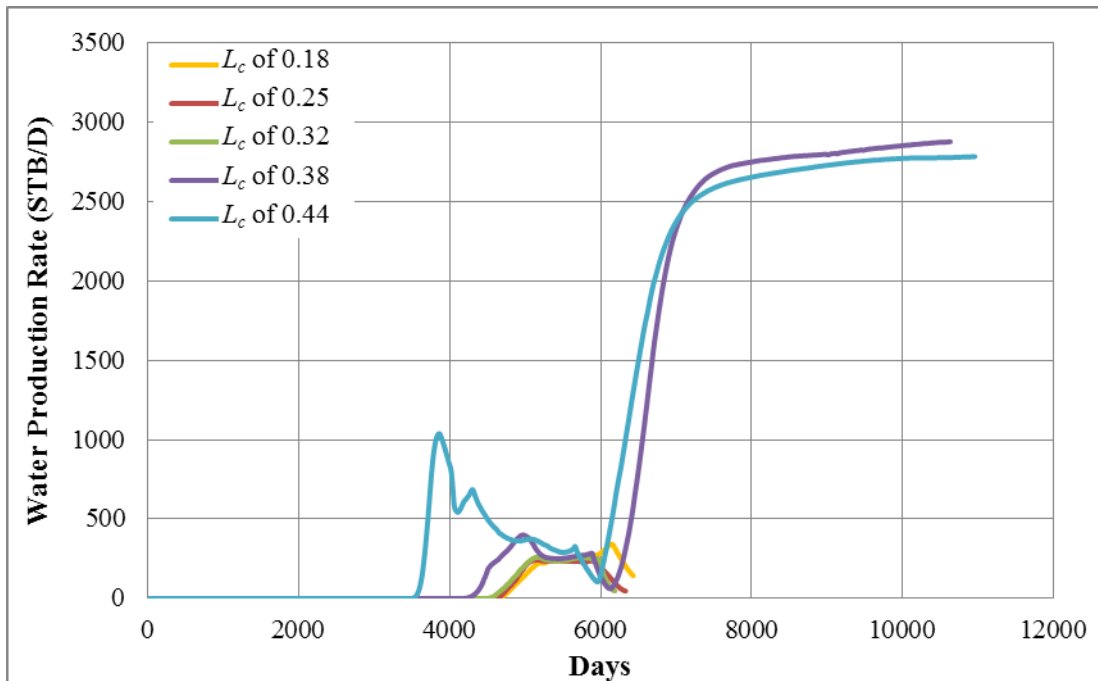
Figure 5.52 Water production rates obtained from CO_2 injection rate of 6 MMSCFD
as functions of time for all heterogeneity index cases on fining upward
reservoir model

It is also observed that the lowest recovery from each injection rate is obtained at different heterogeneity index. Injection rate of 6 MMSCFD gives the lowest point at L_c of 0.32, 8 MMSCFD at L_c of 0.25 and 10, 12, and 14 MMSCFD at L_c of 0.18. For example for case L_c of 0.25, only injection rate of 10 MMSCFD and above yield large oil recovery percentage, differentiating from other two lower injection rates. Investigating from water production profile, it can be seen that an amount of water from the case of 10, 12 and 14 MMSCFD can be significantly produced and it lengthens production duration as shown in Figure 5.53. Similarly, for the model with L_c of 0.32, injection rate of 8 MMSCFD and higher provide high oil recovery compared to injection rate of 6 MMSCFD. This is also an effect from water production which is considered as an arrival of injected water to producer. It sweeps residual oil from the reservoir and, hence, supports oil production rate to be greater than 100 STB/D which is designed production shut-off. Figure 5.55 and 5.56 show oil production rate for the case L_c of 0.25 and 0.32, respectively. It is obvious that

different oil recovery is caused by oil production rate rises up again when it mostly reaches minimum limitation which is align with the time where a big slug of water starts producing.

Figure 5.53 Water production rates from all studied injection rates as functions of time for case L_c of 0.25 on fining upward reservoir model

Figure 5.54 Water production rates from all studied injection rates as functions of time for case L_c of 0.32 on fining upward reservoir model
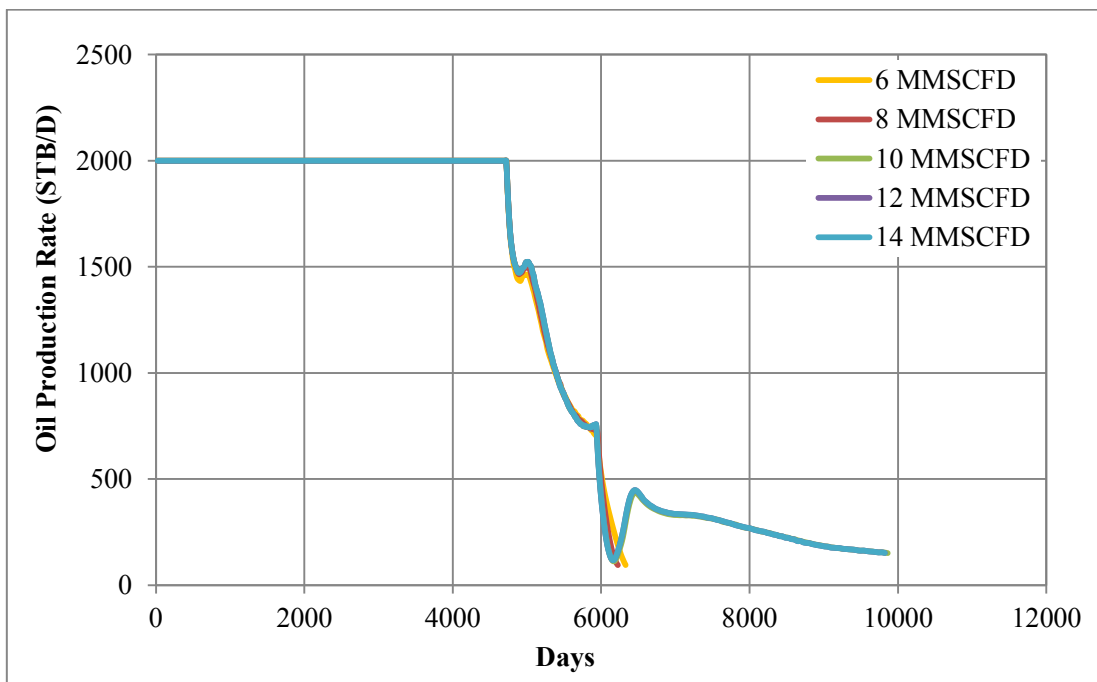
Figure 5.55 Oil production rates from all studied injection rates as functions of time for case L_c of 0.25 on fining upward reservoir model
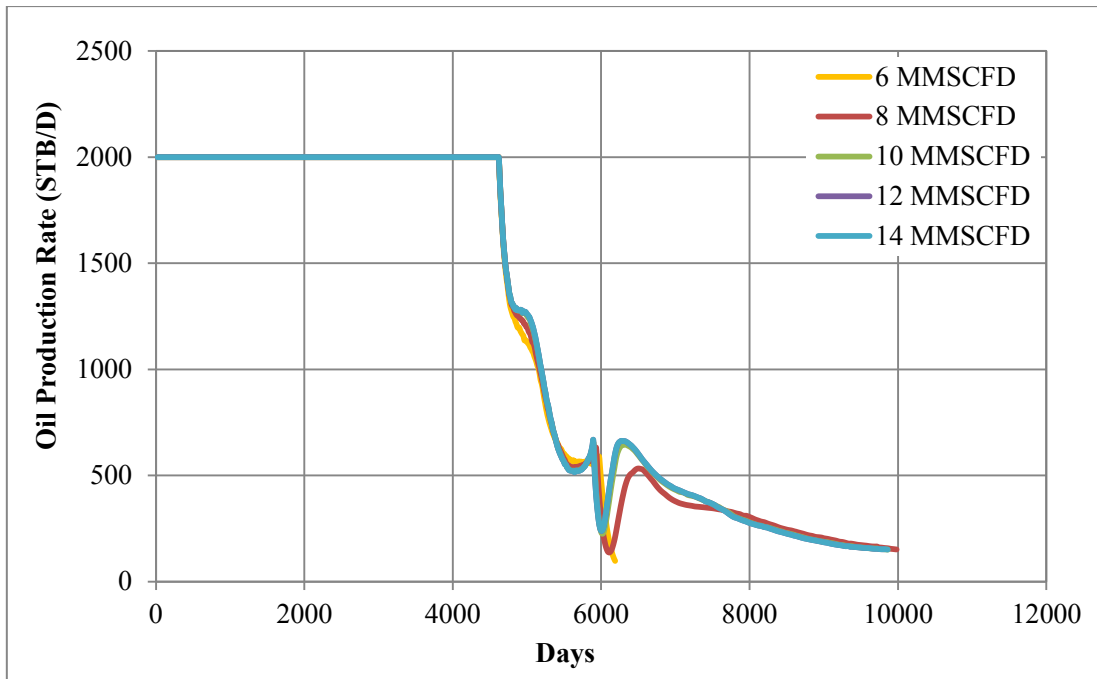
Figure 5.56 Oil production rates from all studied injection rates as functions of time for case L_c of 0.32 on fining upward reservoir model

The reason why water is produced differently from each case even heterogeneity index is the same, can be described as the higher injection rate of CO_2 results in an earlier date to complete a CO_2 injection of 0.4 HCPV slug size, as a designed value, so that chasing water is injected earlier, helping to produce larger amount of water. Table 5.10 summarizes date that a 0.4 HCPV of CO_2 is completely injected and it can also be indicated CO_2 injectivity increases when heterogeneity index increases.

Though, a big slug of water can be produced from all injection rate cases when reservoir possesses high heterogeneity index e.g. 0.38 and 0.44, the injection rate of 10, 12 and 14 MMSCFD is able to achieve the highest oil recovery and it is also because of starting date of chasing water injection, providing the earliest arrival of this big water slug. Therefore, oil production rate when big amount of water breaking through starts increasing earliest as shown in Figure 5.57. In theory, high injection rate of gas causes high viscous force over gravity force, diminishing severe effect of gravity segregation. However, it can be noted from the study that higher gas injection

rate does not show this phenomena due to limitation of fracture pressure at injector which is set at 3,800 psia. At early date of gas injection, pressure at injector is still high as a result of pre-flushed water injection (Figure 5.58), so that amount of CO_2 injected is limited as shown in Figure 5.59. Also obviously seen in injection rate of 12 and 14 MMSCFD from this figure, fracture pressure limits its injection rate. Until the CO_2 slug size is mostly finished, its actual injection rate is still not at its maximum. So, performance from these 2 injection rate is quite the same and also similar to the case of 10 MMSCFD. Gas saturation from these injection rates is also monitored to prove that gas saturation is identical in every case at the early date of CO_2 injection and just slightly different at the late production period due to water injection starts at different period as displayed in Figure 5.60.

Table 5.10 Summary of the date where injection of CO_2 slug of 0.4 HCPV is completed for each injection rate and heterogeneity index on fining upward lithofacies

Heterogeneity index (L_c)	CO_2 Injection Complete Date (days)				
	6 MMSCFD	8 MMSCFD	10 MMSCFD	12 MMSCFD	14 MMSCFD
0.18	5,324	5,234	5,230	5,230	5,230
0.25	5,255	5,140	5,083	5,065	5,065
0.32	5,224	5,093	5,023	5,004	5,014
0.38	5,182	5,043	4,961	4,943	4,934
0.44	5,019	4,860	4,766	4,713	4,713

Figure 5.57 Oil production rates from all studied injection rates as functions of time for case L_c of 0.38 on fining upward reservoir model

Figure 5.58 Bottomhole pressures at injection well from all studied injection rates as functions of time for case L_c of 0.25 on fining upward reservoir model

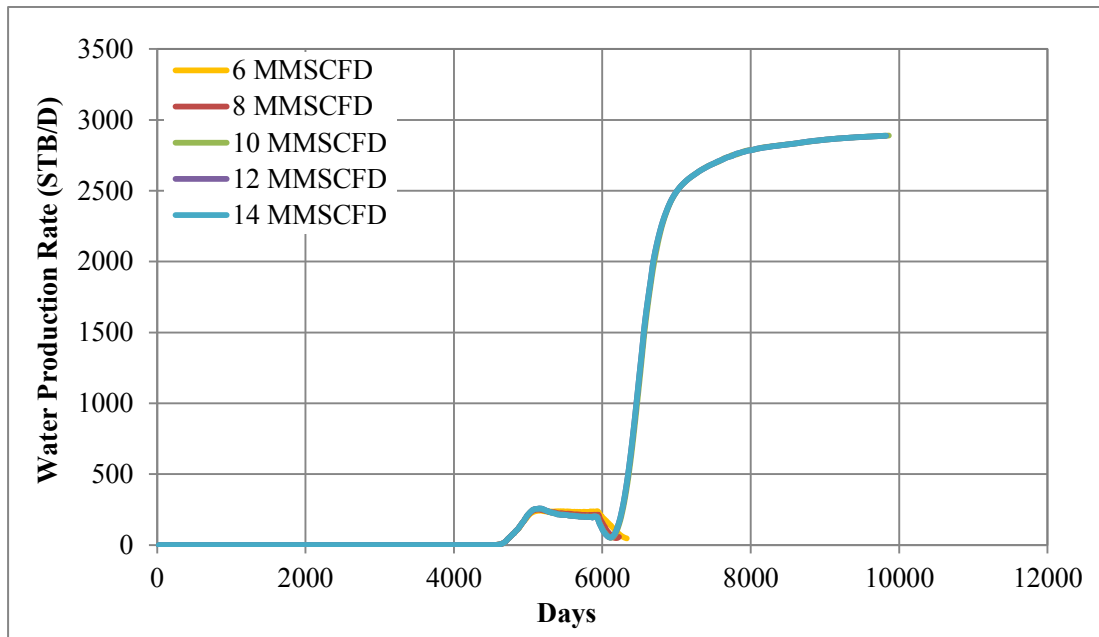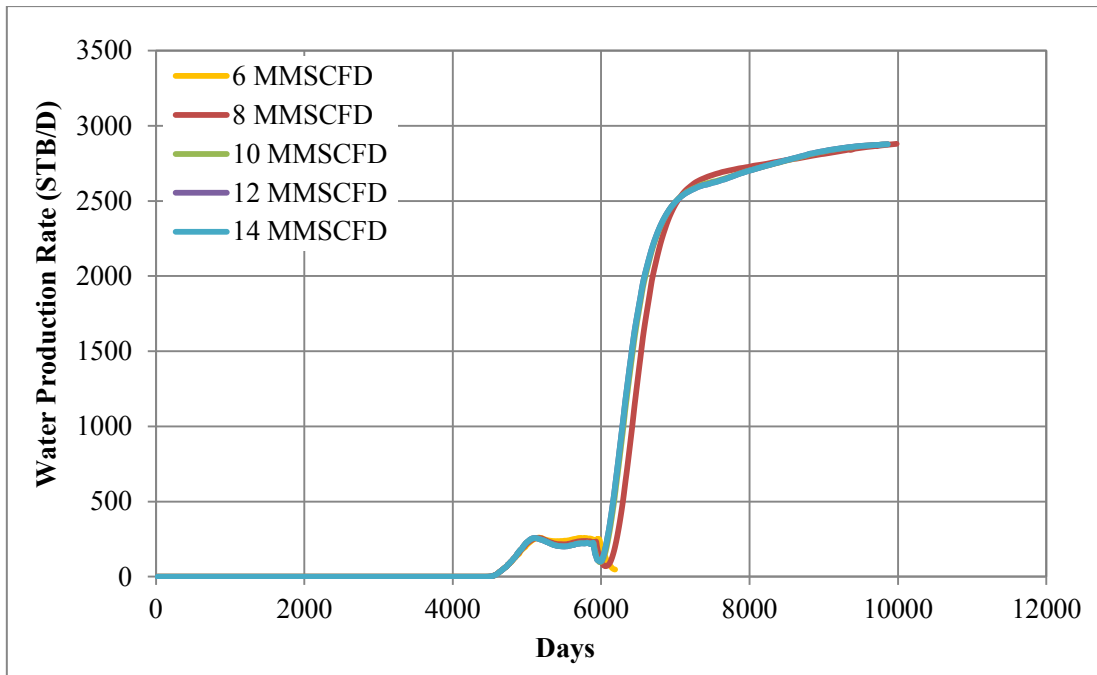Figure 5.59 Actual CO_2 injection rates from all studied injection rates as functions of time for case L_c of 0.25 on fining upward reservoir model
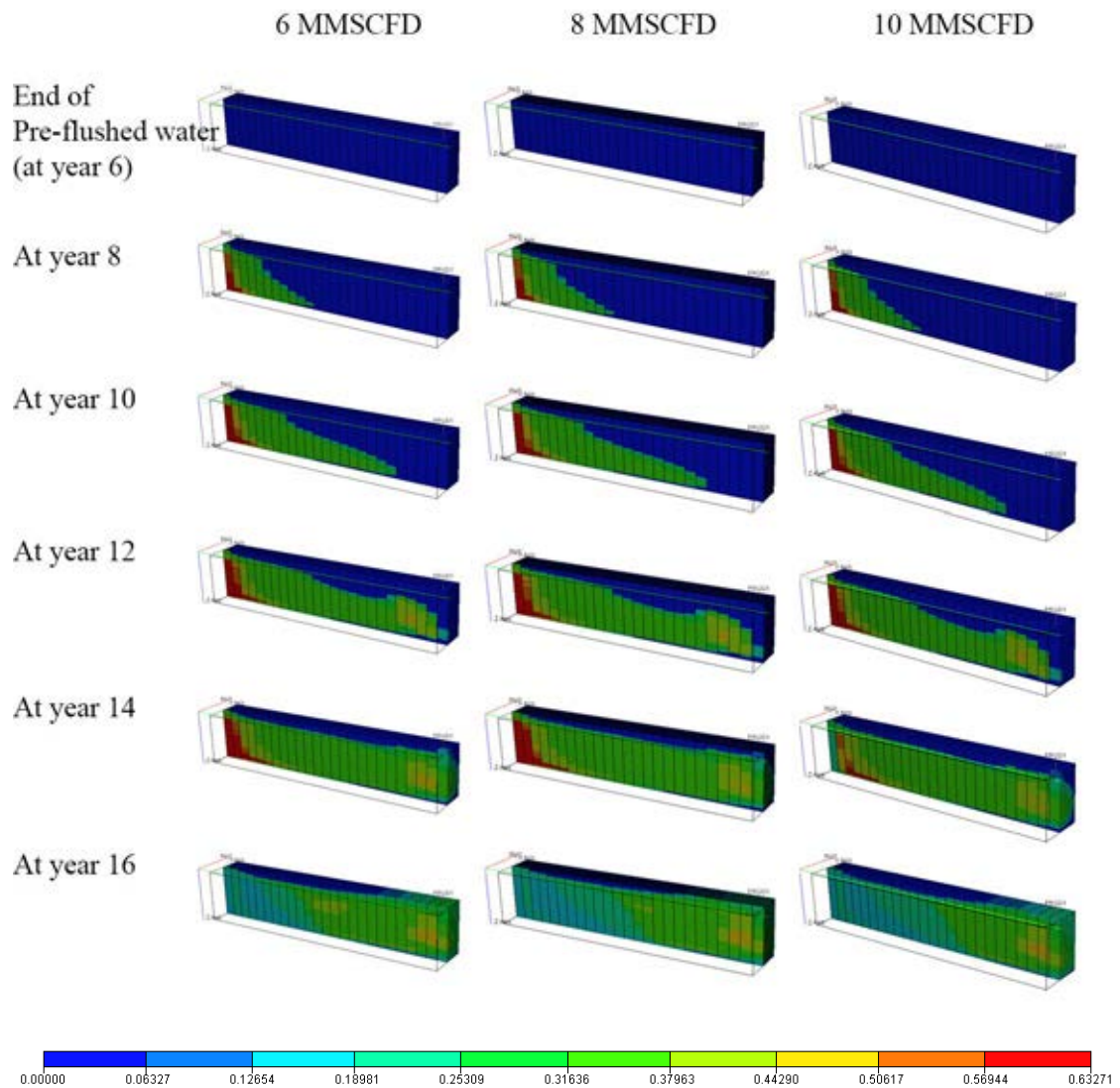
Figure 5.60 Three dimension profile of gas saturation map at different time steps from all studied CO_2 injection rates for case L_c of 0.25 on fining upward reservoir model

In addition, the date where 0.4 HCPV of CO_2 injection is totally injected from the case of 12 and 14 MMSCFD with L_c of 0.18 is the earliest, meaning the soonest start of chasing water injection, oil recovery from this case is still the same compared to other three lower injection rates. This is a result from small variation on permeability constructed on the model, so water flood front is quite stable for all cases and consequently, insignificant water production displacing residual oil arrives to producer.

Considering Figure 5.50 where oil recovery obtained from coarsening upward model is plotted, it gives alike trend for all injection rates and it can be interpreted based on a similar explanation from the case of no dip angle in previous section. The mentioned trend is that oil recovery is small for low heterogeneity index. Then, it increases with moderate heterogeneity index and decreases again at higher value increasing heterogeneity index, but it finally goes up for high heterogeneity index. However, it should be remarked that there are some points differentiated from this trend but it could be said that increasing injection rate provides a better performance on oil recovery.

First of all, with the first studied heterogeneity index, L_c of 0.18, the trend should approximately have the same value of recovery from all injection rates, because there is no water support for sweeping residual oil and, hence, a shorter oil production period is obtained. This is due to the fact that low permeability variation and also coarsening lithofacies enables waterflood front to be stable. Therefore, a significant amount of water does not arrive to producer. However, injection rate of 10, 12 and 14 MMSCFD shows different characteristic and gives the higher oil recovery which is obtained from extension of total production period as seen in Figure 5.61. This results from an arrival of big slug of water because high injection rate means early finish of planned CO_2 slug size and so early chasing water injection is also attained accordingly. Figure 5.62 shows that, with L_c of 0.18, only three cases of 10, 12 and 14 MMSCFD produce a lot of water.

Another point showing much deviation from the trend is from the case of 6 MMSCFD with L_c of 0.32 and this low oil recovery can be explained that it is again impacted from no water production. This case takes the longest time to finish injecting 0.4 HCPV of CO_2, about 260 days later compared to the case of 10 MMSCFD and about 300 days compared to case of 12 and 14 MMSCFD, implying the start date of chasing water injection is consequently late. The producer is shut in early because there is not any extra oil production swept by water to help sustain it to be greater than the minimum limitation.

In summary, from observation on study of injection rate on both lithofacies, increment of heterogeneity index does not seem to affect much on oil recovery for the case of high injection rate (10, 12 and 14 MMSCFD) as less variation on oil recovery

can be seen. The most important parameter that impacts flooding performance in this part is water production. Higher CO_2 injection rate results in sooner date to meet a pre-set slug size of 0.4 HCPV CO_2 and therefore earlier date of water injection, implying that a big slug of water could be produced in some cases. This water production helps in sweeping movable residual oil from pore space and helps pushing this oil to producer. Consequently, oil production rate survives from being lower than production constraint, extending oil production period and enhancing oil recovery. Furthermore, injection rate higher than 10 MMSCFD does not give a better result on oil recovery; this is because injection is limited by fracture pressure and the size of CO_2 slug. It is also noted that in low heterogeneity index cases, a significant amount of water is unlikely to be produced for some cases due to stable flood front and if water is produced, it shows the most rapid in increasing and eventually reaches the maximum water cut limit. Table 5.11 summarizes the simulation results for the study of CO_2 injection rate on both depositional sequences.
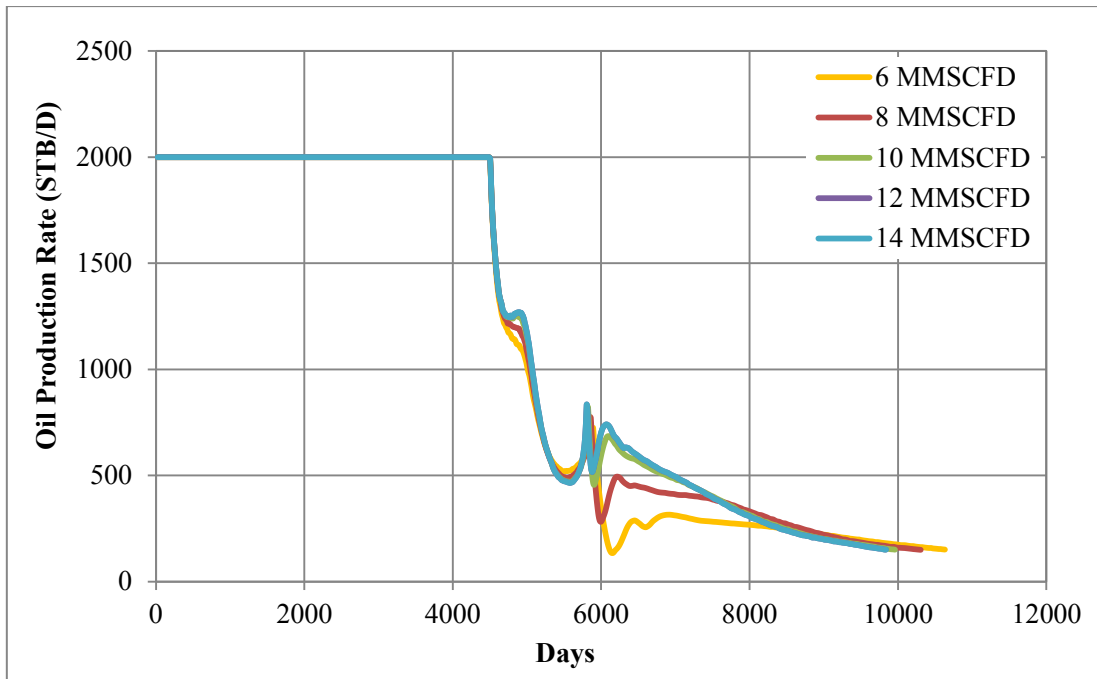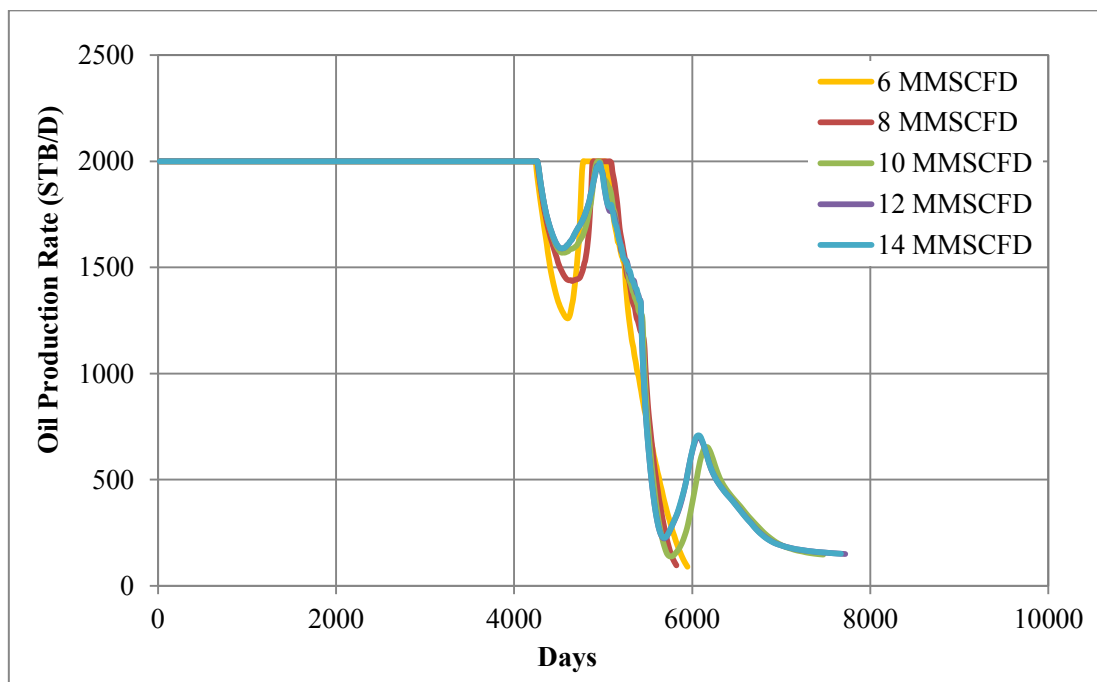

Figure 5.61 Oil production rates from all studied injection rates as functions of time for case L_c of 0.18 on coarsening upward reservoir model
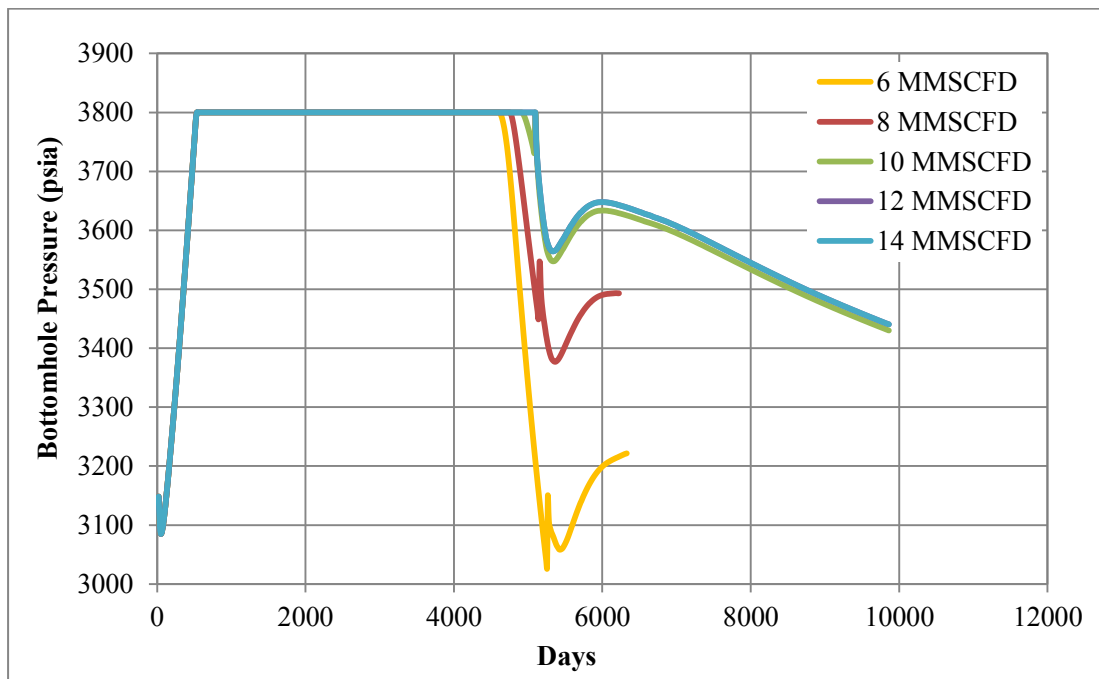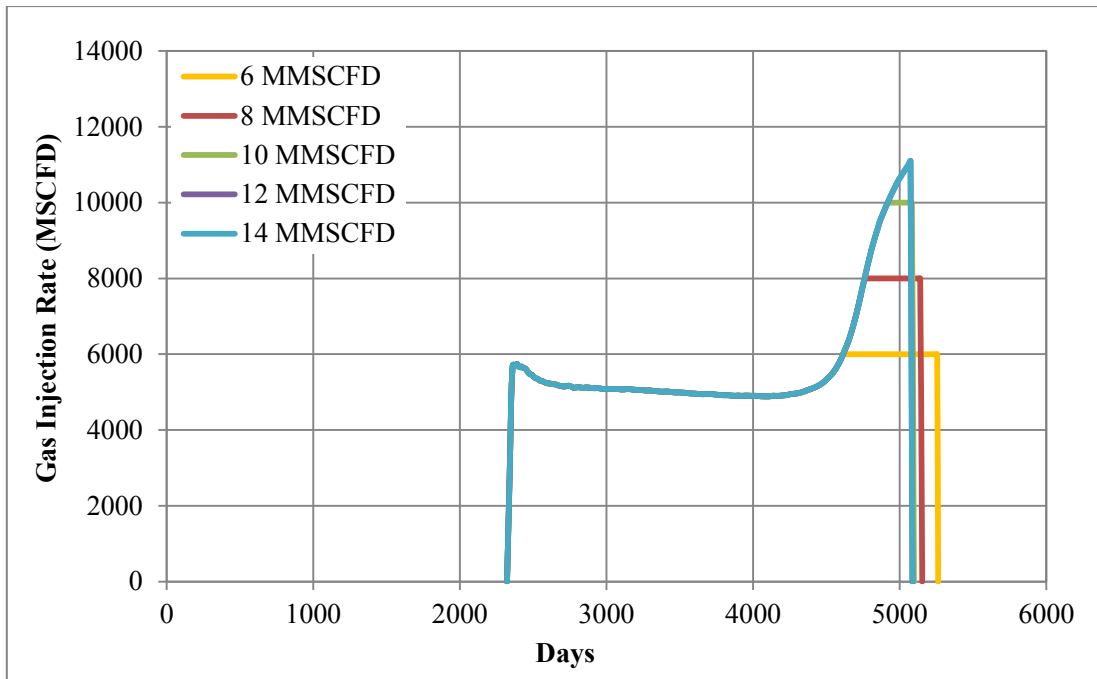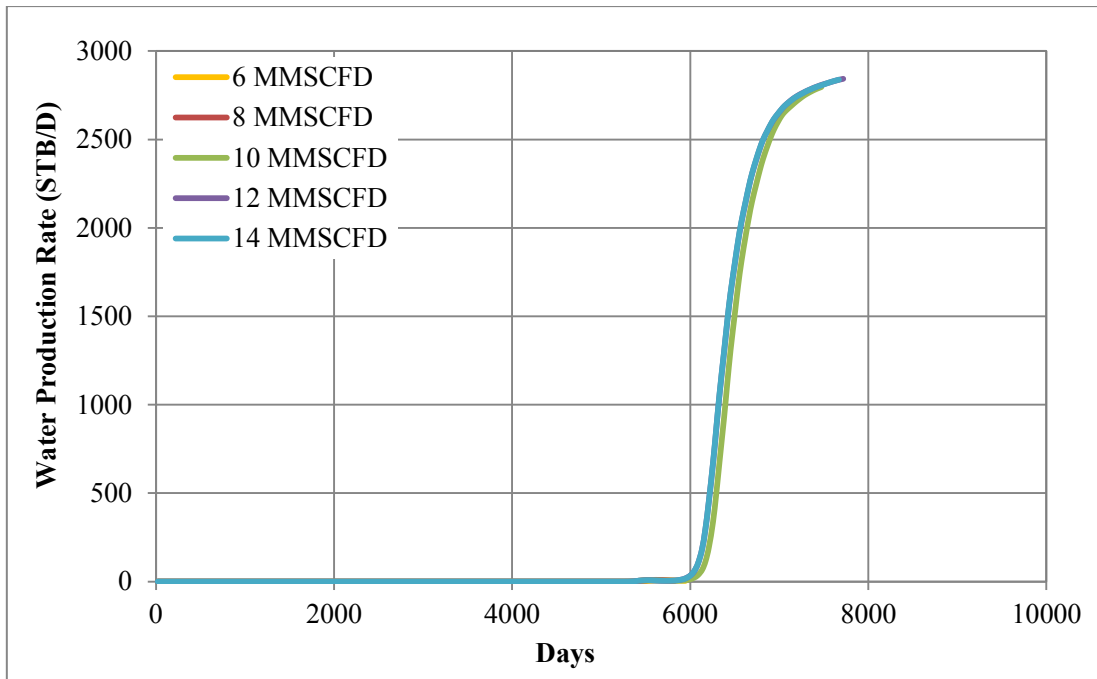
Figure 5.62 Water production rates from all studied injection rates as functions
of time for case L_c of 0.18 on coarsening upward reservoir model

Table 5.11 Summary of simulation results on the study of CO_2 injection rate when
applied with reservoir heterogeneity both fining and coarsening upward sequence

Case	CO₂ Injection Rate (MMSCFD)	L_c	Cumulative Gas Production (BSCF)	Cumulative Water Production (MMSTB)	Oil Recovery (%)	Total Production Period (days)
Fining Upward Sand Model						
01		0.00	15.24	0.2	67.96	6,638
1A		0.18	15.50	0.37	67.93	6,416
1B		0.25	16.40	0.31	66.25	6,316
1C	6	0.32	16.64	0.31	63.05	6,176
1D		0.38	17.13	11.51	60.58	10,633
1E		0.44	17.09	13.20	65.42	10,958

Table 5.11 Summary of simulation results on the study of CO_2 injection rate when applied with reservoir heterogeneity both fining and coarsening upward sequence (continued)

Case	CO₂ Injection Rate (MMSCFD)	L_c	Cumulative Gas Production (BSCF)	Cumulative Water Production (MMSTB)	Oil Recovery (%)	Total Production Period (days)
02		0.00	15.24	0.2	67.96	6,638
2A		0.18	15.07	0.34	66.33	6,376
2B	8	0.25	15.90	0.28	62.94	6,215
2C		0.32	16.42	9.81	67.10	9,982
2D		0.38	16.65	11.05	66.79	10,307
2E		0.44	16.71	13.71	66.57	10,958
03		0.00	15.24	0.2	67.96	6,638
3A		0.18	15.02	0.34	67.96	6,372
3B	10	0.25	15.85	9.47	66.33	9,862
3C		0.32	16.11	9.68	68.37	9,862
3D		0.38	16.29	10.29	67.64	9,981
3E		0.44	16.40	13.96	67.35	10,958
04		0.00	15.24	0.2	67.96	6,638
4A		0.18	15.02	0.34	66.33	6,372
4B	12	0.25	15.82	9.37	68.39	9,823
4C		0.32	16.07	9.71	67.71	9,862
4D		0.38	16.18	10.01	67.45	9,839
4E		0.44	16.23	13.98	68.13	10,914
05		0.00	15.24	0.2	67.96	6,638
5A		0.18	15.02	0.34	66.33	6,372
5B	14	0.25	15.82	9.37	68.39	9,823
5C		0.32	16.07	9.71	67.71	9,862
5D		0.38	16.18	10.01	67.45	9,839
5E		0.44	16.23	13.98	68.13	10,914

Table 5.11 Summary of simulation results on the study of CO_2 injection rate when applied with reservoir heterogeneity both fining and coarsening upward sequence (continued)

Case	CO₂ Injection Rate (MMSCFD)	L_c	Cumulative Gas Production (BSCF)	Cumulative Water Production (MMSTB)	Oil Recovery (%)	Total Production Period (days)
Coarsening Upward Sand Model
06		0.00	15.24	0.2	67.96	6,638
6A		0.18	16.99	Trace	67.93	5,929
6B	6	0.25	17.33	2.43	61.16	7,791
6C		0.32	17.51	Trace	61.49	5,871
6D		0.38	17.82	4.45	55.31	8,446
6E		0.44	17.63	9.28	60.76	9,982
07		0.00	15.24	0.2	67.96	6,638
7A		0.18	16.81	Trace	61.37	5,817
7B	8	0.25	17.13	4.44	63.15	8,243
7C		0.32	17.52	4.08	61.88	8,118
7D		0.38	17.67	4.86	62.08	8,362
7E		0.44	17.63	9.16	63.47	9,701
08		0.00	15.24	0.2	67.96	6,638
8A		0.18	16.60	2.70	64.45	7,473
8B	10	0.25	16.83	5.63	64.36	8,521
8C		0.32	17.25	5.41	63.31	8,521
8D		0.38	17.42	4.87	63.17	8,323
8E		0.44	17.40	8.17	64.19	9,295
09		0.00	15.24	0.2	67.96	6,638
9A		0.18	16.37	3.60	64.99	7,719
9B	12	0.25	16.74	6.03	64.97	8,766
9C		0.32	17.26	5.84	63.81	8,766
9D		0.38	17.48	4.89	63.41	8,401
9E		0.44	17.50	7.94	64.29	9,296

Table 5.11 Summary of simulation results on the study of CO_2 injection rate when applied with reservoir heterogeneity both fining and coarsening upward sequence (continued)

Case	CO_2 Injection Rate (MMSCFD)	L_c	Cumulative Gas Production (BSCF)	Cumulative Water Production (MMSTB)	Oil Recovery (%)	Total Production Period (days)
Coarsening Upward Sand Model						
010		0.00	15.24	0.2	67.96	6,638
10A		0.18	16.37	3.71	65.03	7,755
10B	14	0.25	16.74	6.03	64.97	8,766
10C		0.32	17.26	5.84	63.81	8,766
10D		0.38	17.48	4.89	63.41	8,401
10E		0.44	17.50	7.94	64.29	9,295

5.4.3 Effect of CO_2 Injection Perforation Interval

When CO_2 is injected into reservoir it might easily flow in high permeability streaks since it is gas that possesses high mobility. Especially, when combining this CO_2 injection with coarsening upward lithofacies, low gravity of gas may cause severe gravity segregation, leaving much oil remained unswept inside reservoir and impoverished performance is achieved accordingly. In this section, the study is to determine effect from partial injection of CO_2 through the injector into the location away from high permeability zone, For example, the model, simulated with fining upward sand where high permeability channel is located at lower part of reservoir, is to be partially injected with CO_2 only at upper part. While CO_2 slug is injected through shortened zone, both pre-flushed and chasing water is still remained injected over full reservoir thickness in order to keep water injection as a fixed parameter. This reduced CO_2 injection interval, in practical aspect, can be performed by using a tool called temporary patch which can be set inside tubing during the time at which gas has to be injected. The tool is generally used for the purpose of blocking any undesirable zone to be not produced or injected. This tool can be later pulled out from

the zone in order to get the well operated at full injection zone for chasing water again.

Base case is to be applied with other two partial injection of CO_2, 50% and 75%. CO_2 slug size of 0.4 HCPV is still remained constant for every model in this part. Note that these two selected interval is also confirmed that reservoir pressure is higher than MMP and miscibility is formed. The parameter detail of this study is summarized in Table 5.12.

Table 5.12 Summary of simulated cases on the study of CO_2 injection interval

Group No.	Lithofacies	Heterogeneity Index	CO_2 Injection Interval
1	Fining Upward	0.18	50, 75 and 100%
2		0.25	50, 75 and 100%
3		0.32	50, 75 and 100%
4		0.38	50, 75 and 100%
5		0.44	50, 75 and 100%
6	Coarsening Upward	0.18	50, 75 and 100%
7		0.25	50, 75 and 100%
8		0.32	50, 75 and 100%
9		0.38	50, 75 and 100%
10		0.44	50, 75 and 100%

Main simulation outcome which is oil recovery as a function of reservoir heterogeneity index and CO_2 injection interval are plotted in Figure 5.63 and 5.64, respectively.
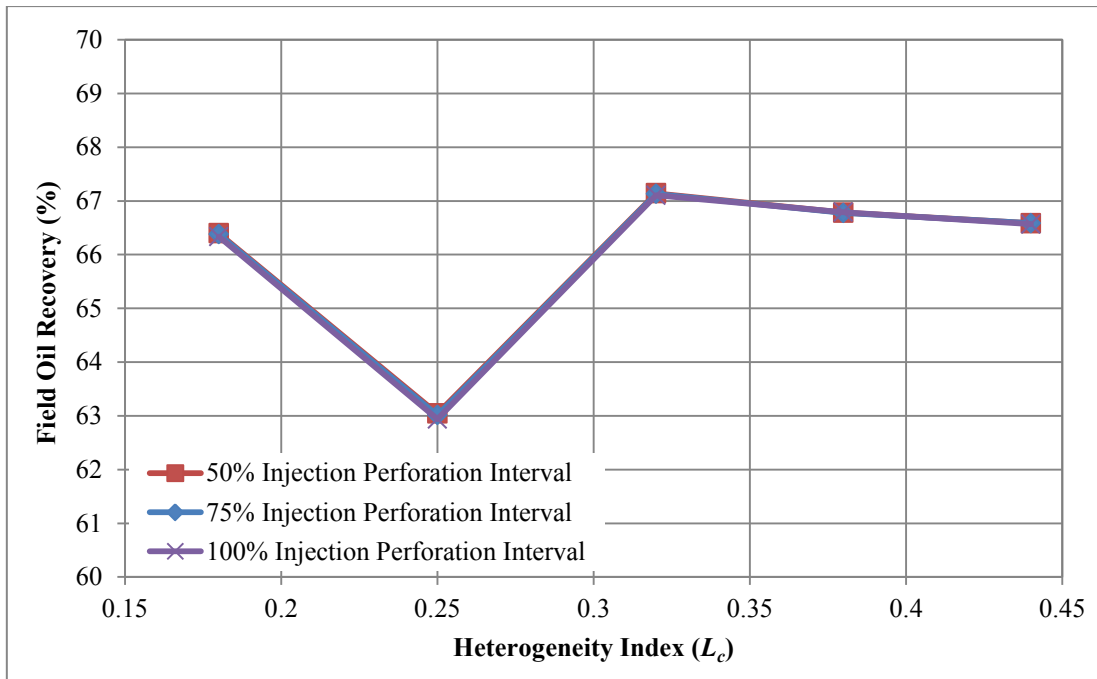
Figure 5.63 Field oil recoveries as functions of heterogeneity index for different injection intervals on fining upward reservoir model
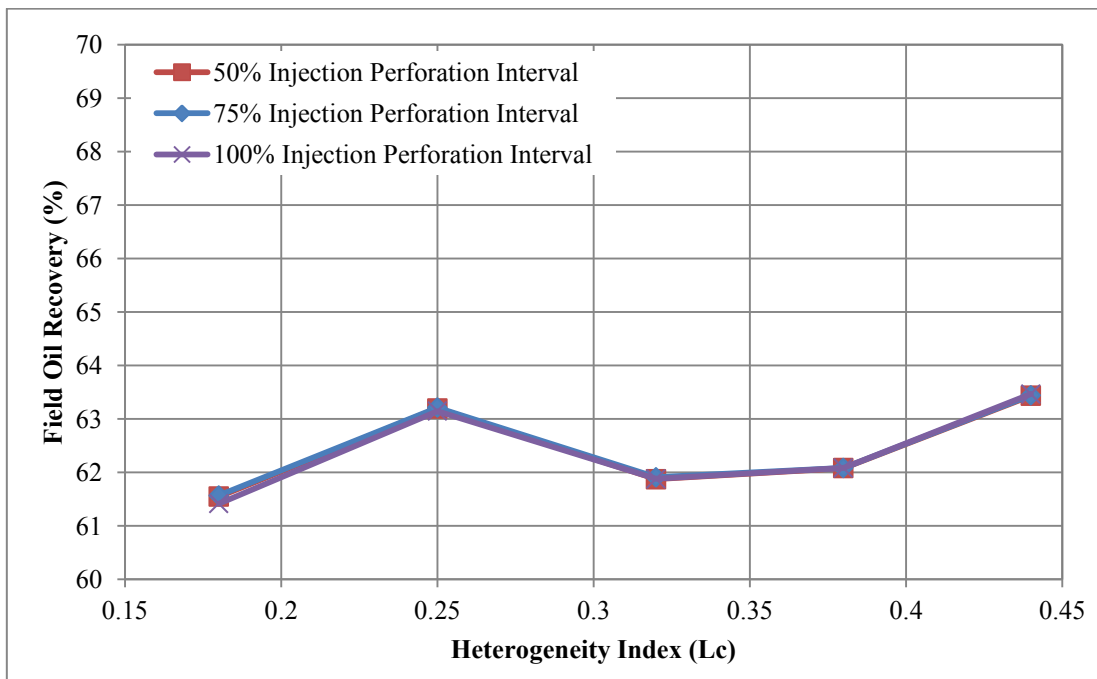
Figure 5.64 Field oil recoveries as functions of heterogeneity index for different injection intervals on coarsening upward reservoir model

Apparently, no difference on oil recovery from varying injection interval of CO_2 and varying heterogeneity index is found for both fining upward and coarsening upward sand model as shown in Figures 5.63 and 5.64. This is due to the fact that gas still shows the same injection behavior such as amount of CO_2 and finishing period of gas injection even the interval is shortened. Gas saturation on three-dimension model and gas injection rate from case L_c of 0.32 on fining upward model is used as an example to interpret result as shown in Figures 5.65 and 5.66, respectively. It is found that, although, CO_2 is injected only at the low permeability channel, it mostly flows in high permeability zone due to high mobility of gas together with connectivity to high permeability zone. As pre-flushed water injection is kept the same rate, the same result of CO_2 injection and the same rate of chasing water injection, so oil recovery is not different for all cases. However, oil recovery from fining upward model can be yielded higher than coarsening upward model. This is due to the reason mentioned previously that coarsening upward model creates more unstable flood front from gas which leads to the larger area unswept by the miscible bank. Besides, reservoir pressure is also presented in Figure 5.67 to confirm that it is higher than MMP.
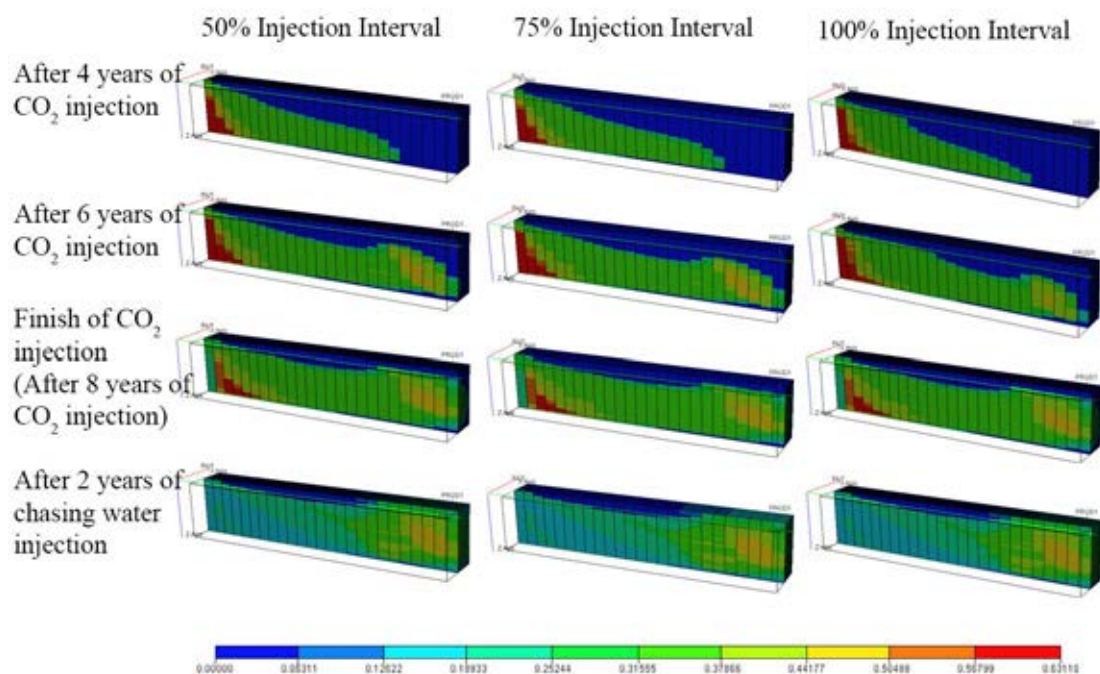
Figure 5.65 Gas saturation profiles from all three injection intervals at different time steps for case L_c of 0.32 on fining upward reservoir model
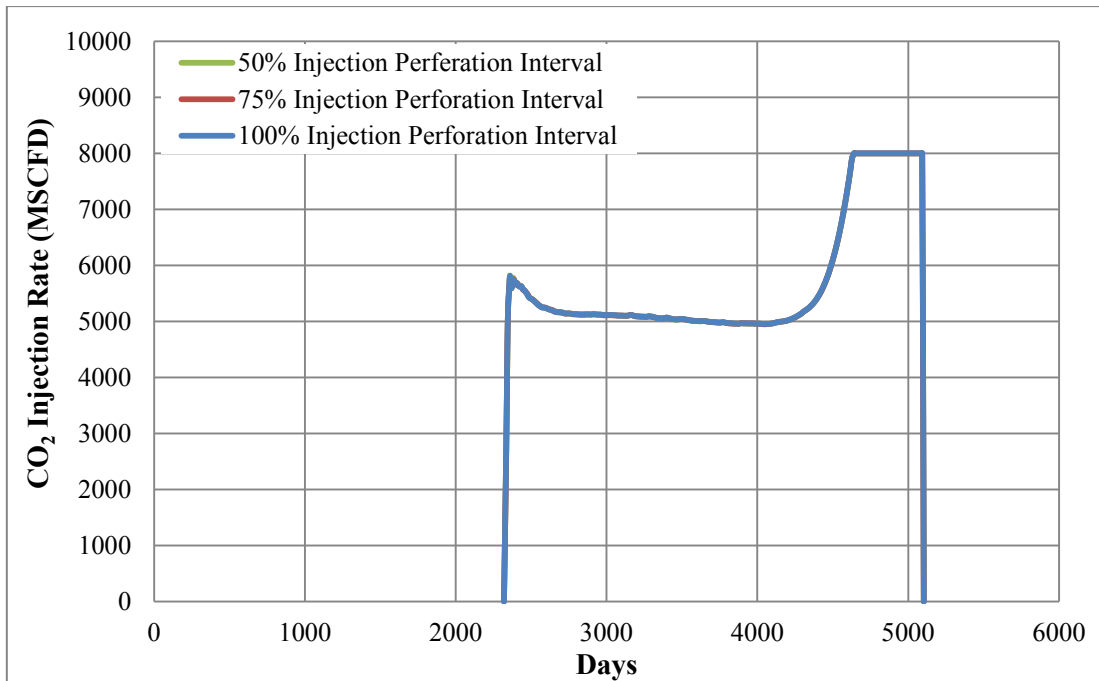
Figure 5.66 Actual CO_2 injection rates as functions of time from all three injection intervals for case L_c of 0.32 on fining upward reservoir model
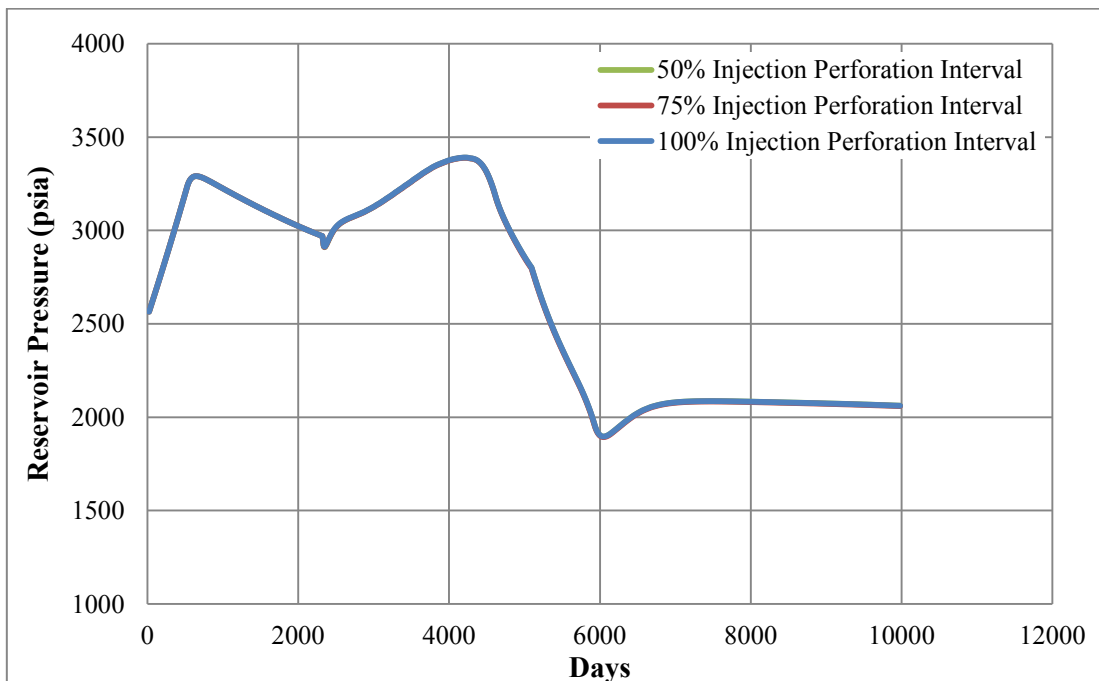
Figure 5.67 Reservoir pressures as functions of time from all three injection intervals for case L_c of 0.32 on fining upward reservoir model

From discussion in this section, it can be concluded that partial interval of CO_2 injection does not show significant effect on oil recovery. This could be due to gas mobility that is extremely high. And when this is combined with reservoir connectivity between each layer (vertical permeability), gas then tends to flow only in high permeability zone, resulting in no difference between cases.

CHAPTER VI

CONCLUSIONS AND RECOMMENDATIONS

In this chapter, results obtained from simulation of CO_2 miscible flooding in multi-layered heterogeneous reservoir are concluded. The effects of both mentioned uncontrollable and controllable parameters implemented with reservoir model are also summarized. Recommendations are included which might be meaningful and helpful for further study.

6.1   Conclusions

There are two sub-sections for conclusions based on the sequence of the study which are optimization of CO_2 miscible flooding and effect of study parameters sections.

6.1.1. Optimization of CO_2 Miscible Flooding

1. Slug size of pre-flushed water shows a visible influence on oil recovery. Optimization of this slug size is required for specific implementation. Since studied reservoir model is water-wet system. Applying pre-flushed water can recover movable oil without wasting large amount of CO_2 to perform miscible flooding since beginning. It is found that the optimal slug size is 0.2 PV.

2. The results from simulation indicates that around 68% of oil recovery can be recovered from implementing designed CO_2 miscible flooding in homogeneous base case where 8% out of this 68% is higher than solely waterflooding implementation. This due to the fact that CO_2 injection does not only assist in increasing reservoir pressure but it also forms miscible bank where increment of oil recovery mainly accomplishes through miscibility mechanism, noticeably seen from a reduction of residual oil

saturation and increase of remaining oil viscosity. Reservoir pressure and oil viscosity reduction illustrate that the miscible bank can exist until it arrives the producer.

6.1.2. Effect of Study Parameters

1. Reservoir heterogeneity acts as a role in effectiveness of CO_2 miscible flooding. This reservoir property impacts flow performance and consequently affects oil recovery. Increasing heterogeneity causes higher unstable flood front and an early breakthrough of injected material can frequently occur. However, this early breakthrough is considered as either positive or negative results in this study. An early breakthrough of gas causes a limit flow of oil to the production well. Therefore, shorter plateau of oil production is observed. On the contrary, an early breakthrough of water could help in slightly bouncing up oil production rate to be greater than minimum constraint and so production can be extended longer, resulting in additional oil recovery.

2. Formation depositional sequence affects the flooding performance. In general, fluid preferentially flows inside high permeability zones. Injected fluids also behave like this. With low gravity of CO_2, coarsening upward lithofacies seems to allow injected CO_2 to flow easily on top part of model, so, larger area is remained unswept from created miscible bank, leaving greater amount of oil. Its recovery is lower as a result.

3. Dip angle of reservoir assists displacement mechanism against gravity segregation of CO_2 by forming more stable flood front. This also results in retarding of breakthrough of gas and hence, higher oil recovery is attained. However, reservoir model with higher dip angle than 30 degree seems to involve with adverse effects since injectant composes of pre-flushed water slug and chasing water slug. As water is injected from updip location, gravity force drags it to flow to producer fast and therefore, maximum water cut is early approached. Thus, poor oil recovery is obtained.

4. Higher CO_2 injection rate theoretically applies to avoid gravity segregation due to lowering gravity number (increase viscous force while gravity force is constant). However, based on the design flooding scheme of CO_2 slug size of 0.4 HCPV, increasing injection rate yields benefit through accelerating completion of this slug size quantity. Hence, early start date of chasing water injection is performed and this results in an on time arrival of water to producer prolonging the total production period to be slightly above limitation of oil production rate before it turns to be lower than minimum constraint.

5. Shortening CO_2 injection perforation interval does not show any difference on this studied flooding. From results, it could be possible that combination of high mobility of CO_2 together with reservoir connectivity in vertical direction leads gas to flow in high permeability zone.

In summary, reservoir with low heterogeneity index shows relatively high recovery when applied with high reservoir dip angle. However, when heterogeneity increases, lower dip angle degree turns to show benefit since effect from water breakthrough could be minimized. High injection rate of 10 MMSCFD provides better oil recovery than other two lower injection rates to all reservoir heterogeneity indexes but injection rate higher than this value could not show any difference on oil recovery due to the limits of fracture pressure and CO_2 slug size. Besides, decreasing injection interval of CO_2 does not give any improvement in term of oil recovery.

6.2   Recommendations

The following points are suggested for applying in further study of CO_2 miscible flooding:

1. Heterogeneity in this study is constructed based on one-way permeability sequence namely low to high value for fining upward lithofacies and high to low value for coarsening upward lithofacies. The unsystematic sequence might be added to represent the permeability variation in reality. Besides,

broader range of permeability value should be studied in order to observe more effects from wider range of heterogeneity index.

2. The reservoir wetting preference in this study is water-wet. Oil-wet rock would be included in the future consideration.

3. Reservoir model with a contact of water or gas would give diversifying conclusions.

4. For more accuracy, the actual reservoir data such as fluid compositions and core analysis should have been included.

References

[1]   Enayati, M., Heidaryan, E. and Mokhtari, B. New Investigations into Carbon Dioxide Flooding by Focusing on Viscosity and Swelling Factor Changes. Paper 2008-064, the Canadian International Conference/SPE Gas Technology Symposium 2008, Calgary, Alberta, Canada, 17-19 June, 2008.

[2]   Majidaie, S., Khanifar, A., Onur, M. and Tan, I.M. A Simulation Study of Chemically Enhanced Water Alternating Gas (CWAG) Injection. Paper SPE 154152, presented at SPE EOR Conference at Oil and Gas West Asia, Muscat, Oman, 16-18 April, 2012.

[3]   Zang, P.Y., Huang, S., Sayegh, S. and Zhou, X.L. Effect of CO_2 Impurites on Gas-Injection EOR Process. Paper SPE 89477, presented at the 2004 SPE/DOE Fourteenth Symposium on Improved Oil Recovery, Tulsa, Oklahoma, USA, 17-21 April, 2004.

[4]   Qin, L.C., Hailong, L. and Yin, X. Q. Application of CO_2 Miscible Flooding on Gao 89-1 Low Permeability Reservoir. Paper SPE 144918, presented at the SPE Asia Pacific Oil and Gas Conference and Exhibition, Jakarta, Indonesia, 20-22 September, 2011.

[5]   Shedid, S.A., Zekri, A.Y. and Almehaideb, R.A. Optimization of Carbon Dioxide Flooding For a Middle-Eastern Heterogeneous Oil Reservoir. Paper 2008-094, prepared for the Canadian International Petroleum Conference/SPE Gas Technology Symposium, Calgary, Alberta, Canada, 17-19 June, 2008.

[6]   Ghasemzadeh, A., Momeni, A. and Vatani, A. Application of Miscible CO_2 injection to Maximize Oil Recovery in One of Iranian Undersaturated Oil Reservoirs: Simulation and Optimization Study. Paper SPE 144476, presented at the SPE Enhanced Oil Recovery Conference, Kuala Lumpur, Malaysia, 19-21 July, 2011.

[7] Yongmao, H., Zenggui, W. and Yueming, J.B.C. Laboratory Investigation of CO_2 Flooding. Paper SPE 88883, Presented at the 28th Annual SPE International Technical Conference and Exhibition, Abuja, Nigeria, 2-4 August, 2004.

[8] Jeschke, P.A., Schoeling, L. and Hemmings, J. CO_2 Flood Potential of California Oil Reservoirs and Possible CO_2 sources. Paper SPE 63305, presented at the 2000 SPE/AAPG Western Regional Meeting, California, 19-23 June, 2000.

[9] Shedid, S.A. Influences of Different Modes of Reservoir Heterogeneity on Performance and Oil Recovery of Carbon Dioxide Miscible Flooding. Journal of Canadian Petroleum Technology, Volume 48, No. 2, pp. 29-36, February 2009.

[10] Ahmed, M., Ahmed, H., and Sayyouh, M.H. Guidelines to Optimize CO_2 EOR in Heterogeneous Reservoirs. Paper SPE 151871, presented at the North Africa Technical Conference and Exhibition, Cairo, Egypt, 20-22 February, 2012.

[11] Mansour, S., Hoier, L., and Kleppe, J. CO_2 Injection and CO_2 WAG in Dipping Gas Condensate and Oil Reservoirs. Paper SPE 154062, presented at the Eighteenth SPE Improved Oil Recovery Symposium, Tulsa, Oklahoma, USA, 14-18 April, 2012.

[12] Abdassah, D., Siregar S., and Kristanto, D. The Potential of Carbon Dioxide Gas Injection Application in Improving Oil Recovery. Paper SPE 64730, Presented at the SPE Seventh International Oil and Gas Conference and Exhibition, Beijing, China, 7-10 November, 2000.

[13] Green, D.W., and Willhite, G.P. Enhanced Oil Recovery. Society of Petroleum Engineers, Richardson, Texas, 1989.

[14] Donaldson, E.C., Chilingarian, G.V., and Yen, T.F. Enhanced Oil Recovery, II: Processes and Operations. Elsevier Science Publishers B.V., Amsterdam, The Netherlands., 1989.

[15] Larry, W.L. Enhanced Oil Recovery. Prentice Hall, USA, 1989.

[16] Latil, M.,Bardon, C., Burger, J., and Sourieau, P. Enhanced Oil Recovery. Gulf Publishing Company Book Division, Texas, U.S.A., 1980.

[17] Yelig, W.F., Metcalfe, R.S. Determination and Prediction of CO_2 Minimum Miscibility Pressures. Paper SPE 7477, Journal of Technology, 1980.

[18] Yuan, H., Johns, R.T., Egwuenu, A.M., and Dindoruk, B. Improved MMP Correlations for CO_2 Floods Using Analytical Gas Flooding Theory. Paper SPE 89359, presented at the SPE/DOE Fourteenth Symposium on Improved Oil Recovery, Tulsa, Oklahoma, USA, 17-21 April, 2004.

[19] Glasø, O. Generalized Minimum Miscibility Pressure Correlation. Paper SPE 12893, SPE Journal, 1985.

[20] Cronquist, C. Carbon Dioxide Dynamic Miscibility with Light Reservoir Oils. Fourth Annual U.S. DOE Symposium on Enhanced Oil and Gas Recovery and Improved Drilling Methods, Tulsa, 1977.

[21] Craig, F.F. The Reservoir Engineering Aspect of Water flooding. Fourth printing, Society of Petroleum Engineering of AIME, New York, U.S.A., 1973.

[22] Tiab, D., and Donaldson, E.C. Petrophysics: theory and practice of measuring reservoir rock and fluid transport properties. Gulf publishing company, Houston, Texas, U.S.A., 2004.

[23] Lake, L.W., and Jensen, J.L. A Review of Heterogeneity Measures Used in Reservoir Characterization. Paper SPE 20156, SPE Journal, 1989.

[24] Tarek, A. Reservoir Engineering Handbook. Second Edition, Gulf Professional Publishing, USA, 2000.

[25] Schlumberger. ECLIPSE Technical Description 2007.1

[26] Heller, J.P., and Kovarik, F.S. Improvement of CO_2 Flood Performance. Fourth Annual Report for the Period, 1 October, 1987 – 30September, 1988.

[27] Lohrenz, J., Bray, B. G., Clark, C.R. Calculating Viscosities of Reservoir Fluids from Their Composition. Paper SPE 915, presented at SPE Annual Fall Meeting, Houston, Texas, 11-14 October, 1964.

APPENDIX

APPENDIX

RESERVOIR MODEL CONSTRUCTION
BY ECLIPSE®300

Reservoir models exploited in this study were developed by using compositional simulator ECLIPSE®300 according to a dynamic change in reservoir fluid compositions. ECLIPSE add-on Software, PVTi, was also used to generate some properties in PVT section. Details in each section and data inserted into the simulator are summarized in this Appendix.

1. **Case Definition**

Simulator	Compositional
Model Dimensions	Number of cell in x-direction 21
	Number of cell in y-direction 25
	Number of cell in z-direction 40
Grid Type	Cartesian
Grid Geometry	Block Centered
Oil-Gas-Water Options	Water, Oil and Gas

2. **Reservoir Geometry and Properties**

X Permeability	Varied from 20-300 mD with constant average value
Y Permeability	Varied from 20-300 mD with constant average value
Z Permeability	Varied from 2-30 mD with constant average value
Porosity	0.2
X Grid Box Sizes	40 ft
Y Grid Box Sizes	200 ft
Z Grid Box Sizes	5 ft
Depth of Top Face	5,000 ft

In this study, the models were categorized into two types based on reservoir dip angle, one of the study parameters, consisting of horizontal and inclined reservoir, respectively. The above mentioned detail is for horizontal reservoir model (no dip angle). However, when constructing, there are slight differences for inclined reservoir model which are shown in section 1 and 2 as follows:

1. Case Definition

        Grid Geometry   Corner Point

2. Reservoir Geometry and Properties

        Grid Block Coordinate Lines   Based on calculated dip angle

        Grid Block Corners   Based on calculated dip angle

3. PVT (imported from PVTi)

Miscellaneous

        Number of Components   11

        Component Names

Component 1	CO_2
Component 2	N_2
Component 3	C1
Component 4	C2
Component 5	C3
Component 6	IC4
Component 7	NC4
Component 8	IC5
Component 9	NC5
Component 10	C6
Component 11	C7+

Lorenz-Bray-Clark Viscosity Correlation Coefficient

Coefficient 1	0.1023
Coefficient 2	0.023364
Coefficient 3	0.058533
Coefficient 4	-0.040758
Coefficient 5	0.0093324

EoS Res Tables

Initial Reservoir Temperature	172°F
Equation of State (Reservoir EoS)	PR

Component	Molecular weight	EoS Omega-a Coefficient	EoS Omega-b Coefficient	Critical Temps (^{o}R)	Critical Pressures (psia)
CO2	44.01	0.4572355	0.07779607	548.46	1071.33
N2	28.01	0.4572355	0.07779607	227.16	492.31
C1	16.04	0.4572355	0.07779607	343.08	667.78
C2	30.07	0.4572355	0.07779607	549.77	708.34
C3	44.10	0.4572355	0.07779607	665.64	615.76
IC4	58.12	0.4572355	0.07779607	734.58	529.05
NC4	58.12	0.4572355	0.07779607	765.36	550.66
IC5	72.15	0.4572355	0.07779607	828.72	491.58
NC5	72.15	0.4572355	0.07779607	845.28	488.79
C6	84.00	0.4572355	0.07779607	913.50	436.62
C7+	267.00	0.4572355	0.07779607	1597.00	124.23

(Continued)

Component	Critical Volumes (ft³/lb-mol)	Critical Z-Factors	EoS Volume Shift	Acentric Factors	Component Parachors
CO2	1.5057	0.2741	-0.0427	0.225	78.0
N2	1.4417	0.2912	-0.1313	0.040	41.0
C1	1.5698	0.2847	-0.1443	0.013	77.0
C2	2.3707	0.2846	-0.1033	0.099	108.0
C3	3.2037	0.2762	-0.0775	0.152	150.3
IC4	4.2129	0.2827	-0.0620	0.185	181.5
NC4	4.0847	0.2739	-0.0542	0.201	189.9
IC5	4.9337	0.2727	-0.0418	0.227	225.0
NC5	4.9817	0.2684	-0.0303	0.251	231.5
C6	5.6225	0.2504	-0.0073	0.299	271.0
C7+	24.1208	0.1755	0.2396	1.184	965.2

(Continued)

Component	Critical Volumes for Viscosity Calculation (ft³/lb-mol)	Critical Z-Factors for Viscosity Calculation	Overall Composition
CO2	1.505735	0.2740778	0.0091
N2	1.441661	0.2911514	0.0006
C1	1.569809	0.2847295	0.3383
C2	2.370732	0.2846348	0.0904
C3	3.203692	0.2761646	0.0799
IC4	4.212855	0.2827370	0.0197
NC4	4.084707	0.2738555	0.0469
IC5	4.933686	0.2727109	0.036
NC5	4.981741	0.2684389	0.0178
C6	5.622479	0.2504175	0.0501
C7+	24.21083	0.1754944	0.3112

Binary Interaction Coefficients

	CO2	N2	C1	C2	C3	IC4	NC4	IC5	NC5	C6	C7+
CO2	0	-0.012	0.1	0.1	0.1	0.1	0.1	0.1	0.1	0.1	0.1
N2	-0.012	0	0.1	0.1	0.1	0.1	0.1	0.1	0.1	0.1	0.1
C1	0.1	0.1	0	0	0	0	0	0	0	0.0279	0.0526
C2	0.1	0.1	0	0	0	0	0	0	0	0.01	0.01
C3	0.1	0.1	0	0	0	0	0	0	0	0.01	0.01
IC4	0.1	0.1	0	0	0	0	0	0	0	0	0
NC4	0.1	0.1	0	0	0	0	0	0	0	0	0
IC5	0.1	0.1	0	0	0	0	0	0	0	0	0
NC5	0.1	0.1	0	0	0	0	0	0	0	0	0
C6	0.1	0.1	0.0279	0.01	0.01	0	0	0	0	0	0
C7+	0.1	0.1	0.0526	0.01	0.01	0	0	0	0	0	0

4. SCAL

Water/ Oil Saturation Functions

No.	S_w	k_{rw}	k_{ro}
1	0.28	0.0000	0.4100
2	0.31	0.0000	0.3378
3	0.34	0.0000	0.2747
4	0.37	0.0002	0.2199
5	0.40	0.0005	0.1730
6	0.43	0.0012	0.1332
7	0.46	0.0026	0.1001
8	0.49	0.0048	0.0730
9	0.52	0.0081	0.0513
10	0.55	0.0130	0.0343
11	0.58	0.0198	0.0216
12	0.61	0.0290	0.0125
13	0.64	0.0411	0.0064
14	0.67	0.0567	0.0027
15	0.7	0.0762	0.0008
16	0.73	0.1004	0.0001
17	0.76	0.1300	0.0000
18	1.00	1.0000	0.0000

Gas/ Oil Saturation Functions

No.	S_g	k_{rg}	k_{ro}
1	0	0.0000	0.4100
2	0.15	0.0000	0.1786
3	0.18	0.0002	0.1452
4	0.21	0.0014	0.1163
5	0.24	0.0048	0.0914
6	0.28	0.0114	0.0704
7	0.31	0.0222	0.0529
8	0.34	0.0384	0.0386
9	0.37	0.0610	0.0271
10	0.40	0.0910	0.0182
11	0.43	0.1296	0.0114
12	0.46	0.1778	0.0066
13	0.49	0.2366	0.0034
14	0.53	0.3072	0.0014
15	0.56	0.3906	0.0004
16	0.59	0.4878	0.0001
17	0.62	0.6000	0.0000
18	0.72	1.0000	0.0000

5. Initialization

Equilibration

Datum Depth	5,000 ft
Pressure at Datum Depth	2,512 psia
WOC Depth	10,000 ft

6. Schedule

6.1 Production Well

Well Specification

Well	PROD1
I Location	11
J Location	25
Datum Depth	5,000 ft

Preferred Phase	Oil
Inflow Equation	STD
Automatic Shut-In Instruction	Shut
Crossflow	Yes
Density Calculation	SEG

Well Connection Data

Well	PROD1
K Upper	1
K Lower	40
Open/Shut Flag	OPEN
Well Bore ID	0.708 ft
Direction	Z

Production Well Control

Well	PROD1
Open/Shut Flag	OPEN
Control	ORAT
Oil Rate	2,000 STB/day
Gas Rate	8,000 MSCF/day
BHP Target	400 psia

Production Well Economic Limits

Well	PROD1
Minimum Oil Rate	100 STB/day
Maximum Water Cut	0.95 STB/STB
Workover Procedure	WELL
End Run	YES
Quantity for Economic Limit	RATE
Secondary Workover Procedure	NONE

6.2 Injection Well

6.2.1 Water injection period

Well Specification

Well	INJ1
I Location	11

J Location	1
Preferred Phase	Water
Inflow Equation	STD
Automatic Shut-In Instruction	SHUT
Crossflow	YES
Density Calculation	SEG

Well Connection Data

Well	INJ1
K Upper	1
K Lower	40
Open/ Shug Flag	OPEN
Well Bore ID	0.708 ft
Direction	Z

Well Injection Targets

Well	INJ1
Injected Fluid	WATER
Injection Rate Control	WATER
Target Water Rate	3,000 STB/day
Target BHP	3,800 psia

6.2.2 CO_2 Injection Period

Well Specification

Well	INJ1
I Location	11
J Location	1
Preferred Phase	Gas
Inflow Equation	STD
Automatic Shut-In Instruction	SHUT
Density Calculation	SEG

Well Connection Data

Well	INJ1
K Upper	1
K Lower	40

Open/Shut Flag	OPEN
Injection Gas Composition	
Well Stream	1
Comp1	1
Comp2	0
Comp3	0
Comp4	0
Comp5	0
Comp6	0
Comp7	0
Comp8	0
Comp9	0
Comp10	0
Comp11	0
Well Injection Targets	
Well	INJ1
Injected Fluid	STREAM
Well Stream	1
Injection Rate Control	Gas
Target Gas Rate	8,000 MSCF
Target BHP	3,800 psia

Vitae

Mr. Satavee Summapo was born on 8th February, 1989, in Bangkok, Thailand. He obtained a second class honors Bachelor's degree in Chemical Engineering, Faculty of Engineering, Chulalongkorn University in 2010. After this degree, he pursued a Master's degree in Petroleum Engineering at Department of Mining and Petroleum Engineering, Chulalongkorn University. During the time of this study, he has also been working for Optimus Oil and Gas Engineering Ltd. as a Process Engineer.